Binding of Self-assembling Peptides to Oligodeoxynucleotides

by

Mei Wang

A thesis
presented to the University of Waterloo
in fulfillment of the
thesis requirement for the degree of
Doctor of Philosophy
in
Chemical Engineering

Waterloo, Ontario, Canada, 2007

Author's Declaration

I hereby declare that I am the sole author of this thesis. This is a true copy of the thesis, including any required final revisions, as accepted by my examiners.

I understand that my thesis may be made electronically available to the public.

Abstract

This thesis is an experimental investigation on the binding of self-assembling peptides to oligodeoxynucleotides (ODNs) and the characterization of the resulting peptide-ODN complexes/aggregates, the first key step in the development of a peptide-based gene delivery system. Effects of pH, charge distribution along the peptide backbone, and oligonucleotide sequences on the peptide-ODN binding were investigated by a series of physicochemical methods.

UV-Vis absorption and fluorescence anisotropy experiments demonstrate that aggregates are formed after mixing the peptide and ODN in aqueous solution. The aggregates in solution can be centrifuged out. Based on this property, the fraction of ODNs incorporated in the peptide-ODN aggregates can be obtained by comparing the UV-Vis absorption of the solution before and after centrifugation. Binding isotherms are generated by a binding density function analysis of the UV absorbance results. The binding parameters are extracted from the analysis of the binding isotherms based on the McGhee and von Hippel model.

Equilibrium binding parameter studies show that the binding of two self-assembling peptides, EAK16-II and EAK 16-IV, to model single and double-stranded ODNs at pH 4 is stronger than at pH 7, and that no binding occurs at pH 11. These results demonstrate that electrostatic interactions play an important role in the EAK-ODN binding because EAKs are more positively charged at low pH. EAKs bind more strongly to dG_{16} than to the other ODN sequences dC_{16} and dGC_{16}. This demonstrates that the hydrogen bond might be involved because they promote the binding of the lysine residues of the peptide to dG_{16} to a greater extent than to dC_{16}. The charge distribution along the peptides is found to have an effect on the binding. EAK16-IV, whose positively charged residues are clustered at one end of the peptide, binds to the ODNs more strongly than EAK16-II, whose positively charged residues are distributed throughout the peptide chain, at the same pH.

The binding process of EAKs to the ODNs was investigated by fluorescence anisotropy and static light scattering experiments. The results show that individual EAK and ODN molecules complex first, followed by the aggregation of these complexes into large aggregates. The nature of the resulting peptide-ODN complexes/aggregates is examined by UV-Vis absorption, fluorescence anisotropy, and PAGE experiments. The results demonstrate that free EAK, free ODNs, and small EAK-ODN complexes, which can not be centrifuged out, exist in the supernatant, and that large aggregates are collected in the pellets after centrifugation of the solution. The size of the resulting EAK-ODN complexes/aggregates measured by AFM and DLS is around a few hundreds of

nanometers at low EAK concentrations. The accessibility of the ODNs to the quencher in the solution is reduced by 40 % and 60 % after binding to EAK16-II and EAK16-IV, respectively, as determined by fluorescence quenching experiments on EAK-ODN mixture solutions.

An ODN protection from Exonuclease 1 degradation is provided by the EAK16-II or EAK16-IV matrix when they are mixed with the ODNs at pH 4. However, the ODNs are protected to a much lower degree when the EAK-ODN aggregates are prepared at pH 7. The EAK-ODN aggregates prepared at pH 7 are found to dissociate more easily than those prepared at pH 4 when they are incubated with exonuclease I solution at pH 9.5. These results suggest that the ODN protection afforded by the EAK-ODN aggregates is correlated with their structural stability after being incubated with the nuclease solution. The stability of the EAK-ODN aggregates after dilution is determined by UV-Vis absorption. No detectable dissociation of the aggregates is observed over 20 hrs after a 5- and 10-fold dilution of the solution in the same buffer used for their preparation. The EAK-ODN aggregates remain stable after the solutions are centrifuged, and re-dissolved in fresh buffer solutions.

The ability of an EAK matix to protect ODNs from nuclease degradation together with its biocompatibility and low-toxicity suggests that EAK self-assembling peptides could be used as carriers for gene delivery.

Acknowledgements

I would like to express my warm and sincere appreciation to my supervisors, Professor Pu Chen and Professor Jean Duhamel. They were always there to meet and talk about my ideas, ask me good questions and help me think through problems, and give constructive comments. They showed me different ways to approach a research problem and the need to be persistent to accomplish any goal. They provided detailed review, beneficial criticism, excellent advice, and revising during the preparation of this thesis. I would have been lost without their constant encouragement and guidance.

I am grateful to my colleagues in the Nano-Bio interfacial engineering group for their valuable discussions and suggestions, and for their help on my work. I thank the staff in the Department of Chemical Engineering for their help in many different ways.

I wish to thank Hye-Young Suk for her assistance with the data collection of the fluorescence quenching experiments, Howard Siu for his help with the time-resolved fluorescence decay experiments, Dan Anderson for stimulating discussions, Professor Elizabeth M. Meiering for letting me use the Zetasizer Nano ZS instrument, Professor Michael Palmer for letting me use the time-resolved fluorometer and giving advice.

The Ph.D and this thesis were financially supported by the Natural Science and Engineering Research Council of Canada (NSERC), the Canadian Foundation for Innovation (CFI), the Canadian Research Chairs (CRC) program, and the Ontario's Premier Research Excellence Award.

Last, but not least, my deep appreciation goes to my family: my husband Dongyu Fang, for loving me with all the good and all the bad, and for being there whenever I needed help; my parents, Fulin Wang and Yuqin Zhang, for giving my life in the first place, and for unconditional support and encouragement for pursuing my interests.

Table of Contents

List of Figures

List of Tables

Chapter 1
Introduction

1.1 Background

Self-assembling peptides have recently drawn intense attention because they can be designed and engineered to provide considerable potential for a number of applications in bionanotechnology. A new class of self-assembling peptides, ionic-complementary peptides, was serendipitously discovered from a Z-DNA binding protein in yeast a decade ago by Shuguang Zhang (Zhang, *et al*., 1993). This class of short peptides was found to spontaneously form a membrane-like structure when added into cell cultures at neutral pH. This observation led to the strategy of using small peptides to construct functional supramolecules.

The molecular structure of these peptides is characterized by alternating hydrophobic and hydrophilic amino acid residues, which contain alternating positive and negative charges, enabling ionic-complementarity. The ionic complementarity, together with hydrogen bonding and hydrophobic interactions, facilitates peptides to self-assemble into very stable nanostructures (Fung, *et al*., 2003; Hong, *et al*., 2003; Chen, 2005). In addition, these peptides elicit minimal cytotoxicity and immune responses and inflammation and are biocompatible (Zhang, 2002). The nano/microstructures constructed from the peptide self-assembly have found many biomedical applications including scaffolding for tissue engineering (Zhang, *et al*., 1995; Holmes, *et al*., 2002), serving as template for nanowire fabrication, and understanding of amyloid fibrillogenesis in protein misfolding diseases (Rochet and Lansbury, 2000; Lynn and Meredith, 2000; Yang, *et al*., 2006b). It has been shown recently that these peptides can stabilize hydrophobic pyrene microcrystals in aqueous solution and unload them into a model cell membrane mimic, egg phosphatidycholine (EPC) vesicle, in a controlled manner (Keyes-Bag, *et al*., 2004). The nanofibers formed from the self-assembly of some of these peptides have shown to be potentially excellent materials for controlled molecular release of various protein growth factors (Nagai, *et al*., 2006; Davis, *et al*., 2006; Lee and Hsieh, 2006). These studies show that self-assembling peptides may be promising candidates as carriers for delivering both hydrophobic and hydrophilic drugs. Our particular interest is the self-assembling peptide-mediated delivery of antisense oligonucleotides.

The major advantage of using self-assembling peptides for gene delivery is the flexibility of this method. The composition of the final peptide-ODN complex can be modified in response to experimental results *in vitro* and *in vivo* to overcome some challenges in the delivery pathways. These

challenges include rapid nucleic acid degradation due to backbone instability and inefficient delivery of nucleic acids into the specific targeted cells (Smith, *et al*., 1998). By design, numerous functional characteristics including DNA binding and protecting sequences, receptor-based targeting sequences, peptides, cell penetrating sequences, fusogenic sequences with properties to release DNA from the endosomes, can be incorporated into the peptide sequence (Smith, *et al*., 1998). This design flexibility is important since there is little quantitative information about how efficiently the vector is processed through each stage of the complex processes of cellular uptake.

The binding of the oligonucleotides (ODNs) to the peptides is the first key step in the formulation procedures for peptide-based DNA delivery systems (Plank, *et al*., 1999; Simeoni, *et al*., 2003). The reasons are as follows. First, the stoichiometry of complexation may affect cellular uptake of the resulting complexes if the cationic peptides interact with the negatively charged phosphate backbone of nucleic acids through electronic interactions. Second, other physicochemical properties of the resulting peptide/ODN assemblies, such as size, morphology, together with surface characteristics, may affect where the ODN is being delivered *in vivo* and ultimately influence the ability of the delivery system to reach its target site. Consequently the choice of any new peptide candidate for a peptide-based ODN delivery system requires the characterization of the binding of the peptide to the ODNs and of the resulting peptide/ODN aggregates.

While there has been no study of binding between self-assembling peptides and oligonucleotides, numerous techniques have been used to examine the interaction between proteins or small ligands and nucleic acids qualitatively and quantitatively (Sauer, 1991; Moss, 2001). Footprinting and cross-linking experiments (Nagaich, *et al*., 1997) have been used to elucidate the binding sites or the overall architecture of the complex between protein and DNA. For quantitative study, isothermal titration calorimetry (Singh, *et al*., 2006) and differential scanning calorimetry (Plotnikov, *et al*., 2004; Franco, *et al*., 2005) are the common methods to determine the equilibrium binding constant directly by measuring the heat evolved during the formation of the protein/DNA complexes. In most instances, quantitative information is obtained indirectly by monitoring the changes in a biological or spectroscopic property of either the ligands or the macromolecule resulting from the formation of complexes. These changes can be probed by techniques such as filter binding (Agou, 1999), electrophoresis mobility shift assay (Stierle, *et al*., 2003; Malonga, *et al*., 2006), surface plasmon resonance (Seimiya and Kurosawa, 1996) and fluorescence (Michel, *et al*., 2003; Endoh, *et al*., 2005). These methods require labeling of the ligand with a chromophore or radioactive isotope, or covalent immobilization of the ligand. Such labeling or immobilization of the ligand might affect their biochemical activity, resulting in an inaccurate binding isotherm. Nevertheless, these techniques are still routinely used to determine the concentrations of the free and bound species, and

generate binding isotherms to obtain the affinity and the stoichiometry of ligand-DNA binding. Other techniques, such as boundary sedimentation velocity (Jensen and von Hippel, 1977; Scott, *et al*., 1999) and UV difference spectroscopy (Boraston, *et al*., 2000; Sitohy, *et al*., 2001), do not require labeling of the molecule of interest, although sensitivity will be enhanced by labeling (Galletto, *et al*., 2003).

The binding of self-assembling peptides to ODNs may cause changes in physicochemical or biological properties in the same way as other basic proteins and peptides do, which may be monitored by the above techniques. However, some unique characteristics are expected to be encountered when studying the self-assembling peptide-ODN interactions. Since these peptides can self-assemble into nanostructures over time, they may bind to the ODN molecules before or after self-assembly occurs, which might result in some challenges in the binding study. The current work will develop a series of experiments to study the binding pathways and equilibrium binding parameters. In addition, due to the potential for self-assembly of the peptides into nanostructures, the ODNs may be surrounded by peptide nanostructures and thus be protected. As rapid degradation of the ODNs is one of the major challenges in the application of oligonucleotides as therapeutic agents (Smith, *et al*., 1998), such protection ability is desired. In comparison to chemical modifications of the oligonucleotide phosphodiester backbone, which is time-consuming and costly (Ghosh, *et al*., 1993), binding of peptides to the ODNs may provide a simple and fast means to protect the ODNs.

In this thesis, detailed binding study may suggest some control strategies for the formulation of appropriate peptide/ODN complexes, and thus have diverse impacts on the application of self-assembling peptides in gene delivery.

1.2 Research Objectives

The research objectives of this study are:

1) to obtain the equilibrium binding parameters of self-assembling peptides to oligonucleotides, understand the binding pathway, and characterize the physicochemical properties of the resulting peptide-ODN complexes/aggregates;
2) to examine the effect of the pH and charge distribution of peptides on their binding to oligonucleotides;
3) to study the nuclease resistance of the ODNs provided by the self-assembling peptide matrices, and examine the stability of the peptide-ODN aggregates.

1.3 Outline of Thesis

This thesis consists of six chapters. The scope of each chapter is as follows:

Chapter 1 briefly introduces the self-assembling peptides and their applications, and the importance of this study. The objectives and scope of this thesis are also given in this chapter.

Chapter 2 reviews self-assembling peptides and their applications. It is followed by an introduction to the current techniques used to study the interactions between protein or peptide and nucleic acids.

Chapter 3 describes a series of physicochemical techniques developed to investigate the complexation and aggregation of a self-assembling peptide, EAK16-II, with oligonucleotides at various pHs.

Chapter 4 investigates the effect of the charge distribution along a self-assembling peptide on its binding to the ODNs. This was done by comparing the binding of EAK16-IV to the ODNs with that of EAK16-II studied in Chapter 3.

Chapter 5 describes how oligonucleotides are protected against nuclease degradation by the self-assembling peptide matrices at different pHs. The stability of the peptide-ODN aggregates with dilution is also investigated.

Finally, Chapter 6 summarises the main findings of this study, the contributions of this research, and some recommendations for future work.

References

Agou, F., S. Raveh, S. Mesnildrey, and M. Veron. 1999. Single Strand DNA Specificity Analysis of Human Nucleoside Diphosphate Kinase B. *J. Biol. Chem.* **274:** 19630-19638.

Boraston, A. B., P. Chiu, R. A. J. Warren, and D. G. Kilburn. 2000. Specificity and affinity of substrate binding by a family 17 carbohydrate-binding module from Clostridium cellulovorans cellulase 5A. *Biochemistry* **39:** 11129-11136.

Chen, P. 2005. Self-assembly of Ionic-complementary Peptides: a Physicochemical Viewpoint. *Colloids Surf. A* **261:** 3-24.

Davis, Michael E., P. C. H. Hsieh, T. Takahashi, Q. Song, S. Zhang, R. D. Kamm, A. J. Grodzinsky, P. Anversa, and R. T. Lee. 2006. Local myocardial insulin-like growth factor 1 (IGF-1) delivery with biotinylated peptide nanofibers improves cell therapy for myocardial infarction. *Proc. Natl. Acad. Sci. USA* **103:** 8155-8160.

Endoh, T., H. Funabashi, M. Mie, and E. Kobatake. 2005. Method for detection of specific nucleic acids by recombinant protein with fluorescent resonance energy transfer. *Anal..Chem.* **77:** 4308-4314.

Franco, R., G. Bai, V. Prosinecki, F. Abrunhosa, G. C. Ferreira, and M. Bastos. 2005. Porphyrin-substrate binding to murine ferrochelatase: effect on the thermal stability of the enzyme. *Biochem. J.* **386:** 599-605.

Fung, S.Y., C. Keyes, J. Duhamel, and P. Chen. 2003. Concentration Effect on the Aggregation of a Self-Assembling Oligopeptide. *Biophys. J.* **85:** 537-548.

Galletto, R., M. J. Jezewska, and W. Bujalowski. 2003. Interactions of the Escherichia coli DnaB helicase hexamer with the replication factor the DnaC protein. Effect of nucleotide cofactors and the ssDNA on protein-protein interactions and the topology of the complex. *J. Mol. Biol.* **329:** 441-465.

Ghosh, M. K., J. S. Cohen, O. Dahl, and K. Ghosh. 1993. Evaluation of some properties of a phosphorodithioate oligodeoxyribonucleotide for antisense application. *Nucl. Acids Res.* **21:** 5761-5766.

Holmes, T. C. 2002. Novel Peptide-Based Biomaterial Scaffolds. *Trends Biotechnol.* **20:** 16-21.

Hong, Y., R. L. Legge, S. Zhang, and P. Chen. 2003. Effect of Amino Acid Sequence and pH on Nanofiber Formation of Self-Assembling Peptides EAK16-II and EAK16-IV. *Biomacromol.* **4:** 1433-1442.

Jensen, D. E., and P. H. von Hippel. 1977. A boundary sedimentation velocity method for determining nonspecific nucleic acid-protein interaction binding parameters. *Anal. Biochem.* **80:** 267-281.

Keyes-Bag, C., S. Y. Fung, J. Bezaire, and P. Chen. 2004. Self-Assembling Peptide as a Potential Carrier of Hydrophobic Compounds. *J. Am. Chem. Soc.* **126:** 7522-7532.

Lee, R. T., and P. Hsieh. 2006. Sustained delivery of PDGF using self-assembling peptide nanofibers. *U.S. Pat. Appl. Publ.* 28pp.

Lynn, D. G. and S. C. Meredith. 2000. Review: model peptides and the physicochemical approach to β-amyloids. *J. Struct. Biol.* **130:** 153-173.

Malonga, H., J. F. Neault, H. Arakawa, and H. A. Tajmir-Riahi. 2006. DNA interaction with human serum albumin studied by affinity capillary electrophoresis and FTIR spectroscopy. *DNA Cell Biol.* **25:** 63-68.

Michel, S. L., A. L. Guerrerio, and J. M. Berg. 2003. Selective RNA binding by a single CCCH zinc-binding domain from Nup475 (Tristetraprolin). *Biochemistry* **42:** 4626-4630.

Nagaich A. K., V. B. Zhurkin, H. Sakamoto, A. A. Gorin, G. M. Clore, A. M. Gronenborn, E. Appella, and R. E. Harrington. 1997. Architectural accommodation in the complex of four p53 DNA binding domain peptides with the p21/waf1/cip1 DNA response element. *J. Biol. Chem.* **272:**14830-14841

Nagai, Y. L. D. Unsworth, S. Koutsopoulos, and S. Zhang. 2006. Slow release of molecules in self - assembling peptide nanofiber scaffold. *J. Control Rel.* **115:** 18-25.

Plank, C., M. X. Tang, A. R. Wolfe, and F. C. Szoka. 1999. Branched cationic peptides for gene delivery: Role of type and number of cationic residues in formation and *in vitro* activity of DNA polyplexes. *Human Gene Ther.* **10:** 319-332.

Plotnikov, V., A. Rochalski, M. Brandts, J. F. Brandts, S. Williston, V. Frasca, and L. Lin. 2004. An autosampling differential scanning calorimeter for study of biomolecular interactions. *Biocalorimetry* **2:** 241-251.

Rochet, J. C., and P. T. Lansbury. 2000. Amyloid fibrillogenesis: themes and variations. *Curr. Opion. Struct. Biol.* **10:** 60-68.

Sauer, R. T. 1991. *Methods in Enzymology, V. 208: Protein-DNA Interactions* .Academic Press, San Diego, California.

Scott, D. J., S. Leejeerajumnean, J. A. Brannigan, R. J. Lewis, A. J. Wilkinson, and J. G. Hoggett. 1999. Quaternary re-arrangement analysed by spectral enhancement: the interaction of a sporulation repressor with its antagonist. *J. Mol. Biol.* **293:** 997-1004

Seimiya, M., and Y. Kurosawa. 1996. Kinetics of binding of Antp homeodomain to DNA analyzed by measurements of surface plasmon resonance. *FEBS Lett.* **398:** 279-284.

Simeoni, F., M. C. Morris, F. Heitz, and G. Divita. 2003. Insight into the mechanism of the peptide-based gene delivery system MPG: implications for delivery of siRNA into Mammalian Cells. *Nucl. Acids Res.* **31:** 2717-2724.

Singh M, L. D'Silva, and T. A. Holak. 2006. DNA-binding properties of the recombinant high-mobility-group-like AT-hook-containing region from human BRG1 protein. *Biol. Chem.* **387:** 1469-1478.

Sitohy, M., J. M. Chobert, M. Schmidt, A. Gozdzicka-Jozefiak, and T. Haertle. 2001. Interactions between esterified whey proteins (alpha-lactalbumin and beta-lactoglobulin) and DNA studied by differential spectroscopy. *J. Protein Chem.* **20:** 633-640.

Smith, L. C., J. Duguid, M. Wadhwa, M. J. Logan, C. H. Tung, V. Edwards, J. T. Sparrow. 1998. Synthetic peptide-based DNA complexes for nonviral gene delivery. *Adv. Drug Deliv. Rev.* **30:** 115-131.

Stierle, V., J. Couprie, C. Ostlund, I. Krimm, S. Zinn-Justin, P. Hossenlopp, H. J. Worman, J. C. Courvalin, and I. Duband-Goulet. 2003. The carboxyl-terminal region common to lamins A and C contains a DNA binding domain. *Biochemistry* **42:** 4819- 4828.

Yang, H., M. Pritzker, S. Y. Fung, Y. Sheng, W. Wang, and P. Chen. 2006b. Anion Effect on the Nanostructure of a Metal Ion Binding Self-Assembling Peptide. *Langmuir* **22:** 8553-8562.

Zhang, S., T. Holmes, C. Lockshin, and A. Rich. 1993. Spontaneous assembly of a self-complementary oligopeptide to form a stable macroscopic membrane. *Proc. Natl. Acad. Sci. USA* **90:** 3334-3338.

Zhang, S., T. C. Holmes, M. Dipersio, R. O. Hynes, X. Su, and A. Rich. 1995. Self-complementary Oligopeptide Matrices Support Mammalian Cell Attachment. *Biomaterials* **16:** 1385-1393.

Zhang, S. 2002. Emerging biological materials through molecular self-assembly. *Biotechnol. Adv.* **20:** 321-339.

Chapter 2
Literature Review

2.1 Self-assembling Peptide Systems

Synthetic self-assembling peptides are derived from segments of naturally occurring proteins or through molecular design. Their common feature is the capability of self-assembling in aqueous solution. Self-assembling peptides have recently emerged as one of the most promising biological materials because they can be designed and engineered to provide a broad range of applications, including modeling for fibrillogenesis, scaffolding for tissue repair and tissue engineering, drug delivery of molecular medicine and fabrication of nanowires (Zhang, 2002; Chen, 2005). Molecular self-assembly relies on chemical complementarity and structural compatibility. These fundamentals are key to the design of the molecular units required for the fabrication of functional macrostructures, which in turn permit the application of molecular self-assembly in bio-nanotechnology. A number of self-assembling peptides have been designed and developed (Table 2.1).

2.1.1 Ionic-complementary Peptides

Among the new self-assembling peptides is a class of ionic-complementary peptides, e.g., EAK made of glutamic acid (E), alanine (A), and lysine (K) residues, discovered from a Z-DNA binding protein in yeast a decade ago by Shuguang Zhang (Zhang, *et al*., 1993). Analysis of the Z-DNA binding protein revealed an unusual 16-amino-acid sequence with repetitive polar and nonpolar residues, EAK16. The observation that this short peptide formed a membrane-like structure when added into cell cultures led to the strategy of using small peptides to construct functional supramolecules. Detailed investigation into this peptide indicated that its ionic-complementarity might play an important role in its unusually stable self-assembly. This class of biological materials has shown considerable potential for a number of applications in bionanotechnology (Zhang, 2002; Chen, 2005).

Table 2.1. The family of self-assembling peptide

Name	Charge distribution sequence (n→c)	Type	Structure
DN1	+−: n-QQRFQWQFEQQ-c	I	α/β
DN1-QF	+−: n-QQRFQFQWQFEQQ-c	I	α/β
DN1-2E	+−: n-QQRFEWEFEQQ-c	N/A	α/β
DN1-3O	+−: n-QQOFOWOFQQQ-c	N/A	α/β
A_6D	−: n-AAAAAAD-c	N/A	N/A
V_6D	−: n-VVVVVVD-c	N/A	N/A
RAD16-I	+−+−+−+−: n-RADARADARADARADA-c	I	β
RAD16-II	++−−++−−: n-RARADADARARADADA-c	II	β
RAD16-IV	++++−−−−: n-RARARARADADADADA-c	IV	β
DAR16-IV	−−−−++++: n-ADADADADARARARAR-c	IV	α/β
DAR16-IV^T	−−−−++++: n-DADADADARARARARA-c	IV	α/β
DAR32-IV	−−−−++++: n-$(ADADADADARARARAR)_2$-c	IV	α/β
RADA8-I	+−+−: n-RADARADA-c	I	r.c
RAD8-II	++−−: n-RARADADA-c	II	r.c
RGDA16-I	+−+−+−+−: n-RADARGDARADARGDA-c	I	r.c
RAEA16-I	+−+−+−+−: n-RAEARAEARAEARAEA-c	I	β
RAEA8-I	+−+−: n-RAEARAEA-c	I	r.c
KADA16-I	+−+−+−+−: n-KADAKADAKADAKADA-c	I	β
KADA8-I	+−+−: n-KADAKADA-c	I	r.c
EAH8-II	−−++: n-AEAEAHAH-c	II	r.c
EFK16-II	−−++−−++: n-FEFEFKFKFEFEFKFK-c	II	β
EFK12-I	−+−+−+: n-FEFKFEFKFEFK-c	I	β
EFK8-I	−+−+: n-FEFKFEFK-c	I	β
ELK16-II	−−++−−++: n-LELELKLKLELELKLK-c	II	β
ELK8-II	−−++: n-LELELKLK-c	II	β
EAKA16-I	+−+−+−+−: n-AEAKAEAKAEAKAEAK-c	I	β
EAKA8-I	−+−+: n-AEAKAEAK-c	I	r.c
EAK16-II	−−++−−++: n-AEAEAKAKAEAEAKAK-c	II	β
EAK12-a	++−−++: n-AKAKAEAEAKAK-c	II	r.c
EAK12-b	+−−++: n-AKASAEAEAKAK-c	N/A	r.c
EAK12-c	+−−−++: n-AKAEAEAEAKAK-c	N/A	r.c
EAK12-d	−−−−++: n-AEAEAEAEAKAK-c	IV/II	α/β
EAK8-II	−−++: n-AEAEAKAK-c	II	r.c
KAE16-IV	++++−−−−: n-KAKAKAKAEAEAEAEA-c	IV	β
EAK16-IV	−−−−++++: n-AEAEAEAEAKAKAKAK-c	IV	β
KLD12-I	+−+−+−: n-KLDLKLDLKLDL-c	I	β
RADSC-14	+−+−: n-RADSRADSAAAAAC-c	I	N/A
RADSC-16	+−+−+−: n-RADSRADSRADSAAAC-c	I	N/A

β: β-sheet; α: α-helix; r.c.: random coil; N/A: not applicable. Modified from Refs (Zhang, 2002; Chen, 2005).

Ionic-complementary peptides are characterized by an alternating hydrophobic and hydrophilic amino acid residue. These peptides have been classified into several types. The classification is based on the hydrophilic surfaces of the molecules, which have alternating positively

and negatively charged amino acids alternating by one residue, two residues, and three residues and so on. The most simple and widely studied charge distribution of peptides are − + − + − + − +, − − + + − − + +, and − − − − + + + + referred to as type I, type II, and type IV, respectively. These charge distributions can be repeated, or the orientation of these charges can be reversed to yield entirely different molecules. These well-defined sequences allow the peptides to undergo self-assembly because of their amphiphilicity and ordered charged residues. Self-assembly is driven by electrostatic interactions, hydrogen bonds, and/or van der Waals' forces. Studies of a broad range of peptides have shown the importance of ionic complementarity in their self-assembly and applications in bionanotechnology.

Hecht and his group performed a well controlled experiment using ionic-complementary peptides to understand the relationship between secondary structure and molecular structure (Xiong, *et al*., 1995). They designed four peptides: two of them made of L, E, and K residues possessed α-helical intrinsic propensities, and the other two made of I, D, and R had non-α-helical intrinsic propensities. The two peptides with the same intrinsic propensities have different charge distributions: α-helical periodicity (− − + + − − + +) and β-strand periodicity (− + − +). With this design, they were able to determine that the secondary structure is dominated by periodicity, if the periodicity is different from the intrinsic propensity. This demonstrates the importance of charge distribution in determining the secondary structure of peptides. However, this is not always the case. An ionic-complementary peptide EAK16 discovered in 1993 showed that the secondary structure detected was entirely different from that predicted by computer simulation (Pennisi, 1993). This surprising observation may be due to the unique molecular structure of this particular peptide. EAK16 is an amphiphilic peptide containing alternative hydrophobic and hydrophilic amino acid residues (Figure 2.1). Different from the surfactant-like molecules, EAK16 self-assembles into β-sheets conformation (Figure 2.2) and further forms stable membrane-like structures upon addition of salts to the solution. The amphiphilic character together with the ionic complementarity contributes to the stable macrostructure formation. The resulting membranes can withstand high temperatures of up to 90 °C for more than 4 h in 1 % sodium dodecyl sulfate (SDS) solution. They are also resistant to digestion with several proteases, including trypsin, α-chymotrypsin, papain, and protease K.

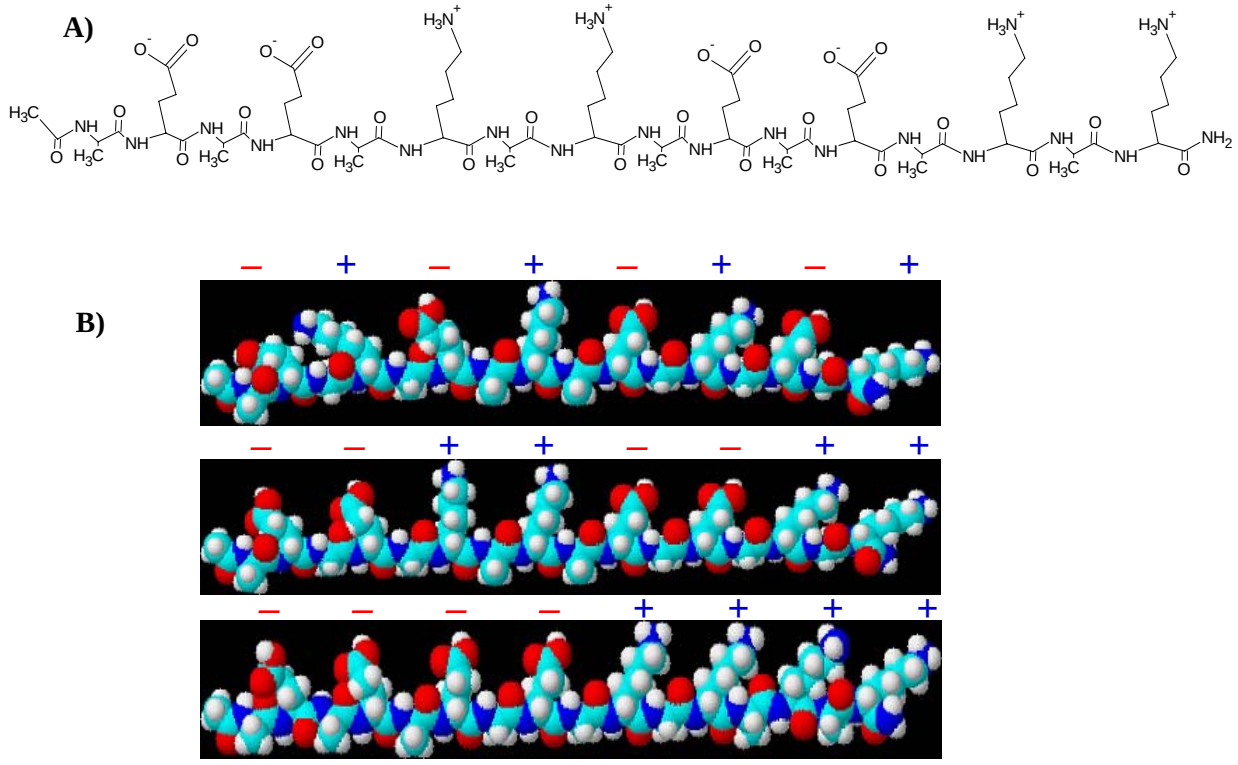

Figure 2.1. (A) Chemical structure of an ionic-complementary self-assembling peptide-EAK16-II. It contains alternating hydrophobic (A) and hydrophilic (E and K) residues, which generates a unique amphiphilic structure with a hydrophobic region on one side and a hydrophilic one on the other. The charged residues are arranged in a fashion as type II, where pairs of negatively (E) and positively (K) charged side chains alternate in sequence. (B) The 3-D molecular model of EAK16s. The top, middle, and bottom scheme represent the molecular structures of EAK16-I, EAK16-II, and EAK16-IV, respectively. The length of the backbone of EAK16s is around 7 nm while the width ranges from 0.3 to 0.7 nm (image generated from ACD/3D freeware, Toronto, Ont., Canada) (Chen, 2005).

There are several important features of ionic-complementary peptides. First, their charge distribution can be altered through simple molecular design, resulting in several types of peptides, such as the I, II and IV-types. Figure 2.1 shows the results of a sequence design based on the same components (E, A, and K), which generate EAK16-I, EAK16-II, and EAK16-IV. The design of the charge distribution has an impact on the secondary structure and self-assembly.

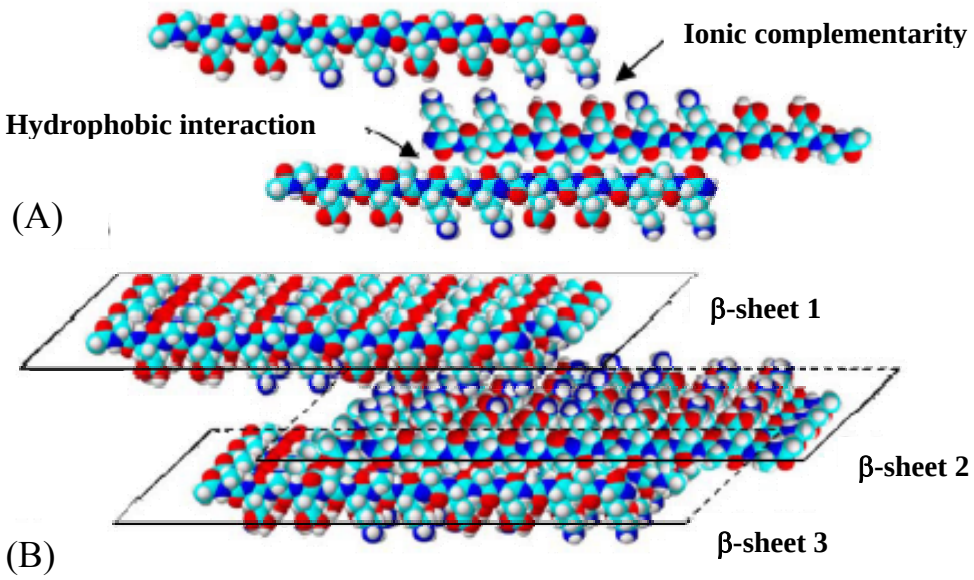

Figure 2.2. (A) A scheme of EAK16-II self-assembly through hydrophobic interaction and ionic-complementarity. Electrostatic interactions together with hydrogen bonds and hydrophobic interactions drive peptides to form stable β-sheets. (B) A proposed model of EAK16-II self-assembly into β-sheet-based aggregates. The peptides are proposed to self-assemble in an antiparallel fashion to favor the minimum energy state. In fact, some evidence has shown that EAK16-I and -II have a high frequency peak from Fourier-transform infrared (FTIR) measurements, which implies the antiparallel β-sheet formation (Chen, 2005).

A second important feature is the ease with which the ionic-complementary peptide family can be expanded with the same charge distribution using different amino acids. For instance, the positively and negatively charged residues of EAK16 can be substituted with positively and negatively charged R and D while maintaining the ability to self-assemble into macroscopic materials. DAR is such a self-assembling peptide. However, if the positively charged residues, K and R, were replaced by negatively charged residues, E and D, the peptide would not be able to self-assemble and form macroscopic materials, although β-sheet structures have been observed in the presence of salt. If the A is changed to a more hydrophobic residue, such as L, I, F or W, the molecule will have a greater tendency to self-assemble.

A third feature particularly important for the class of ionic-complementary peptides discovered by Zhang *et al*. is that a minimum number of amino acids are required in order to have the ionic self-complementarity. For example, the minimum number of amino acids required to build aggregates with type IV peptides is sixteen, while the creation of type I and type II peptidic

aggregates requires four and eight amino acids, respectively. The sequence of these short peptides can also be applied in the construction of polypeptides such as poly-EAK (Goeden-Wood, *et al*., 2003).

Since ionic-complementarity plays an important role in determining the stable conformation of a peptide through electrostatic interactions, the change of charge status of amino acids in the peptides obtained by changing pH is anticipated to affect their self-assembly. Such pH effect was observed by Aggeli *et al*. in the study of the DN1 peptide (QQRFQWQFEQQ) (Aggeli, *et al*., 2003). This peptide formed a stable gel at a pH less than 5. At pH above 5, the fibrils were observed to flocculate, rendering the gel unstable. At this pH, both E and R were charged, making the peptides stack together in various ways, which led to amorphous aggregates. This study suggests an effective method of controlling the macroscopic properties of the aggregates of self-assembling peptides by changing the pH of the solution. This method would prove useful for the encapsulation and controlled release of biologically important molecules from the peptide gels.

The pH-dependence of nanostructure formation reported by Hong *et al*. using the EAK16-II and EAK16-IV peptides did not match the above expectation (Hong, *et al*., 2003). EAK16-II formed fibrillar assemblies regardless of pH values. EAK16-IV formed globular assemblies only at near neutral pH conditions (pH 6.5-7.5). When prepared above pH 7.5 or below pH 6.5, EAK16-IV formed fibrillar assemblies, whose structures were indistinguishable from the fibrils formed by EAK16-II.

Concentration is another parameter affecting peptide self-assembly. The concentration dependence of peptide self-assembly is expected to resemble that of surfactants. Atomic force microscopy (AFM) studies revealed that EAK16-II or Aβ peptide formed isolated filaments and globules even at concentrations below the critical aggregation concentration (CAC) (Walsh, *et al*., 1999; Fung, *et al*., 2003; Hong, *et al*., 2004 & 2005). The isolated structures are referred to as protofibrils, which are formed prior to the self-assembly of larger fibrils. The observation of protofibrils at concentrations below the CAC seems to contradict the micellization theory. Surfactants are only present as monomers when the concentration is below the critical micelle concentration (CMC). The difference may be explained with a nucleation mechanism: the nuclei are formed either through the peptide itself at the concentrations above the CAC, or by the impurities present as "seeds" at the concentrations below the CAC.

2.1.2 Lipid-like Self-assembling Peptides

A class of short lipid-like amphiphilic peptides (peptide detergents) can self-assemble into nanotubes or nanovesicles, which can stabilize membrane proteins outside their natural cell membrane milieu, incorporate segments of homopolymeric, natural amino acids, or serve as template for fabrication of

nanowires. Each peptide in this class has a tail consisting of consecutive hydrophobic amino acids and a polar head consisting of one or two charged residues.

. Although a variety of detergents and lipids as surfactants have been used to stabilize and crystallize membrane proteins for several decades, they are still unable to significantly maintain structural stability of membrane proteins during experimental handling. New types of surfactants are needed, such as A_6D (AAAAAAD) and V_6D (VVVVVVD). These peptides were able to stabilize the photosystem complexes and glycerol-3-phosphate dehydrogenase in solid-state devices (Yang and Zhang, 2006). This new type of peptide detergents was very effective in stabilizing membrane proteins and maintaining their functions, providing a powerful tool for membrane proteins research and application (Yang and Zhang, 2006).

2.2 Applications of Self-assembling Peptides

2.2.1 Drug Delivery

Rapid progress in genomics and proteomics has generated a large number of novel drugs, which have been designed to act against specific targets in the body. However, these drugs have experienced only limited success in clinical studies, due to low solubility, poor stability, low cellular uptake across plasma membrane, or lack of specific targeting (Anderson, 1998; Gorecki and MacDermot, 1997). Thus, effective drug delivery vehicles are being researched to make new therapies available for clinical use. Viral vectors and cationic polymers, lipids, polypeptides, and proteins have been the predominant drug delivery carriers (Selvam, *et al*., 2006; Pietersz, *et al*., 2006; Torchilin, 2005; Jones, *et al*., 2006). To date, there has been little lasting impact in the clinical practice of medicine conferred by these delivery systems.

Peptide-mediated drug delivery agents are emerging as alternatives since they possess the safety of nonviral systems and preserve some ideal cell penetration characteristics of viral systems. Peptides are a fundamental component of all living cells and of many substances that are necessary for the proper functioning of an organism, such as enzymes, hormones, and antibodies. Self-assembling peptides spontaneously form nanostructures, which have shown potential in encapsulation of a broad range of therapeutic agents from hydrophilic gene therapeutics to hydrophobic chemotherapeutics. The main attraction for these peptides is their versatility. They can be easily synthesized and tailored to exhibit the desired encapsulation and cell penetration properties.

A self-assembling peptide RAD16-II (Davis, *et al*., 2006) has been used to prolong delivery of insulin-like growth factor 1 (IGF-1), a cardiomyocyte growth and differentiation factor, to the myocardium, using a "biotin sandwich" approach. Biotinylated IGF-1 was complexed with tetravalent

streptavidin and then bound to biotinylated self-assembling peptides. This biotin sandwich strategy allowed binding of IGF-1 but did not prevent self-assembly of the peptides into nanofibers within the myocardium. After injection into rat myocardium, biotinylated nanofibers provided sustained IGF-1 delivery for 28 days, and targeted delivery of IGF-1 in vivo increased activation of protein kinase B in the myocardium.

Recently, this peptide has also been used to deliver platelet-derived growth factor (PDGF)-BB into myocardium by the same group. Intramyocardial delivery of PDGF by RAD16-II nanofibers leads to long-term improvement of the cardiac performance after experimental infarction without apparent pulmonary toxicity. Local myocardial protection may allow prevention of heart failure without systemic toxicity (Hsieh, *et al*., 2006; Lee and Hsieh, 2006).

EAK16-II has been successfully used to stabilize pyrene microcrystals in aqueous solution, up to ten-thousand times beyond its solubility limit in water of 7×10^{-7} M, and unload molecular pyrene into a cell membrane mimic, egg phosphatidycholine (EPC) vesicle, in a controlled manner. The complete transfer of pyrene crystals occurred within a few hours (Keyes-Bag, *et al*., 2004).

The biological hydrogels formed from the self-assembly of RAD16-I are promising materials for various controlled molecular release applications (Nagai, *et al*., 2006). The diffusion properties of dyes, such as bromophenol blue, 8-hydroxypyrene-1,3,6-trisulfonic acid trisodium salt and 1,3,6,8-pyrenetetrasulfonic acid tetrasodium salt, and Coomassie Brilliant Blue G-250, through RADA16 hydrogels have been reported. The apparent diffusivities of the dyes decreased with increasing peptide concentration, providing an alternate route of controlling release kinetics. In addition, strong electrostatic interactions between nanofiber and promophenol blue result in no release from the hydrogels, suggesting the release profiles can be tailored through controlling the nanofiber-diffusant interactions at the molecular level.

Controlled delivery of drugs in response to environments has the potential of targeting therapies and personalized treatments. Two self-assembling peptide motifs KLD12-I, which adopt stable β-sheet structures spontaneously in aqueous solution induced by the repetition of alternating ionic hydrophilic and hydrophobic amino acids, were linked with a peptide sequence SGRSANA which is specifically cleaved by a disease-associated protease (Law, *et al*., 2006). In aqueous solution, this peptide self-assembles as a gel scaffold, where drugs are encapsulated. Upon treatment of this peptide solution with the appropriate protease, the matrix can be degraded in a controlled fashion, where the degradation rate is fine-tuned by varying the peptide composition and the release therapeutic payloads.

Self-assembling peptide DN1 and its derivatives have been found to form β-barrel channels that are incorporated in the lipid bilayers of vesicles loaded with an active ingredient (Agelli, *et al*.,

2003). This active compound can be a small biological molecule, a protein, or DNA. If these molecules can not penetrate the lipid bilayer, then the β-barrels are the only means of release of the active compound outside the vesicle. Thus the β-barrel in this case acts as a component of a formulation of slow or sustained release of an active compound. On a particular note, the self-assembly of the monomeric peptide into β-barrel aggregates can be triggered in response to changes in the pH of the aqueous solution.

A series of surfactant peptides made of a hydrophobic tail attached to a polar head group consisting of one or two positively charged residues at the *C*- or *N*-terminus have been shown to self-assemble in aqueous solution to produce nanovesicles or nanotubes (Zhang and Zhao, 2004; Guler, *et al*., 2005). One example is the hydrophilic, bioactive peptide RGDS covalently linked to a cholesterol hydrophobic moiety (Chol-AAAAGGGKRGDS), which is able to encapsulate a hydrophobic molecule during self-assembly into cylindrical nanostructures (Guler, *et al*., 2005). This encapsulation can stabilize hydrophobic cargoes such as pyrene in the core of these nanostructures. These supramolecular systems could be used to combine encapsulation of hydrophobic drugs with presentation of bioactive epitopes for targeted drug delivery since the RGD peptide is also known to bind to integrins that are more highly expressed in blood vessels of human tumors (Arap, *et al*., 1998). Another group of surfactant self-assembling peptides was created by Shugang Zhang and his coworker (Zhang and Zhao, 2004). By choosing and linking specific sequences of amino acids, they generated short peptides with a positively charged end made of the amino acids lysine or histidine, such as LLLLLLKK. When placed in a solution of DNA, the positively charged peptides self-assembled into nano-capsules and tubes, encapsulating the negatively charged DNA. This “minivan” was then able to deliver the DNA to at least some cells growing on laboratory plates as the minivan surface can be tagged with a receptor that is specific to a particular cell (Gorman, 2003).

In summary, self-assembling peptides combine a large loading capacity with cell targeting/penetrating abilities designed atn the molecular level to form a versatile drug construct. The ability to optimize the balance between hydrophilic and hydrophobic peptide residues to enhance the loading and release capacity should make these peptides effective biocompatible carriers in gene therapy and chemotherapy.

2.2.2 Model for Studying Amyloid Fibrillogenesis

The structural transition of amyloid disease-related proteins such as prion proteins from α-helix to insoluble and cytotoxic β-sheet amyloid fibrils plays a key role in a variety of fatal diseases known as Alzheimer's and prion diseases (Watson, *et al*., 2005). The amyloid fibril is a misfolded and undesirable state for proteins and its formation may block cell-to-cell communications and damage

neuronal pathways. It is necessary to study the nature of the proteins in such critical diseases in order to clarify the folding pathway of proteins. Many fibrous peptides and proteins including both natural and designed amyloid and fibrous peptides have been investigated to provide useful information for constructing and manipulating peptide conformations. Notable examples include islet amyloid polypeptide (IAPP) from endocrine hormones, tansthyretin (TTR) from transport molecules, and Aβ and prion protein from the nervous system (Kowalewski and Hotzman, 1999; Walsh, *et al*., 1999; Sipe and Cohen, 2000; Kundu, *et al*., 2003).

There are similarities between the self-assembly process of self-assembling peptides and amyloid fibrils. First, self-assembling peptides produce fibrillar nanostructures similar to those formed from a typical amyloid peptide Aβ. Second, some self-assembling peptides can undergo conformational transitions identical to amyloid peptides. Third, both self-assembly processes follow the nucleation and growth mechanism. Fibril formation is triggered above a critical concentration. (Fung, *et al*., 2003; Hong, *et al*., 2004 & 2005). Finally, the protofibrils play an important role in both self-assembly processes. Therefore, self-assembling peptides can be a good model for understanding amyloid fibril formation.

The ionic self-complementary peptide KTEAETKTEAKVDAKADVE, derived from the C-domain of *Arabidopsis thaliana* copper metallochaperone (CCH), adopts an extended conformation in solution with a high content of β-sheet structure that induces a pH-dependent fibril formation. Freeze drying electron microscopy reveals the existence of well ordered amyloid-like fibrils in the solutions of this peptide (Mira, *et al*., 2004).

Mihara and his group have designed a class of self-assembling peptides that undergo a self-initiated and spontaneous α–helix-to-β–sheet (α-to-β) transition and self-assemble into amyloid fibrils in a neutral aqueous solution (Takahashi, *et al*., 1999a & 2000). A series of these peptides are composed of two amphiphilic α-helices with double-heptad repeats $(ALEQKLA)_2$. The two peptide chains are linked by a disulfide bond between Cys residues at the C-terminus. A 1-adamantanecarbonyl (Ad) group as a hydrophobic domain is attached to the N-terminus of the peptide. The peptide initially shows an α-helix structure that gradually changes to β-structure in a neutral aqueous solution, whereupon the Ad group causes intermolecular peptide association through hydrophobic interactions. This structural transition results in amyloid fibril formation, which seems to follow a nucleation process and a subsequent autocatalytic transition reaction. The α-to-β transition was studied under different conditions including peptide concentration, temperature, pH, solvent, salt, and detergent by Mihara *et al*. Increases of peptide concentration or temperature enhance the α-to-β conformation transition. The highest transition rate is observed at neutral pH. The addition of

organic solvents and salts can retard and even inhibit the transition. Both cationic and anionic detergents similarly retard or inhibit the structural transition in a concentration-dependent manner. Furthermore, hydrophobic domains generated by these peptides seem to create the same conformational defects that may form unstable α-helices in the aggregates. When a critical amount of α-helices accumulate in the aggregates, they give rise to long-range (intermolecular) interactions and the peptide undergoes an α-to-β transition in an autocatalytic manner. It has been shown that the hydrophobicity of the peptide affects the stability of the intermediate α-helical aggregates, which controls the α-to-β transition. The same group has also found that the ionic complementarity is important for amyloid fibril assembly (Takahashi, *et al*., 1999b & 2002; Mihara, *et al*., 2005).

The study of the self-assembly mechanism of amyloid may lead to a treatment for conformational diseases. Since amyloid fibril formation has been characterized as pathogenic, the major strategy for treatment of conformational diseases is to inhibit the amyloid fibril formation. This can be achieved by inhibiting various pathways to amyloid fibril assembly. For example, adding small inhibitors or adjusting physiological condition has been found to affect amyloid fibril formations (Yang, *et al*., 1999). Some researchers focus on intermediate α-helix aggregates, which may be the major cause of cellular toxicity. It is found that when the amino acids controlling the kinetics of intermediate formation are replaced, fibrillogenesis kinetics is significantly altered (Kirkitadze, *et al*., 2001).

2.2.3 Tissue Engineering

Advanced tissue engineering requires biocompatible materials that serve as substrates for cell growth, differentiation and biological function. Self-assembling peptides are being developed as biomaterials for creating cartilage, blood vessels, and other tissues, or as substrates for nerve cell growth and synapse formation, immobilized peptides, and proteins (Holmes, 2002). A major benefit of synthetic materials is that they minimize the risk of biological contamination. Self-assembling peptides also frequently show favourable properties concerning biocompatibility, immunogenicity and biodegradability, producing non-toxic waste products.

One of these peptides, EAK16-II, has been found to be nontoxic; it has no effect on the growth-rate of nerve growth factor-differentiated rat PC-12 cells when added into the cell culture medium (Zhang, *et al*., 1993). Meanwhile, two ionic-complementary peptides, EAK16-II and RAD16-II, have been reported to form matrices that support mammalian cell attachment (Zhang, *et al*., 1995). The cells that attached to a peptide-coated substrate exhibited a flat, spread morphology, similar to the morphology that was observed when the cells attached to a fibronectin-coated substrate. In contrast, the same cells retain a round shape and do not spread on the malleable RAD16-II

membranes. The cells remained well attached, even after transferring the membrane to a fresh culture well.

The RAD16-I nanofiber scaffold creates a permissive environment for axons not only to regenerate through the site of an acute injury but also to knit the brain tissue together. The regenerated axons reconnect to target tissues with sufficient density to promote functional return of vision, as evidenced by the fact that the presence of sunflower seeds in the binding site can induce response from treated rates (Ellis-Behnke, 2006). RAD16-II scaffolds are able to establish a three-dimensional environment for *in vitro* promotion of angiogenesis (Narmoneva, *et al*., 2005).

In summary, self-assembling peptides may be promising scaffolding materials in tissue engineering applications such as neurite outgrowth, cartilage repair, and responsive gel formation. Not only are these peptide matrices highly biocompatible and biodegradable, they also possess diverse biological functionalities. Ease of molecular design and engineering will make these small peptides smart biological materials for future tissue engineering.

2.2.4 Fabrication of Nanowires

The design and fabrication of complex nanostructures with specific geometry and composition is one of the main challenges of nanotechnology. In the computing industry, the fabrication of nanowires using the "top-down" approach faces tremendous challenges. Thus, the possibility of fabricating conducting nanowires by molecular means using self-assembled nanotubes is of particular interest to the electronics industry. One can readily envision that nanotubes might serve as templates for metallization. Once the template has been removed, a pure conducting wire is left behind and immobilized on a surface.

Self-assembling peptide, such as A_6D and V_6D, mimic the structure of phospholipids with the D polar head group and the A_6 or V_6 apolar tail. They have been shown to form nanotubes readily (Yang and Zhang, 2006). These nanotubes have the potential to act as templates for the formation of nanowires. Furthermore, the nanotubes may be useful as an encapsulating vesicle for drug delivery. Chemical modification of the peptide monomer may expand the function of these structures. For example, a specific cell-surface ligand can be directly incorporated into a vesicle for targeted delivery of insoluble drugs to particular cells (Zhao and Zhang, 2006).

A Phe-Phe dipeptide, the Alzheimer's β-amyloid diphenylalanine structural motif, has been applied to construct nanowires (Reches and Gazit, 2003). This dipeptide can self-assemble into discrete and stable nanotubes. The resulting nanotubes were added to boiling ionic silver solution, and the silver within the nanotubes was reduced with citric acid. The peptide in the nanotube was

degraded by a proteinase K enzyme to reveal discrete nanowires with a long persistence length. The procedure is shown in Figure 2.3.

Based on the understanding of the peptide nanotube assembly process, the same group recently designed a method for surface decoration of the peptide nanotube to form a tri-layered (silver-peptide-gold) coaxial nanowire (Carny, *et al*., 2006). After peptide nanotubes were self-assembled from the FF dipeptide, a linker peptide, whose sequence was CFF, FFC or CGSGFF, was added. These linker peptides contained a FF motif, which can interact with the peptide nanotube surface, and a cysteine residue, which provided the reactive thiol group for binding to gold. Gold particles were found to bind evenly on the surface of the nanotubes.

These early studies suggest that the construction of nanostructures using self-assembling peptides as templates may become an alternative to the more conventional methods used currently in nanotechnology.

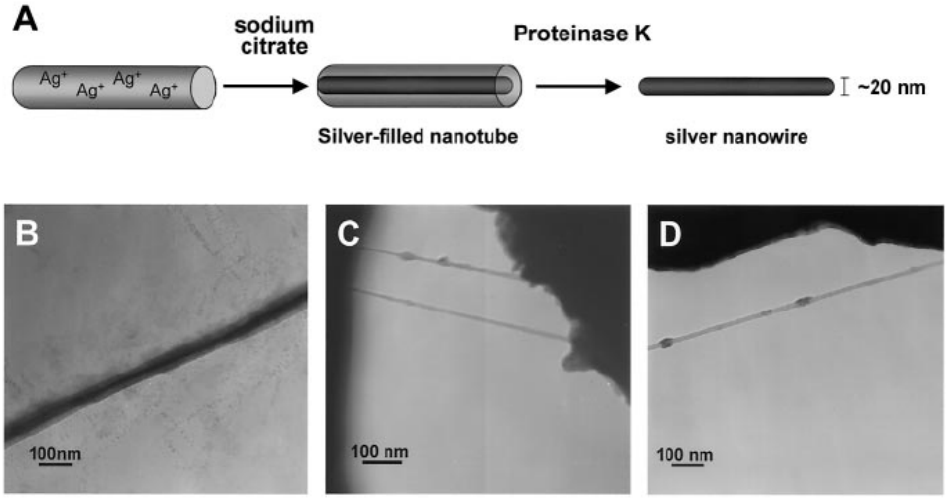

Figure 2.3. The process of nanowire fabrication.

2.3 Protein-DNA Interactions and Characterization Techniques

Although binding of self-assembling peptides to oligonucleotides has not been reported, protein-DNA interactions have been widely studied to understand basic cellular processes including DNA metabolism and gene expression. Most protein-DNA interactions in these processes are specific, which have been examined to identify the binding sites on the DNA or on the protein surface facing the DNA by techniques like filter binding, gel retardation, footprinting, and southwestern blotting (Moss, 2001). In contrast, most single-stranded DNA-binding proteins (SSBs) bind non-specifically to single-stranded DNA (ssDNA), such as *Eco*SSB, gp32 of T4 bacteriophage, *Taq*SSB, *Tth*SSB, and replication protein A (RPA) in eukaryotes (Kur, *et al*., 2005). These non-specific interactions have

been studied quantitatively using techniques that monitor changes in the biological or physicochemical properties resulting from the formation of complexes (Bujalowski and Lohman, 1987). In most instances, these techniques are gel mobility shift assay (Morii, *et al*., 1996; Stierle, *et al*., 2003), filter binding assay (Agou, *et al*., 1999), boundary sedimentation velocity (Galletto, *et al*., 2003), surface plasmon resonance (Seimiya and Kurosawa, 1996), UV difference spectra (Boraston, *et al*., 2000), and fluorescence assay (Michel, *et al*., 2003; Endoh, *et al*., 2005). Except boundary sedimentation velocity and UV difference spectra, all these methods require labeling of the ligand with a chromophore or radioactive isotope, or covalent immobilization of the ligand. Other characterization approaches, such as differential scanning calorimetry (Singh, *et al*., 2006) and isothermal titration calorimetry (Plotnikov, *et al*., 2004), directly measure the heat evolved in the binding to estimate the forces stabilizing a given complex. Structures or morphologies of protein-DNA complexes can be obtained by X-ray crystallography and nuclear magnetic resonance (NMR) at atomic resolution for small complexes. Large multiprotein complexes, beyond the scope of these two techniques, are generally examined by electron microscopy and atomic force microscopy (Dodson and Echols, 1991).

The focus of this review is the applications of these techniques which were used in this thesis to study the nonspecific interactions of proteins or cationic peptides with nucleic acids or oligonucleotide.

2.3.1 Electrophoresis Mobility Shift Assay (EMSA)

A gel mobility retardation assay is based on the electrophoretic mobility of a DNA fragment bound to a protein being lower than that of either the DNA fragment or protein alone. This technique typically requires radioactive labeling of the DNA which is used as the probe. The mixture of bound and free species is separated on a polyacrylamide gel, which is subsequently exposed to a radiographic film. The eventual protein/DNA interaction is visualized by the presence of a radiographic band on the film.

This method has been used to identify DNA sequences that were bound specifically by the sunflower homeodomain leucine-zipper protein Hahb-4 (Palena, *et al*., 1999). Binding analysis suggests that Hahb-4 preferentially binds the dyad-symmetrical sequence CAAT(A/T)ATTG. A prerequisite to such a DNA binding ability is that Hahb-4 forms a dimer as implied by the non-hyperbolic plot of the percentage of DNA bound as a function of protein concentration. This specific interaction had a dissociation constant (K_d) of 1.31×10^{-14} M^2, which was increased 2-4 folds when the nucleotides at positions 1, 5, or 9 of the dyad-symmetrical sequence were replaced. The removal

of the leucine zipper also promoted a decrease in specificity and an increase in dissociation constant ($K_d = 5.03 \times 10^{-5}$ M) due to the absence of dimer formation.

This method has also been used to study the binding of peptides to nucleic acids. The gel retardation analysis revealed that a synthetic 73-residue peptide from human Tristetraprolin (TTP) bound to the tumor necrosis factor (TNF) AU-rich elements (AREs) with a TTP-RNA dissociation constant of 10 nM (Blackshear, *et al*., 2003). The value was comparable with the results obtained from fluorescence anisotropy experiments, another technique used in the same study. The electrostatic interaction between 9-residue (GRKKRRQRRR) or 12-residue (RKKRRQRRRGGC) fragments of the Tat peptide and an 18-mer antisense oligonucleotide against RIα mRNA was also studied by gel retardation analysis (Zhang, *et al*., 2003). The ODNs were completely bound at a Tat/ODN ratio as low as 2:1.

Although traditional gel mobility shift assay is one of the most common methods to study certain macromolecular systems, it may be not suitable for some systems where the species distribution obtained at equilibrium is changed during the experimental procedure. First, there may be dissociation or association of the various species when the sample is loaded in the gel well due to the change in ionic strength from the equilibration buffer to the electrophoresis buffer. Second, there may be dissociation of some complexes during electrophoresis due to the effect of mass action. These concerns have motivated the development of a cryogenic method that would obviate the potential problems associated with labile dissociation or association (Cann, 1989). In this low-temperature gel mobility shift technique, solutions of protein and DNA mixtures at equilibrium are rapidly quenched to -40°C via an ethylene glycol-based carrier medium. The quenched samples are then electrophoresed at -35°C in a polyacrylamide gel matrix. The rapid and sustained drop in temperature results in almost complete stabilization of the equilibrium species distribution. Autoradiogram analysis of the relative abundances for the bound and free DNA sites is carried out over a range of initial binding ratios to yield the binding curve and equilibrium constant as in the usual gel-shift assay. This cryogenic version of the gel-shift method has been successfully used in the λcI repressor-O_R binding study (Bain and Ackers, 1998), for which conventional gel-shift assay has not been feasible due to the instability of the protein/DNA complex at room temperature (Dixon, *et al*., 1991).

Another approach developed on the basis of electrophoresis mobility shift assay (EMSA) is capillary electrophoresis with high sensitivity laser-induced-fluorescence (LIF) detection. Capillary electrophoresis (CE) separates analytes on the basis of their mass-to-charge ratio. The key features of the method are the rapid separation and quantification of bound and free DNA in uncoated capillaries with no gel matrices. The effect of the gel matrix on dissociation constant measurements is absent in this method (Glenn and Etzkorn, 1998). CEMSA has the advantages of automation, no radioactivity,

high resolution, on-line detection, and the use of small amounts of samples (Glenn and Etzkorn, 1998). The dissociation constant for GCNK58, a DNA-binding-region of the yeast transcription factor GCN4, binding to the AP1 DNA site, was investigated by CEMSA with LIF detection of fluorescein-labeled DNA (Glenn and Etzkorn, 1998), which was 35 ± 4 nM. The interaction of calf-thymus DNA with human serum albumin (HSA) in aqueous solution under physiological conditions was investigated using CE at constant DNA concentrations of 12.5 mM (phosphate) and various HSA contents 0.04 to 0.3 mM (Malonga, 2006). The results revealed two types of HSA-DNA complexes with a strong and weak binding characteristed by $K_1 = 4.5 \times 10^5\ M^{-1}$ and $K_2 = 6.1 \times 10^4\ M^{-1}$, respectively. The two major binding sites were located at the G-C base pairs and the backbone phosphate groups. The protein-DNA interaction stabilized the HSA secondary structure and a minor alteration of the B-DNA structure was observed, while no major protein conformational changes occurred.

2.3.2 UV Difference Spectroscopy

The protein interaction with the sugar-phosphate backbone of DNA may perturb the base stacking in DNA molecules, allowing the bases to absorb more UV-Vis light energy and resulting in difference in the absorption spectra, which can be used to quantify such binding. In Figure 2.4, The UV absorbance difference between complexed and naked DNA is measured while titrating a fixed amount of DNA with a protein. The UV absorbance difference initially increases when increasing protein concentration and eventually reaches a plateau. The stoichiometry ratio for the binding of the protein to DNA can be easily determined from Figure 2.4B,.

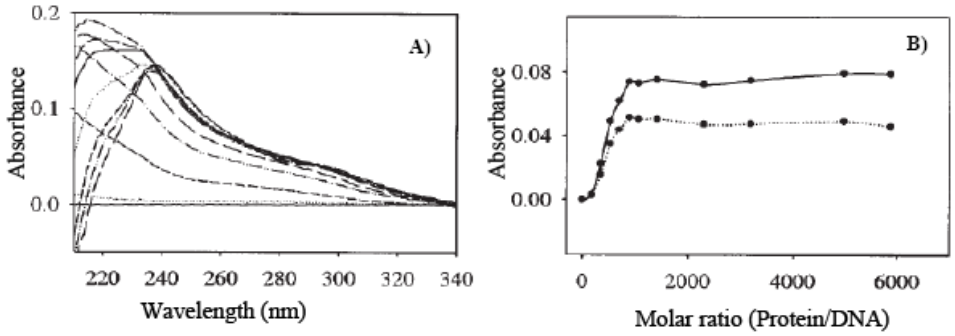

Figure 2.4. (A) UV-Vis differential spectra of DNA interacting with methylated β-lactoglobulin protein. Each successive curve represents the absorption of one accumulative addition of the protein solution to a fixed amount of DNA solution. (B) Plots of absorbance as a function of molar ratio of concentrations of protein to DNA. Solid and dash line refer to absorbance obtained at 260 nm and 280 nm, respectively (Sitohy, *et al*., 2001).

Sitohy *et al.* (2001) applied UV differential spectra to study the binding of esterified or native whey proteins and nucleic acids. Adding native forms of whey proteins to DNA did not produce any difference in the spectra. In contrast, positive differential spectra between 210 and 340 nm were observed after addition of methylated α-lactalbumin proteins corresponding to a molar ratio (MR) of protein/DNA as low as 138 at neutral pH. UV absorption differences increased with increasing MR and leveled off at DNA saturation. The saturation point with methylated α-lactalbumin proteins was reached at a MR of 1100. In contrast, a relatively higher MR of 2750 was required to reach saturation with the ethylated form of the proteins. Lysozyme, a native basic protein, showed a behavior similar to what was observed in the case of the methylated α-lactalbumin but with a relatively lower MR of 700. The amounts of proteins needed to saturate the nucleic acids were found to be much higher than those needed to neutralize it. This phenomenon demonstrated some specific protein-binding sites along the DNA other than the negative charges on the sugar-phosphate DNA backbones. The observation that addition of 0.1 % SDS suppressed completely all spectral differences and the presence of 5 M urea only partially reduced the spectral differences suggested that hydrophobic interactions played an important role. Peptidic hydrolysates of esterified and native proteins or their cationic fractions produced negative differential spectra when mixed with DNA at pH > 7. The negative differences in the UV absorption spectra were most promising in the case of peptidic hydrolysates of methylated derivatives of whey proteins.

2.3.3 Fluorescence Spectroscopy

Changes in the fluorescence emission spectrum of a protein upon binding to DNA are often used to determine the stoichiometry of binding and equilibrium binding constants. In some cases the data can also give an indication of the location of particular residues within the protein with which DNA binds. Similar to CD, titration curves of changes in fluorescence parameters, such as intensity, anisotropy, fluorescence energy transfer, or lifetime, as a function of protein or DNA concentration are normally fitted with binding models to extract the binding parameters. As one of the most sensitive spectroscopic techniques, fluorescence spectroscopy can yield the binding constants of many protein-DNA interactions at low concentrations, typically in the nanomolar to micromolar range. This technique is generally quick and easy to perform. Among different fluorescence techniques, fluorescence anisotropy and steady-state fluorescence are the most commonly used methods (Lakowicz, 1999).

Fluorescence anisotropy was employed to study the binding of ICP8, the major single-stranded DNA (ssDNA) binding protein of the *Herpes simplex* virus type I, to a 5'-fluorescein-labeled

32-mer oligonucleotide (Gourves, *et al*., 2000). The model-free binding isotherms were generated from plots of the fluorescence anisotropy as a function of ICP8 concentration using the binding density function method developed by Lohman and Bujalowski (Bujalowski and Lohman, 1987; Lohman and Bujalowski, 1991). Fitting the binding isotherm with the method of Epstein (Epstein, 1978) revealed that ICP8 formed a nucleoprotein filament on ssDNA with a binding site size of 10 nucleotides/ICP8 monomer, an association constant $K = 0.55 \pm 0.05 \times 10^6\ M^{-1}$, and a cooperativity $\omega = 15 \pm 3$. The equilibrium constant was largely independent of salt concentration. In comparison with other ssDNA-binding proteins, such as phage T4 and gp32, ICP8 bound weakly to ssDNA with low cooperativity. In addition, the reaction product was more stable at high salt concentrations, and fluorescence enhancement of etheno-ssDNA by ICP8 was higher than for other ssDNA binding proteins.

Arosio and his coworkers also used fluorescence anisotropy to study the binding of the Ku heterodimer to DNA with fluorescein attached at the 5'-end (Arosio, *et al*., 2004). The dissociation constant (K_d) for the binding of Ku to a DNA binding site of the proper length (>20 bp) was found to be 22-29 nM at 300 mM NaCl. The binding isotherms for the DNA complexes with heterodimers were analyzed with two independent models, Adair's equation using multiple identical binding sites, that did not overlap, and the McGhee and von Hippel model that considered the presence of overlapping binding sites. The analysis demonstrated that there was no or very weak nearest-neighbor cooperativity among the Ku molecules. These models can most likely be applied to study the interaction of Ku with duplexes of any length. Furthermore, salt dependence studies indicated that electrostatic interactions played a major role in the binding of Ku to DNA. The K_d decreases approximately 60-fold as the salt concentration is lowered from 300 to 200 mM.

The complexation of a synthetic peptide (PGEk) with phosphodiester $d(TTAGGG)_4$ (TMO) and phosphorothioate $Sd(TTAGGG)_4$ (TMS) oligonucleotides was studied by steady-state fluorescence (Besschetnova, *et al*., 2006). The PGEk peptide consisted of 64 amino acids and comprised a hydrophobic domain derived from the human epidermal growth factor (hEGF) as cell targeting moiety and a hydrophilic domain derived from the nuclear localization signal sequence (NLS). The intrinsic fluorescence intensity of PGEk and fluorescence polarization were respectively found to decrease and increase upon PGEk binding to the ODNs. Binding isotherms were examined by Scatchard plot and the stoichiometry of the complexes was found to be three PGEk peptides per one ODN. The binding of the first two PGEk molecules to TMO and TMS occurred noncooperatively with the high association constants K_1(TMO) of $7 \pm 1 \times 10^7\ M^{-1}$ and K_1(TMS) of $3 \pm 0.5 \times 10^7\ M^{-1}$, respectively. The third PGEk molecule bound to TMO cooperatively with a still high association

constant K_2(TMO) of 4.0 ± 1.5 × 10^6 M^{-1}. The third PGEk molecule bound rather weakly to the TMS oligonucleotide with K_2 (TMS) of 8 ± 2 × 10^5 M^{-1}.

The binding of the drug, quinolones, Nal, or Oxo to the polynucleotides under low-salt buffer conditions were determined for poly(dA)·(dT), poly[d(A-T)], poly(dG)·(dC), poly[d(G-C)] and *E. coli* DNA by steady-state fluorescence spectroscopic techniques (Jain and Rajeswari, 2002). The fluorescence data were analyzed using a two step mechanism which involved two different drug-nucleic acid complexes. Complex $[DN]_1$ was formed through nonspecific interaction and the formation of complex $[DN]_2$ involved intercalation of the drug into DNA bases. The order of binding for Nal and Oxo was: poly[d(G-C)] > poly[d(A-T)] > *E. coli* > poly(dG)·(dC) > poly(dA)·(dT). Quinolones bound more avidly to alternating than to block copolymers of dG/dC and dA/dT stretches. Such a two-step process was also identified in the binding of KWGK to a 21-mer duplex of the GC-rich region of the c-myc gene under low-salt conditions using UV-Vis absorption, fluorescence and circular dichroism. The first step was driven by electrostatic interaction only, and the second step by intercalation only. The resulting stacking structure increased progressively the melting temperature of the duplex and two lysine residues beside tryptophan formed hydrogen bonds with DNA bases and stabilized the DNA (Jain and Rajeswari, 2003).

DNA binding to a 29-residue GCN4 basic region peptide, GCN4br, as well as to br-C peptide, a monomeric basic-region analogue with a stabilized α-helix at its C-terminal end, was studied by fluorescence spectroscopy (Zhang, *et al*., 2002b). The fluorophore NBD was attached at the N-terminus of the br-C peptide as a fluorescent probe. Quantitative analysis of the fluorescence quenching of the NBD-br-C peptide caused by the major groove of the duplex DNA facing toward the bound peptide indicated the formation of a 1:1 complex with a dissociation constant of 1.41 ± 0.22 μM. Competitive displacement fluorescence assays for the binding of the br-C and GCN4br peptides to DNA gave dissociation constants of 0.65 ± 0.09 μM and 3.9 ± 0.5 μM, respectively. The difference in the dissociation constants for these two peptides corresponded to a free energy difference of 1.1 kcal/mol that was attributed to the helix stabilization achieved in the br-C peptide.

Intrinsic fluorescence experiments were used to characterize the interaction between variants of the HIV-1 Tat (32-72) BP1 peptide and TAR RNA (Metzger, *et al*., 1997). The dissociation constants for both the wild-type BP1 and cysteine-defective BP1 peptides were found to be in the range of 60 to 70 nM, which indicated that the free sulfhydryl groups of the cysteines within the peptide BP1 were not required to bind to the TAR RNA with a high affinity. This finding triggered the authors to use an extrinsic fluorescence assay to study the binding of the Tat peptide to TAR RNA by using a mutant BP1 peptide (C34S, C37W) (BP1SW) as probe. The dissociation constant for the binding of BP1SW to TAR RNA was 9 nM. The change of the BP1SW fluorescence intensity upon

TAR RNA binding was used to investigate the binding kinetics by stopped-flow experiments. The results suggested a two-step binding model, with a rapid diffusion-limited formation of a tight, but unspecific complex, followed by a relatively slow structural rearrangement step ($k \approx 60\ s^{-1}$) to form specific BP1SW-TAR complexes.

Porschke and Ronnenberg have studied the kinetics of interaction between a DNA duplex and the KWK lysine oligopeptides by the field-jump method using fluorescence detection (Porschke and Ronnenberg, 1981). The binding process was identified to be a two-step association mechanism, where a bimolecular step driven by electrostatic interaction was followed by a slow intramolecular transition where the aromatic residues (W) stacked via intercalation with the DNA base pairs. The equilibrium binding studies of KWK to DNA yielded the stacking constant of 0.3 and 6 for native and denatured DNA in the second step, respectively (Montenay-Garestier, *et al*., 1981). It suggested that stacking was strongly favored in ssDNA. The dissociation rate constant was 4000 s^{-1} for the first step, and 440 s^{-1} for the second step, which corresponded to halftimes of 0.17 and 1.6 ms, respectively. The dissociation of the KWK-DNA complex first involved a slow extraction of the aromatic amino acids from the DNA helix, followed by rapid release of the cationic peptide from the DNA template. Apparently, such fast dissociation of KWK from complexes with a halftime of about 1.6 ms could not provide the KWK-DNA complexes with sufficient circulation time for their application in gene delivery. One way to slow down dissociation was to increase the number of lysine residues. The rationale is that the rate constant for the disruption of electrostatic bonds between DNA and lysine oligopeptides decreases with increasing number of lysines. Such expectation was proved by Smith *et al.* (Smith, *et al*., 1998). They designed a series of peptides based on the K_nWK family, where n = 4, 5, 6, 7, 8, 10 and 12. To facilitate the characterization of the DNA complexes, a ^{125}I- or ^{131}I-labeled tyrosine (Y) was added at the N-terminus of the peptide. A lysine (K) was added on the left side of tyrosine to provide a branching residue for attachment of receptor ligands and reporter groups at its ε-amino group. Since molecular simulation indicated that the series of such designed peptides would have an α-helical configuration, the peptide would orientate at the surface of the DNA after insertion of the tryptophan (W) into the DNA helix. Thus, an alanine (A) residue was included in the sequence to the side chains of tryptophan and the second Lys to the N-terminus on opposite sides of the putative helix. The obtained $YKAK_nWK$ peptide was noncovalently bound to DNA through electrostatic interaction. By dynamic light scattering, small complexes (<100 nm) were formed with all the peptides at phosphate-to-lysine ratios that ranged from 1:0.1 to 1:10, except at charge ratios of 1:1 where large aggregates (>1000 nm) formed. These complexes were stable at room temperature for at least 5 days, overcoming the problem of rapid dissociation experienced by the KWK-DNA

complexes. Application of the $YKAK_nWK$ peptides to the transfer of DNA into HepG2 cells showed that only the peptides with $n \geq 8$ were able to enhance gene transfection (Smith, *et al*., 1998).

Lohman *et al.* (Lohman, *et al*., 1980) have found that the binding constant for pentalysine-DNA interactions decreased dramatically with both increasing NaCl concentration and pH. The data were consistent with an electrostatic interaction between the cationic peptide and DNA, driven by the entropic contribution of counterion release to the free energy of binding. This work was extended with oligolysines containing tryptophan by examining the thermodynamics of binding of KWK_n with n = 1, 2, 4, or 6 to polynucleotides (Mascotti and Lohman, 1993). The quenching of the tryptophan fluorescence upon interaction with the polynucleotides was monitored to generate binding isotherms. Then, the equilibrium binding constants were determined by analysis of the binding isotherms using the non-cooperative McGhee and von Hippel (1974) model. As observed with pentalysine, the free energy of binding of these peptides was entirely entropy driven. Fluorescence studies also found that other oligolysine and lysine-rich peptides such as KGWGK, KWK_6, and K_n (n=3-8) bound to oligo- and polynucleotides with binding constants in the range of 1×10^3~1×10^5 M^{-1} (Matsuno, *et al*., 2001; Roy, *et al*., 1992; Ballin, *et al*., 2004).

An amphiphilic peptide MPG (GALFLGFLGAAGSTMGAWSQPKKKRKV), containing a hydrophobic domain derived from the fusion sequence of HIV gp41 and a hydrophilic domain derived from the NLS of SV40 T-antigen, was designed by Divita's group to deliver antisense ODN, plasmid DNA, and siRNA (Morris, *et al*., 1997; Morris, *et al*., 1999; Simeoni, *et al*., 2003). The quenching of intrinsic fluorescence of MPG was used to monitor the binding of MPG to the oligonucleotides (Morris, *et al*., 1997). The MPG-ODN induced a remarkable quenching of the intrinsic fluorescence emitted by the Trp residue of MPG. The maximum emission peak did not shift suggesting that the environment of the Trp residue was not modified. The quenching of the intrinsic fluorescence was most likely due to direct interaction of MPG with the phosphate or with the nucleoside moiety of the oligonucleotides. A quadratic equation was used to fit the fluorescence quenching data to determine the binding parameters. Best fits were obtained for a ratio of four and eight peptide molecules per the 18-mer single- and 18/36-mer double-stranded oligonucleotides, respectively. MPG exhibited relatively high affinity for all oligonucleotides tested with apparent dissociation constants in the $1-2\times10^{-8}$ M range. The resulting compact structure (with a 20-fold excess of peptide) not only stabilizes the nucleic acids and protects them from nuclease degradation in cell culture media but also drives them efficiently to mammalian cells in culture. Similar experiments were done to study the binding of MPG to plasmid DNA (Morris, *et al*., 1999). The results revealed high affinity for binding of MPG to pRL-SV40 (3.2 kb) and pJ30-antisense-Hucdc25C plasmid (4.9 kb) with respective dissociation constants of 0.5×10^{-8} M and 1.8×10^{-8} M.

Pep-2 (KETWFETWFTEWSQPKKKRKV), an analogue of the Pep-1 peptide, has been used to deliver a short 15-mer antisense HypNA-pPNA chimera directed specifically against cyclin B1 (Morris, *et al*., 2004). Binding of cargoes to Pep-2 was monitored by fluorescence spectroscopy. Pep-2 exhibited a high affinity for PNAs with a dissociation constant of 22 ± 4 nM, and formed stable peptide-based nanoparticles around the cargo with an estimated diameter between 100 and 200 nm.

In general, fluorescence methods enable the determination of the binding parameters of peptides to DNA at equilibrium with no need to separate the interacting species. Thus this technique is generally quick and easy to perform.

2.3.4 Summary

In the above sections, various techniques were presented to study the binding of proteins or peptides to nucleic acids. These techniques are based on the biological or spectroscopic changes observed upon the formation of the complexes. Traditional or other advanced EMSA techniques typically require the radioisotope labeling of the interesting species. In addition, separation of the unbound and bound species on a polyacrylamide gel or an electrical field may cause the dissociation or association of complexes and affect the measured binding parameters. Other techniques, such as fluorescence spectroscopy, difference CD spectroscopy, or difference UV absorption spectroscopy, detect spectroscopic changes resulting from the formation of protein-DNA complexes. These spectroscopic techniques permit the study of interactions at equilibrium in solution, without separation of the unbound and bound species. They are generally fast and easy to perform. However, the determination of the binding parameters from the experimental data needs careful interpretation and analysis. Nevertheless, these spectroscopic methods are still the primary techniques used for any binding study.

2.4 Construction of Binding Isotherms

In order to generate binding isotherms from the experimental data obtained by spectroscopic techniques, such as UV-Vis absorbance or fluorescence, it is commonly assumed that a linear relationship exists between the signal change and the degree of binding. However, if a linear relationship does not hold, then the calculated apparent isotherms will be incorrect. In the general case, where multiple ligands bind to a macromolecule or a large supramolecular aggregate (micelle, lipid mono- or bilayer), the fractional signal change and the extent of binding often do not have a simple linear relationship. It is thus essential that true binding isotherms be built even when a direct proportionality does not exist between the fractional signal change and the degree of binding. The binding density function (BDF) analysis provides a means to achieve this aim.

The thermodynamic basis for the BDF analysis is that the distribution of ligands bound in different states (average number of ligands bound per macromolecule) is strictly determined at equilibrium by the free ligand concentration (Bujalowski and Lohman, 1987; Schwarz, *et al.*, 1987). From the thermodynamic point of view, the free and the bound ligand can be considered as existing in different states at equilibrium in the system where there is no aggregate formation. This statement requires that the respective chemical potentials be equal at equilibrium. This requirement results in Equation 2-1 (Schwarz, 1977),

$$\mu_f^o + RT\,ln\,f_f L_f = \mu_b^o + RT\,ln\,\varphi(\nu) \qquad (2\text{-}1)$$

where the subscripts f and b refer to the free and bound ligand state, respectively. The chemical potentials μ_f^o and μ_b^o are obtained under standard conditions. f_f and L_f are the activity coefficient and the concentration of the free ligand, respectively. $\varphi(\nu)$ is the activity of the bound ligand, which is a function of the average binding density ν. ν is defined as the amount of bound ligand per macromolecule given by $\nu = L_b/M_t$, where M_t is the concentration of the macromolecule. Equation 2-1 can be rewritten into Equation 2-2

$$KL_f = \varphi(\nu) \qquad (2\text{-}2)$$

where $K = f_f \exp\{(\mu_f^o - \mu_b^o)/RT\}$ represents the basic binding constant. At equilibrium, any given binding system can be quantitatively characterized by a thermodynamic association isotherm which reveals the relationship between binding density and the concentration of free ligand. This relationship holds irrespective of the possibility that bound and/or free ligand molecules assume any number of different structural states. According to Equation 2-2, the ligand binding density ν at equilibrium is a unique function of the free ligand concentration L_f under a given solution condition. The relationship between ν and L_f reflects the underlying molecular binding mechanism (Schwarz, 2000; Schwarz and Reiter, 2001).

It results from Equation 2-2 that if the average ligand binding density ν is the same for x solutions containing different ligand and macromolecule total concentrations $(L_t, M_t)_x$, then the free ligand concentration L_f will also be the same in each solution. The mass conservation equation shown in Equation 2-3 can be applied for a set of x concentration pairs $(L_t, M_t)_x$ which have the same ν and L_f values.

$$L_t = \nu \cdot M_t + L_f \tag{2-3}$$

In practice, ν and L_f can be determined from the slope and intercept of the plot of L_t *vs* M_t for *x* solutions which have the same ν and L_f.

In order to obtain the L_f and ν values, a set of concentration pairs $(L_t, M_t)_x$ that correspond to pairs of L_f and ν values have to be found, which is achieved through the BDF analysis described in the following section. A commonly adopted experimental routine to monitor binding takes advantage of the changes in a signal Φ (e.g., UV absorbance, fluorescence intensity, or CD ellipticity) upon the formation of complexes. If the signal is from the macromolecule, then it is related to the individual concentrations according to Equation 2-4

$$\Phi = s_f \cdot M_f + \sum_i s_i \cdot M_i \tag{2-4}$$

where, M_f and M_i are the concentrations of free and bound macromolecule, respectively. s_f is the molar signal of the free macromolecule. s_i is the molar signal of each macromolecular species at concentration M_i with *i* ligands bound.

The mass conservation equation, which relates M_f and M_i to the total concentration of macromolecule M_t, is given in Equation 2-5 (Lohman and Bujalowski, 1991)

$$M_t = M_f + \sum_i M_i \tag{2-5}$$

Equation 2-4 can be converted to Equation 2-6 by applying the mass conservation given in Equation 2-5 and taking into account the fact that $v_i = iM_i/M_t$

$$\Phi = s_f \cdot M_t + \sum_i M_t (s_i - s_f)(v_i / i) \tag{2-6}$$

Equation 2-6 can be used to define a relative change in Φ (Lohman and Bujalowski, 1991).

$$\Delta\Phi = (\Phi - s_f \cdot M_t)/s_f M_t = \sum_i (\frac{s_i - s_f}{s_f})(v_i / i) \qquad (2\text{-}7)$$

In Equation 2-7, $(s_i - s_f)/s_f$ is the molecular signal change in the complex containing i ligands, which is an intrinsic molecular property of the system. Equation 2-7 indicates that $\Delta\Phi$ is a unique function of v_i, where $\Delta\Phi$ is referred to as the macromolecular binding density function (MBDF). At equilibrium, each separate value of v_i is a function of the free ligand concentration L_f only, which is strictly determined by the average binding density ν as indicated in Equation 2-2 (Lohman and Bujalowski, 1991; Schwarz, 1977 & 2000). Therefore, $\Delta\Phi$ is a function of L_f and hence ν only. The solutions with a set of x pairs of total concentrations $(L_t, M_t)_x$ for which $\Delta\Phi$ is the same, will have the same ν and L_f values. Consequently, $\Delta\Phi$ is an appropriate function to use in finding the set of concentration pairs $(L_t, M_t)_x$ which have the same ν and L_f values. The outcome can determine the true values of L_f and ν from the slope and intercept of the plot of L_t *vs* M_t for a given $\Delta\Phi$ value. Such a procedure is illustrated in Figure 2.5 and Figure 2.6.

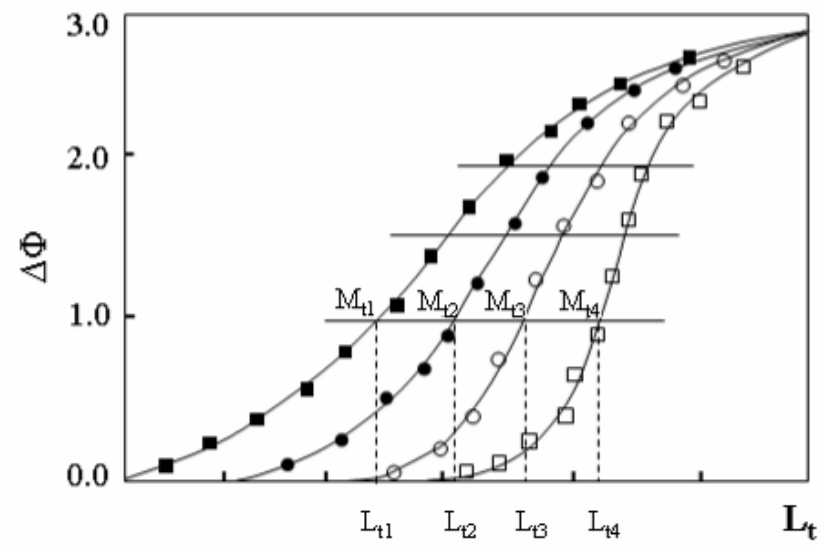

Figure 2.5. Theoretical titration curves of the signal $\Delta\Phi$ as a function of ligand concentration for two different macromolecule concentrations. The figure is reprinted from Jezewska and Bujalowski (1996).

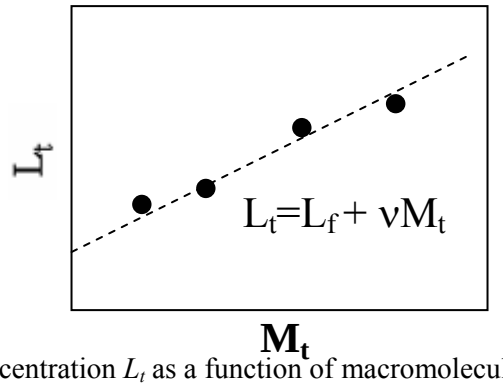

Figure 2.6. Plot of ligand concentration L_t as a function of macromolecule concentration M_t for a given $\Delta\Phi$. The slope is the binding density ν, and the intercept is the free peptide concentration L_f.

In Figure 2.5, the horizontal line intersecting four titration curves is characterized by the same $\Delta\Phi$ value. The points where this horizontal line intersects each titration curve defines the four sets of $(L_t, M_t)_x$ (x = 1 to 4) concentrations which have the same ν and L_f values. One set of (ν, L_f) values can be obtained from the slope and intercept of the plot of L_t *vs.* M_t in Figure 2.6 for a given $\Delta\Phi$ value. A binding isotherm can be generated by drawing several such horizontal lines and determining the ν and L_f values. Such a derivation is independent of specific binding models and as such, can be generalized to any binding system. Execution of this procedure requires to generate $\Delta\Phi$ *vs.* ligand concentration plots for different macromolecule concentrations.

The above derivation works when the signal arises from the macromolecule. If the observed signal arises from the ligand, then the binding density function requires a slightly different analysis. Although the expression of the BDF depends on whether the observed signal arises from the macromolecules or the ligands, it remains a unique function of the binding density. Accordingly the above procedure for generating the binding isotherm is suitable for both cases as long as the systems exhibit a change in the physicochemical or biological signals (Lohman and Bujalowski, 1991). Tables 2.2 and 2.3 (Lohman and Bujalowski, 1991) summarize the expressions of the BDF when the experimentally observed signal is due to changes in the fluorescence or absorbance of the macromolecule and ligand, respectively.

The expressions for the binding density function listed above are for spectroscopic changes, but they can be universally extended to any kind of change which is only function of the average binding density. The basic idea about the binding density function (BDF) analysis was independently proposed in 1987 by two groups who applied it to protein-nucleic acid binding (Bujalowski and Lohman, 1987) and peptide-liposome interaction (Schwarz, *et al.*, 1987). However, the underlying concept can be applied to any macro- or supramolecular binding system (Schwarz, 2000).

Table 2.2. Macromolecular binding density functions (MBDF) for different spectroscopic signals

Method	ΔΦ (MBDF)	Comments
Absorbance	$\Delta A = \sum_i (\Delta\varepsilon_i / i)\nu_i$ where $\Delta A = (A - A_o)/A_o$ $\Delta\varepsilon_i = (\varepsilon_i - \varepsilon_f)/\varepsilon_f$	ε_f and ε_i are the extinction coefficients for the free and bound macromolecule. A_o and A are the absorbance of the macromolecule solution in the absence and presence of ligand, respectively.
Fluorescence	$Q = \sum_i (\Delta F_i / i)\nu_i$ where $Q = (I - I_o)/I_o$ $\Delta F_i = (F_i - F_f)/F_f$	F_f and F_i are the molar fluorescence for the free and bound macromolecule. I_o and I are the fluorescence of the macromolecule solution in the absence and presence of ligand, respectively.

Table 2.3. Ligand binding density functions (LBDF) for different spectroscopic signals

Method	ΔΦ (LBDF)	Comments
Absorbance	$\Delta A(L_t/M_t) = \sum_i (\Delta\varepsilon_i / i)\nu_i$ where $\Delta A = (A - A_o)/A_o$ $\Delta\varepsilon_i = (\varepsilon_i - \varepsilon_f)/\varepsilon_f$	ε_f and ε_i are the extinction coefficients for the free ligand and each state of the bound ligand. A_o and A are the absorbance of the ligand solution in the absence and presence of macromolecule, respectively.
Fluorescence	$Q(L_t/M_t) = \sum_i (\Delta F_i / i)\nu_i$ where $Q = (I - I_o)/I_o$ $\Delta F_i = (F_i - F_f)/F_f$	F_f and F_i are molar fluorescence for the free ligand and each state of the bound ligand. I_o and I are the fluorescence of the ligand solution in the absence and presence of macromolecule, respectively.

In the self-assembling peptide-oligonucleotide binding system, the binding may result in the formation of aggregates due to the potential for self-assembly of peptides into nanostructures. In that case, an oligonucleotide molecule is either in the aggregated or soluble state. This situation is likely to occur since it is not uncommon that the ligand-nucleic acid binding causes aggregate formation or

condensation of the DNA (Morris, *et al.*, 1997 & 1999; Teif, *et al.*, 2005). How to extend the BDF analysis to such a binding system and to generate binding isotherms is of interest. Although the research for extending the BDF analysis to such a binding system has not been conducted yet, some studies may provide insights/hints to identify the experimental signal that yields the binding density function $\Delta\Phi$, which is the key element in the BDF analysis. Such an example is found in the investigation of the ligand-induced DNA aggregation or condensation (Teif, *et al.,* 2001 & 2005) where the fraction of condensed/aggregated DNA has been shown to be a unique function of the binding density. The following section reviews the arguments made by Teif *et al*.

The principles of the calculation of the equilibrium binding of large ligands to DNA were formulated in the late 1960s to the 1970s (Crothers, 1968; McGhee and von Hippel, 1974). DNA condensation is one of the processes that may be treated using this formalism. There are several possible descriptions of DNA condensation caused by ligand binding. The two-state model is one of them (Figure 2.7). This model implies that a DNA molecule is either in the starting (soluble) or condensed (aggregated) state, intermediate state being forbidden. The ligands may reversibly bind each DNA state with different binding constants and different stoichiometric parameters.

The parameters corresponding to the soluble or condensed DNA are denoted by the subscript j (= 1 or 2, respectively). Each DNA molecule consists of L base pairs (units). n_j DNA molecules are in state j with g_j bound ligands. C_o is the molar concentration of free ligands in solution, while $c_j = g_j/(n_jL)$ is the relative concentration of ligands bound to DNA in the form i; in other words, the binding density for the DNA in state j. The binding is supposed to be reversible, *i.e.*, each ligand can change its location at the DNA chain, dissociate, and bind again to other DNA molecules.

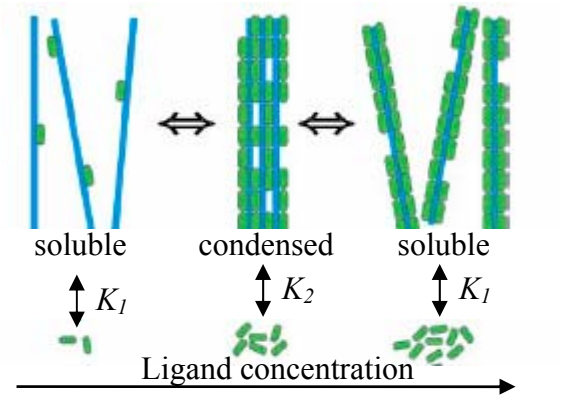

Figure 2.7. The two-state model. DNA may be in one of the two states: soluble or condensed. The two DNA states bind ligands with different binding constants, K_1 and K_2, and different stoichiometries.

The change in the free energy [ΔF (g_1,g_2,c_o)] resulting from the binding of g_j ligands to n_j DNA molecules is determined by the expression (Teif, *et al.,* 2001) given in Equation 2-8,

$$\Delta F(g_1, g_2, C_o) = \sum_{j=1}^{2} (n_j F_j + g_j \psi_j - g_j \mu) - RT \ln(W) \qquad (2\text{-}8)$$

where F_j is the free energy of a DNA molecule in the j state in the absence of adsorbed ligands; ψ_j is the free energy corresponding to a DNA molecules in the state j with g_j bound ligands; μ is the chemical potential of the free ligand, which has the same expression as the left-hand side of Equation 2-1; W is the number of ways in which the bound ligands can be arranged on the DNA molecule of L units at the same energetic state. W is expressed in Equation 2-9 (Teif, *et al.,* 2001).

$$W = \prod_j \frac{[n_j L / r_j - (m_j - 1) g_j]!}{g_j!(n_j L / r_j - m_j g_j)!} \frac{(n_1 + n_2)!}{n_1! n_2!} \qquad (2\text{-}9)$$

Minimization of ΔF with respect to n_j and g_j gives the mass action law for the system

$$K_j = \frac{r_j c_j [1 - r_j (m_j - 1) c_j]^{m_j - 1}}{C_o (1 - r_j m_j c_j)^{m_j}} \qquad (2\text{-}10)$$

K_j is the binding constant for the ligands that are bound to DNA in the state j; m_j is the number of DNA base pairs covered by one ligand molecule upon binding to DNA in state j; and r_j equals 0.5 or 1 depending on whether a bound ligand interacts with one or two DNA strands of double-stranded DNA, respectively. Equation 2-10 suggests that the binding density c_j is strictly determined by the free ligand concentration C_o since r_j and m_j are constant values. Thus, the Equation 2-10 can be rewritten under the form $K_j C_o = \varphi(c_j)$; in other words, the thermodynamic basis for the BDF analysis is fulfilled.

The expression of the fraction of condensed DNA molecules ϑ is also obtained by minimizing ΔF and its expression is given in Equation 2-11

$$\vartheta = US_{12} / (1 + US_{12}) \qquad (2\text{-}11)$$

where S_{12} is the equilibrium constant for the transition between the soluble and condensed states of DNA in the absence of ligands. The expression of U is presented in Equation 2-12 (Teif, *et al.,* 2001).

$$U = \prod_{j=1,2} \left[\frac{1 - r_j (m_j - 1) c_j}{1 - r_j m_j c_j} \right]^{(-1)^j (L/r_j)} \qquad (2\text{-}12)$$

Given that r_j and m_j are constant values, Equation 2-12 suggests that U is only function of the binding density c_j, which is determined by the free ligand concentration C_o, as indicated in Equation 2-10. Thus, U is a unique function of the free ligand concentration and hence the average binding density, and so is ϑ thanks to Equation 2-11. In other words, ϑ can be considered as an appropriate binding density function (*i.e.* $\vartheta = \Delta\Phi = f(L_f) = \varphi(\nu)$), whose expression can be expected to be more complicated than those listed in Tables 2.2 and 2.3.

In the case where a peptide binds to DNA, ϑ can be calculated from the UV-Vis absorbance of the DNA solution in the absence of ligand and that of the supernatant of the peptide-DNA solutions after they have been centrifuged. Once plots of the fraction of condensed DNA molecules ϑ *vs.* ligand concentration for different DNA concentrations are obtained, the binding isotherms can be generated based on the BDF analysis. This thesis draws heavily from these considerations to characterize the binding of two self-assembling peptides to DNA molecules.

References

Aggeli, A., M. Bell, L.M. Carrick, C.W.G. Fishwick, R. Harding, P.J. Mawer, S.E. Radford, A.E. Strong, and N. Boden. 2003. pH as a trigger of peptide b-sheet self-assembly and reversible switching between nematic and isotropic phases. *J. Am. Chem. Soc.* **125:** 9619-9628.

Agelli, A., N. Boden, M. Hunter, and P. Knowles. 2003. Self-assembling β-barrel channel-forming peptides for wound dressing and other pharmaceutical uses. *PCT Int. Appl.* 28 pp.

Agou, F., S. Raveh, S. Mesnildrey, and M. Veron. 1999. Single Strand DNA Specificity Analysis of Human Nucleoside Diphosphate Kinase B. *J. Biol. Chem.* **274:** 19630-19638.

Anderson, W. F. 1998. Human gene therapy. *Nature* **392:** 25-30.

Arap, W., R. Pasqualini, and E. Ruoslahti. 1998. Cancer treatment by targeted drug delivery to tumor vasculature. *Science* **279:** 377-380.

Arosio, D., S. Costantini, Y. Kong, and A. Vindigni. 2004. Fluorescence anisotropy studies on the Ku-DNA interaction: anion and cation effects. *J. Biol. Chem.* **279:**42826-42835.

Bain, D. L., and G. K. Ackers. 1998. A quantitative cryogenic gel-shift technique for analysis of protein-DNA binding. *Anal. Biochem.* **258:** 240-245.

Ballin, J. D., I. A. Shkel, and M. T. Record. 2004. Interactions of the KWK6 Cationic Peptide with Short Nucleic Acid Oligomers: Demonstration of Large Coulombic End Effects on Binding at 0.1-02 M Salt. *Nucl. Acids Res.* **32:** 3271-3281.

Besschetnova, I.A., G. E. Pozmogova, A. N. Chuvilin, A. K. Shchelkina, and O. F. Borisova. 2006. Complexes of telomeric oligonucleotide d(TTAGGG)4 with the new recombinant protein PGEk-nucleic acid carrier into proliferating cells. *Mol Biol (Mosk).* **40:** 489-496.

Blackshear, P.J., W. S. Lai, E. A. Kennington, G. Brewer, G. M. Wilson, X. Guan, P. Zhou. 2003. Characteristics of the interaction of a synthetic human tristetraprolin tandem zinc finger peptide with AU-rich element-containing RNA substrates. *J. Biol. Chem.* **278:** 19947-19955.

Boraston, A. B., P. Chiu, R. A. J. Warren, and D. G. Kilburn. 2000. Specificity and affinity of substrate binding by a family 17 carbohydrate-binding module from Clostridium cellulovorans cellulase 5A. *Biochemistry* **39:** 11129-11136.

Bujalowski, W., and T. M. Lohman. 1987. A General Method of Analysis of Ligand-Macromolecule Equilibria Using a Spectroscopic Signal from the Ligand to Monitor Binding. Application to E. coli SSB Protein-Nucleic Acid Interactions. *Biochemistry* **26:** 3099-3106.

Cann, J. R. 1989. Phenomenological theory of gel electrophoresis of protein-nucleic acid complexes. *J. Biol. Chem.* **264:** 17032-17040.

Carny, O., D. E. Shalev, and E. Gazit. 2006. Fabrication of Coaxial Metal Nanocables Using a Self - Assembled Peptide Nanotube Scaffold. *Nano Lett.* **6:** 1594-1597.

Chen, P. 2005. Self-assembly of Ionic-complementary Peptides: a Physicochemical Viewpoint. *Colloids Surf. A* **261:** 3-24.

Crothers, D. M. 1968. Calculation of binding isotherms for heterogeneous polymers. *Biopoly.* **6:** 575-584.

Davis, M. E., P. C. H. Hsieh, T. Takahashi, Q. Song, S. Zhang, R. D. Kamm, A. J. Grodzinsky, P. Anversa, and R. T. Lee. 2006. Local myocardial insulin-like growth factor 1 (IGF-1) delivery with biotinylated peptide nanofibers improves cell therapy for myocardial infarction. *Proc. Natl. Acad. Sci. USA* **103:** 8155-8160.

Dixon, W. J., J. J. Hayes, J. R. Levin, M. F. Weidner, A. B. Dombrowski, and T. D. Tullius. 1991. *Methods Enzymol.* **208:** 380-413.

Dodson, M., and H. Echols. 1991. Electron Microscopy of Protein-DNA Complexes. *Methods Enzymol.* **208:** 168-196.

Ellis-Behnke, R. G., Y. X. Liang, S. W. You, D. K. Tay, S. Zhang, K. F. So, and G. E. Schneider. 2006. Nano neuro knitting: Peptide nanofiber scaffold for brain repair and axon regeneration with functional return of vision. *Proc. Natl. Acad. Sci. USA* **103:** 5054-5059.

Epstein, I. R. 1978. Cooperative and non-cooperative binding of large ligands to a finite one-dimensional lattice. A model for ligand-oligonucleotide interactions. *Biophy. J.* **8:** 327-339.

Endoh, T., H. Funabashi, M. Mie, and E. Kobatake. 2005. Method for detection of specific nucleic acids by recombinant protein with fluorescent resonance energy transfer. *Anal..Chem.* **77:** 4308-4314.

Fung, S.Y., C. Keyes, J. Duhamel, and P. Chen. 2003. Concentration Effect on the Aggregation of a Self-Assembling Oligopeptide. *Biophys. J.* **85:** 537-548.

Galletto, R., M. J. Jezewska, and W. Bujalowski. 2003. Interactions of the Escherichia coli DnaB helicase hexamer with the replication factor the DnaC protein. Effect of nucleotide cofactors and the ssDNA on protein-protein interactions and the topology of the complex. *J. Mol. Biol.* **329:** 441-465.

Glenn, J. F., and F. A. Etzkorn. 1998. A capillary electrophoresis mobility shift assay for protein–DNA binding affinities free in solution. *Nucl. Acids Res.* **26:** 4304-4305.

Gorman, J. 2003. Delivering the goods: gene therapy without the virus. *Sci. News* **163:** 43-44.

Goeden-Wood, N.L., J.D. Keasling, and S.J. Muller. 2003. Self-assembly of a designed protein polymer into b-sheet fibrils and responsive gels. *Macromol.* **36:** 2932-2938.

Gorecki, D.C., and K. D. MacDermot. 1997. Gene therapy: Panacea or placebo? II. Main applications of gene therapy. *Arch. Immunol .Ther. Exp.* ***45:*** 375-381.

Gourves, A.S., N. Tanguy Le Gac, G. Villani, P. E. Boehmer, and N. P. Johnson. 2000. Equilibrium binding of single-stranded DNA with herpes simplex virus type I-coded single-stranded DNA-binding protein, ICP8. *J. Biol. Chem.* **275:** 10864-10869.

Guler, M. O., C. C. Randal, and S. I. Stupp. 2005. Encapsulation of pyrene within self-assembled peptide amphiphile nanofibers. *J. Mater. Chem.* ***15:*** 4507-4512.

Holmes, T. C. 2002. Novel Peptide-Based Biomaterial Scaffolds. *Trends Biotechnol.* **20:** 16-21.

Hong, Y., R. L. Legge, S. Zhang, and P. Chen. 2003. Effect of Amino Acid Sequence and pH on Nanofiber Formation of Self-Assembling Peptides EAK16-II and EAK16-IV. *Biomacromol.* **4:** 1433-1442.

Hong, Y., L. Lau, R. Legge, and P. Chen. 2004. Critical Self-Assembly Concentration of an Ionic-Complementary Peptide EAK16-I. *J. Adhesion* **80:** 913-931.

Hong, Y., M. D. Pritzker, R. Legge, and P. Chen. 2005. Effect of NaCl and peptide concentration on the self-assembly of an ionic-complementary peptide EAK16-II. *Colloids Surf., B: Biointerfaces* **46:** 152-161.

Hsieh, P. C., C. MacGillivray, J. Gannon, F. U. Cruz, and R. T. Lee. 2006. Local controlled intramyocardial delivery of platelet-derived growth factor improves postinfarction ventricular function without pulmonary toxicity. *Circulation* **114:** 637-644.

Jain, A. A., and M. R. Rajeswari. 2002. Preferential binding of quinolones to DNA with alternating G, C / A, T sequences: a spectroscopic study. *J. Biomol. Struct. Dyn.* **20:** 291-299.

Jain, A. A., and M. R. Rajeswari. 2003. Binding studies on peptide-oligonucleotide complex: intercalation of tryptophan in GC-rich region of c-myc gene. B*iochim. Biophys. Acta.* **1622:** 73-81.

Jensen, D. E., and P. H. von Hippel. 1977. A boundary sedimentation velocity method for determining nonspecific nucleic acid-protein interaction binding parameters. *Anal. Biochem.* **80:** 267-281.

Jezewska, M. J. and W. Bujalowski. 1996. A General Method of Analysis of Ligand Binding to Competing Macromolecules Using the Spectroscopic Signal Originating from a Reference Macromolecule. Application to *Escherichia coli* Replicative Helicase DnaB Protein-Nucleic Acid Interactions. *Biochemistry* **35:** 2117-2128.

Jones, M. C., P. Tewari, C. Blei, K. Hales, D. J. Pochan, and J. C. Leroux. 2006. Self-Assembled Nanocages for Hydrophilic Guest Molecules. *J. Am. Chem. Soc.* **128:** 14599-14605.

Keyes-Bag, C., S. Y. Fung, J. Bezaire, and P. Chen. 2004. Self-Assembling Peptide as a Potential Carrier of Hydrophobic Compounds. *J. Am. Chem. Soc.* **126:** 7522-7532.

Kirkitadze, M. D., M. M. Condron, and D. B. Teplow. 2001. Indentification and characterization of key kinetic intermediates in amyloid β-protein fibrillogenesis. *J. Mol. Biol.* **312:** 1103-1119.

Kowalewski, T., and D. M. Hotzman. 1999. *In situ* atomic force microscopy study of Alzheimer's β–amyloid peptide on different substrates: new insights into mechanism of β–sheet formation. *Proc. Natl. Acad. Sci. USA* **96:** 3688-3693.

Kundu, B., N. R. Maiti, E. M. Jones, K. A. Surewicz, A. Krystyna, D. L. Vanik and W. K. Surewicz. 2003. Nucleation-dependent conformational conversion of the Y145Stop variant of human prion protein: Structural clues for prion propagation. *Proc. Natl. Acad. Sci. USA* **100:** 12069-12074.

Kur, J., M. Olszewski, A. Długołęcka, and P. Filipkowski. 2005. Single-stranded DNA-binding proteins (SSBs)-sources and applications in molecular biology. *Acta Biochim. Polonica* **52:** 569–574.

Law, B., R. Weissleder, and C. H. Tung. 2006. Peptide-Based Biomaterials for Protease-Enhanced Drug Delivery. *Biomacro.* **7:** 1261-1265.

Lee, R. T., and P. Hsieh. 2006. Sustained delivery of PDGF using self-assembling peptide nanofibers. *U.S. Pat. Appl. Publ.* 28pp.

Lohman, T. M., P. L. deHaseth, M. T. Record. 1980. Pentalysine-deoxyribonucleic acid interactions: a model for the general effects of ion concentrations on the interactions of proteins with nucleic acids. *Biochemistry* **19:** 3522-3530.

Lohman, T. M., and W. Bujalowski. 1991. Thermodynamic methods for model-independent determination of equilibrium binding isotherms for protein-DNA interactions: spectroscopic approaches to monitor binding. *Methods Enzymol.* **208:** 258-290.

Malonga, H., J. F. Neault, H. Arakawa, and H. A. Tajmir-Riahi. 2006. DNA interaction with human serum albumin studied by affinity capillary electrophoresis and FTIR spectroscopy. *DNA Cell Biol.* **25:** 63-68.

Mascotti, D. P., and T.M. Lohman. 1993. Thermodynamics of single-stranded RNA and DNA interactions with oligolysines containing tryptophan. Effects of base composition. *Biochemistry* **32:** 10568-10579.

Matsuno, H., K. Niikura, and Y. Okahata. 2001. Design and Characterization of Asparagine- and Lysine-Containing Alanine-Based Helical Peptides That Bind Selectively to A·T Base Pairs of Oligonucleotides Immobilized on a 27 MHz Quartz Crystal Microbalance. *Biochemistry* **40:** 3615-3622.

McGhee, J. D., and P. H. von Hippel. 1974. Theoretical Aspects of DNA-Protein Interactions: Co-operatice and Non-co-operative Binding of Large Ligands to a One-dimensional Homogeneous Lattice. *J. Mol. Biol.* **86:** 469-489.

Metzger AU, Bayer P, Willbold D, Hoffmann S, Frank RW, Goody RS, Rosch P. 1997. The interaction of HIV-1 Tat (32-72) with its target RNA: a fluorescence and nuclear magnetic resonance study. *Biochem. Biophys. Res. Commun.* **241:** 31-36.

Michel, S. L., A. L. Guerrerio, and J. M. Berg. 2003. Selective RNA binding by a single CCCH zinc-binding domain from Nup475 (Tristetraprolin). *Biochemistry* **42:** 4626-4630.

Mihara, H., S. Matsumura, and T. Takahashi. 2005. Construction and Control of Self-Assembly of Amyloid and Fibrous Peptides. *Bull. Chem. Soc. Jpn.* **78:** 572-590.

Mira, H., M. Vilar, V. Esteve, M. Martinell, M. J. Kogan, E. Giralt, D. Salom, I. Mingarro, L. and

Montenay-Garestier, T., J. Fidy, J. C. Brochon, and C. Helene. 1981. Dynamics of peptide-nucleic acid complexes. Fluorescence polarization studies. *Biochimie.* **63:** 937-940.

Morii, T., J. Yamane, Y. Aizawa, K. Makino, and Y. Sugiura. 1996. Cooperative Oligomerization Enhances Sequence-Selective DNA Binding by a Short Peptide. *J. Am. Chem. Soc.* **116:** 10011-10017.

Morris, M. C., P. Vidal, L. Chaloin, F. Heitz, and G. Divita. 1997. A new peptide vector for efficient delivery of oligonucleotides into mammalian cells. *Nucl. Acids Res.* **25:** 2730-2736.

Morris, M. C., L. Chaloin, J. Mery, F. Heitz, and G. Divita. 1999. A novel potent strategy for gene delivery using a single peptide vector as a carrier. *Nucl. Acids Res.* **27:** 3510-3517.

Morris, M. C., L. Chaloin, M. Choob, J. Archdeacon, F. Heitz, and G. Divita. 2004. Combination of a new generation of PNAs with a peptide-based carrier enables efficient targeting of cell cycle progression. *Gene Ther.* **11:** 757-764.

Moss, T. 2001. *Methods in Molecular Biology, v.148: DNA-Protein Interactions: Principles and Protocols*. Humana Press, Totowa, New Jersey.

Nagai, Y. L. D. Unsworth, S. Koutsopoulos, and S. Zhang. 2006. Slow release of molecules in self - assembling peptide nanofiber scaffold. *J. Control Rel.* **115:** 18-25.

Narmoneva, D. A., O. Oni, A. L. Sieminski, S. Zhang, J. P. Gertler, R. D. Kamm, and R. T. Lee. 2005. Self-Assembling Short Oligopeptides and the Promotion of Angiogenesis. *Biomaterials* **26:** 4837-4846.

Palena, C. M., D. H. Gonzalez, and R. L. Chan. 1999. A monomer-dimer equilibrium modulates the interaction of the sunflower homeodomain leucine-zipper protein Hahb-4 with DNA. *Biochem. J.* **341:** 81-87.

Pennisi, E., 1993. Material Peptide: A piece of yeast protein becomes a building block for scientists. *Sci. News* **143:** 316-317.

Pietersz, G. A., C. K. Tang, and V. Apostolopoulos. 2006. Structure and design of polycationic carriers for gene delivery. *Mini-Reviews in Med. Chem.* **6:** 1285-1298.

Plotnikov, V., A. Rochalski, M. Brandts, J. F. Brandts, S. Williston, V. Frasca, and L. Lin. 2004. An autosampling differential scanning calorimeter for study of biomolecular interactions. *Biocalorimetry* **2:** 241-251.

Porschke, D., and J. Ronnenberg. 1981. The reaction of aromatic peptides with double helical DNA. Quantitative characterization of a two step reaction scheme. *Biophys. Chem.* **13:** 283-290.

Reches, M., and E. Gazit. 2003. Casting Metal Nanowires Within Discrete Self-Assembled Peptide. *Science* **300:** 625-627.

Roy, K. B., S. Kukreti, H. S. Bose, V. S. Chauhan, and M. R. Rajeswari. 1992. Hairpin and duplex forms of a self-complementary dodecamer, d-AGATCTAGATCT, and interaction of the duplex form with the peptide KGWGK: can a pentapeptide destabilize DNA? *Biochemistry* **31:** 6241-6245.

Schwarz, G., 1977. On the analysis of linear binding effects associated with curved Scatchard plots. *Biophys. Chem.* **6:** 65-76.

Schwarz, G., H. Gerke, V. Rizzo, and S. Stankowski. 1987. Incorporation Kinetics in a Membrane, Studied with the Pore-Forming Peptide Alamethicin. *Biophys. J.* **52:** 685-692.

Schwarz, G., 2000. A universal thermodynamic approach to analyze biomolecular binding experiments. *Biophys. Chem.* **86:** 119-129.

Schwarz, G., and R. Reiter. 2001. Negative cooperativity and aggregation in biphasic binding of mastoparan X peptide to membranes with acidic lipids. *Biophys. Chem.* **90:** 269-277.

Seimiya, M., and Y. Kurosawa. 1996. Kinetics of binding of Antp homeodomain to DNA analyzed by measurements of surface plasmon resonance. *FEBS Lett.* **398:** 279-284.

Selvam, S., P. B. Thomas, S. F. Hamm-Alvarez, J. E. Schechter, D. Stevenson, A. K. Mircheff, and M. D. Trousdale. 2006. Current status of gene delivery and gene therapy in lacrimal gland using viral vectors. *Adv. Drug Deliv. Rev.* **58:** 1243-1257.

Simeoni, F., M. C. Morris, F. Heitz, and G. Divita. 2003. Insight into the mechanism of the peptide-based gene delivery system MPG: implications for delivery of siRNA into Mammalian Cells. *Nucl. Acids Res.* **31:** 2717-2724.

Singh M, L. D'Silva, and T. A. Holak. 2006. DNA-binding properties of the recombinant high-mobility-group-like AT-hook-containing region from human BRG1 protein. *Biol. Chem.* **387:** 1469-1478.

Sipe, J. D., and A. S. Cohen. 2000. Review: history of the amyloid fibril. *J. Struct. Biol.* **130:** 88-98.

Sitohy, M., J. M. Chobert, M. Schmidt, A. Gozdzicka-Jozefiak, and T. Haertle. 2001. Interactions between esterified whey proteins (alpha-lactalbumin and beta-lactoglobulin) and DNA studied by differential spectroscopy. *J. Protein Chem.* **20:** 633-640.

Smith, L. C., J. Duguid, M. Wadhwa, M. J. Logan, C. H. Tung, V. Edwards, J. T. Sparrow. 1998. Synthetic peptide-based DNA complexes for nonviral gene delivery. *Adv. Drug Deliv. Rev.* **30:** 115-131.

Stierle, V., J. Couprie, C. Ostlund, I. Krimm, S. Zinn-Justin, P. Hossenlopp, H. J. Worman, J. C. Courvalin, and I. Duband-Goulet. 2003. The carboxyl-terminal region common to lamins A and C contains a DNA binding domain. *Biochemistry* **42:** 4819- 4828.

Takahashi, Y., A. Ueno, and H. Mihara. 1999a. Optimization of hydrophobic domains in peptides that undergo transformation from to α-helix to β-fibril. *Bioorg. Med. Chem.* **7:** 177-185.

Takahashi, Y., T. Yamashita, A. Ueno, and H. Mihara. 2000. Construction of peptides that undergo structural transition from α-helix to β-sheet and amyloid fibril formation by the introduction of N-terminal hydrophobic amino acids. *Tetrahedron* **56:** 7011-7018.

Takahashi, Y., A. Ueno, and H. Mihara. 1999b. Peptides undergoing secondary structural transition and self-assembly into amyloid fibril based on structural complementarity. *Peptide Sci.* **36:** 57-60.

Takahashi. Y, A. Ueno, and H. Mihara. 2002. Amyloid architecture: Complementary assembly of heterogeneous combinations of three or four peptides into amyloid fibrils. *ChemBioChem.* **3:** 637-642.

Teif, V.B., and D. Y. Lando. 2001. Calculations of DNA Condensation Caused by Ligand Adsorption. *Mol. Biol.* **35:** 106-107.

Teif, V.B. 2005. Ligand-Induced DNA Condensation: Choosing the Model *Biophys. J.* **89:** 2574-2587.

Torchilin, V. P. 2005. Lipid-core micelles for targeted drug delivery. *Curr. Drug Deliv.* **2:** 319-327.

Walsh, D. M., D.M. Hartley, Y. Kusumoto, Y. Fezoui, M.M. Condron, A. Lomakin, G.B. Benedek, D.J. Selkoe, and D.B. Teplow. 1999. Structure and biological activity of protofibrilliar intermediates. *J. Biol. Chem.* **274:** 25945-25952.

Watson, D., E. Castano, T. A. Kokjohn, Y. Kuo, Y. Lyubchenko, D. Pinsky, E. S. Connolly, C. Esh, D. C. Luehrs, W. B. Stine, L. M. Rowse, M. R. Emmerling, and A. E. Roher. 2005. Physicochemical characteristics of soluble oligomeric Aβ and their pathologic role in Alzheimer's disease. *Neuro. Res.* **27:** 869-881.

Xiong, H., B. L. Buckwalter, H. Shieh, and M. H. Hecht. 1995. Periodicity of Polar and Nonpolar Amino Acids is the Major Determinant of Secondary Structure in Self-Assembling Oligomeric Peptides. *Proc. Natl. Acad. Sci. USA* **92:** 6349-6353.

Yang, D. S., C. M. Yip, T. H. Huang, A. Chakrabartty, and P. E. Fraser. 1999. Manipulating the amyloid-β aggregation pathway with chemical chaperones. *J. Biol. Chem.* **271:** 32970-32974.

Yang, S. J., S. Zhang. 2006. Self-assembling behavior of designer lipid-like peptides. *Supramol. Chem.* **18:** 389-396.

Zhang, M., B. Wu, H. Zhao, J. W. Taylo. 2002b. The effect of C-terminal helix stabilization on specific DNA binding by monomeric GCN4 peptides. *J. Pept. Sci.* **8:** 125-136.

Zhang, S., T. Holmes, C. Lockshin, and A. Rich. 1993. Spontaneous assembly of a self-complementary oligopeptide to form a stable macroscopic membrane. *Proc. Natl. Acad. Sci. USA* **90:** 3334-3338.

Zhang, S., T. C. Holmes, M. Dipersio, R. O. Hynes, X. Su, and A. Rich. 1995. Self-complementary Oligopeptide Matrices Support Mammalian Cell Attachment. *Biomaterials* **16:** 1385-1393.

Zhang, S. 2002. Emerging biological materials through molecular self-assembly. *Biotechnol. Adv.* **20:** 321-339.

Zhang, S., and X. Zhao. 2004. Design of molecular biological materials using peptide motifs. *J. Mater. Chem.* **14:** 2082- 2086.

Zhao, X. J., and S. Zhang. 2006. Self-Assembling Nanopeptides Become a New Type of Biomaterial. *Adv. Polym. Sci.* **203:** 145-170.

Chapter 3
Interaction of a Self-Assembling Peptide with Oligonucleotides: Complexation and Aggregation

3.1 Introduction

Self-assembling peptides have recently emerged as one of the most promising biomolecular materials in bio-nanotechnology research (Zhang, *et al*., 1993 & 1994 & 2002; Aggeli, *et al*., 1999; Chen, 2005). The self-assembly of peptides not only relates to many naturally occurring states of proteins, such as amyloid fibrillogenesis (Aggeli, *et al*., 1999), but also provides useful biomolecular building blocks for a wide variety of supramolecular fabrications (Zhang, *et al*., 1993 & 2002; Chen, 2005). Among the new self-assembling peptides is a class of ionic-complementary, amphiphilic peptides, e.g., EAK made of glutamic acid (E), alanine (A), and lysine (K) residues (Zhang, *et al*., 1993). This new class of peptides originates from zuotin, a yeast protein that preferentially binds to left-handed Z-DNA (Zhang, *et al*., 1993). The molecular structure of these peptides contains alternating positive and negative charges, enabling ionic-complementarity. This ionic complementarity, together with hydrogen bonding, hydrophobic, and van der Waals interactions promotes self-assembly of the peptide molecules into highly stable aggregates (Hong, *et al*., 2003; Fung, *et al*., 2003; Chen, 2005). The nano/microstructures constructed from the peptide self-assembly have found many biomedical applications, including scaffolding for tissue engineering (Zhang, *et al*., 1995; Holmes, *et al*., 2000) and biological surface patterning (Zhang, 2002). It has been shown recently that these peptides can encapsulate a hydrophobic organic compound and unload it into a model cell membrane in a controlled manner (Keyes-Bag, *et al*., 2004). It is interesting to see if these self-assembling peptides can also be used for carrying DNA or RNA in gene delivery, which is the current bottleneck to gene therapy (Plank, *et al*., 1999; Simeoni, *et al*., 2003). Our particular interest is the self-assembling peptide-mediated delivery of antisense oligonucleotides and short-interfering RNAs (siRNAs) (Bergen and Pun, 2005).

The first key step to develop an oligonucleotide delivery system is to form peptide-oligonucleotide complexes (Plank, *et al*., 1999; Simeoni, *et al*., 2003). This entails the study of the binding of the peptide to oligonucleotides and the conformations of the resulting peptide-oligonucleotide complexes. The peptide and oligonucleotides used in this work are EAK16-II, a well-studied self-assembling peptide (Zhang, *et al*., 1993) referred to as EAK later on, and both single- and double-stranded oligodeoxynucleotides (ODNs), namely a guanine hexadecamer (dG_{16}), a cytosine

hexadecamer (dC_{16}), and their duplex (dGC_{16}). It has been argued that many peptide-nucleic acid interactions are not sequence-specific, resulting from non-covalent molecular interactions (Schwarz and Watanabe, 1983; McGhee and von Hippel, 1974; Muller, *et al*., 1991; Scatchard, 1949; Latt and Sober, 1967; Crothers, 1968; Schwarz, 1970; Epstein, 1978; Tsodikov, *et al*., 2001; Bujalowski and Lohman, 1987; Morii, *et al*., 1996). Thus, the dG_{16} and dC_{16} hexadecamers were chosen to assess how a purine or a pyrimidine affects the binding of a self-assembling peptide to an oligonucleotide. Since most therapeutic antisense oligonucleotides and siRNAs are short nucleic acids of less than 22 nucleotides in length, the choice of 16 mers is somewhat arbitrary but within the usual therapeutic oligonucleotide length range.

While there has been no study of binding between self-assembling peptides and oligonucleotides, numerous investigations have been done on the binding between proteins and nucleic acids (Plank, *et al*., 1999; Simeoni, *et al*., 2003). Characterization of the binding between a ligand protein and a nucleic acid requires the determination of the concentrations of the free and bound species involved. These quantities can be obtained by relating them to changes in the physicochemical or biological properties resulting from the formation of complexes (Bujalowski and Lohman, 1987). In most instances, these changes can be probed by techniques such as gel mobility shift assay (Morii, *et al*., 1996; Stierle, *et al*., 2003), filter binding assay (Agou, *et al*., 1999), surface plasmon resonance (Seimiya, *et al*., 1996), and fluorescence (Michel, *et al*., 2003; Endoh, *et al*., 2005). These last methods require labeling of the ligand with a chromophore or radioactive isotope, or covalent immobilization of the ligand. Besides being time consuming, labeling or immobilization of ligands can affect their biochemical activity, resulting in an inaccurate binding isotherm. Other characterization methods, such as boundary sedimentation velocity (Jensen and von Hippel, 1977) and UV difference spectra (Boraston, *et al*., 2000), do not require labeling of the molecule of interest, although labeling can be used if the behavior of a specific species needs to be isolated (Galletto, *et al*., 2003).

In this work, UV absorption measurements were adopted in conjunction with centrifugation of solutions of oligonucleotide and peptide, where the concentration of the oligonucleotide left in the supernatant could be determined. This method, also referred to as the depletion method (Creagh, *et al*., 1996), has the advantage of not requiring large quantities of samples or any chemical labelling. As will be shown later, this combination of UV absorption and centrifugation may be used for a wide range of solution systems where both molecular binding and subsequent aggregation occur. Oligodeoxynucleotides naturally exhibit a characteristic absorbance in the UV-Vis range. Upon peptide binding, aggregates made of peptide-ODN complexes formed. These aggregates could be centrifuged out, leaving behind a mixture of unbound ODNs and some EAK-ODN complexes in the

supernatant. The concentration of ODN in the supernatant was determined by UV absorption. The experimental results were treated with a binding density function analysis (Bujalowski, and Lohman, 1987; Bujalowski, and Klonowaka, 1994) to generate isotherms of the binding between peptide and ODNs. The outcome was analyzed further with the modified non-cooperative McGhee and von Hippel (MvH) model for the purpose of comparing the effects of solution conditions and ODN types (McGhee and von Hippel, 1974; Tsodikov, *et al*., 2001).

Some unique challenges are encountered when studying the interaction of a self-assembling peptide with an ODN. Since the peptide can self-assemble into nanostructures, EAK nanofibers in the present case (Zhang, *et al*., 1993; Fung, *et al*., 2003), there is a question as to whether EAK would bind to the ODN molecules directly, or EAK would first self-assemble into its aggregates to which the ODN binds subsequently. This paper presents a series of experiments designed to demonstrate that EAK binds to ODNs in molecular form, before the peptide self-assembly takes place. The peptide-ODN aggregates are believed to form after an initial step of molecular binding between peptide and ODN molecules, and a subsequent association of the peptide-ODN (intermediate) complexes into aggregates, possibly assisted by the inherent self-assembly capability of the peptide.

After binding and nanostructure formation with the peptide, the ODN was further evaluated for its accessibility to solvent species by fluorescence quenching experiments, as this property is critically important to assess the stability and potency of ODNs during their delivery both *in vitro* and *in vivo* (Plank, *et al*., 1999; Simeoni, *et al*., 2003). This study represents the first example in the literature where the binding of a self-assembling peptide to oligonucleotides is characterized.

3.2 Experimental Section

Materials and Methods

All reagents were of analytical grade and obtained from BDH (Poole, UK). The pH dependence of the binding of EAK to the ODNs was investigated by performing experiments at three different pHs. The pH 4 buffer was made with 0.171 M acetic acid and 0.029 M sodium acetate adjusted with acetic acid (Akinrimisi, *et al*., 1963); the pH 7 buffer was made with 0.01 M tris(hydroxymethyl)methylamine and 0.005 M sodium sulfate adjusted with sulfuric acid (Akinrimisi, *et al*., 1963); the pH 11 buffer was made with 0.1 M glycine and 0.1 M sodium chloride adjusted with sodium hydroxide (Bolumar, *et al*., 2003).

The EAK16-II peptide whose sequence is shown in Table 3.1 and the C-terminus carboxyfluorescein labeled EAK (FAM-EAK) were purchased from Research Genetics (Alabama, USA) and used without further purification.

Four single-stranded oligodeoxynucleotides (ssODNs), namely dG_{16}, dC_{16}, FAM-dC_{16} (dC_{16} labeled with carboxyfluorescein at the 5'-end), and dC_{16}-Rh (dC_{16} labeled with carboxytetramethylrhodamine at the 3'-end) were obtained with 95 % purity from Eurogentec North America (San Diego, USA) with HPLC purification. The ODN sequences are listed in Table 3.1. Solutions of the double-stranded ODNs (dsODNs) at different pHs were prepared one day before use by mixing two equimolar amounts of complementary ssODNs in the corresponding buffer in Eppendorf tubes, placing the tubes in a 95 ºC water bath for 5 minutes, turning off the water bath, and letting the solution slowly cool to room temperature.

Table 3.1. Type, name, and sequence of oligonucleotides (ODNs) and self-assembling peptide.

Type	Name	Sequence
Single-stranded ODN (ssODN)	dG_{16}	5'-GGG GGG GGG GGG GGG G-3'
	dC_{16}	5'-CCC CCC CCC CCC CCC C-3'
	FAM-dC_{16}	5'-Fluorescein-CCC CCC CCC CCC CCC C-3'
	dC_{16}-Rh	5'-CCC CCC CCC CCC CCC C-Rhodamine-3'
Double-stranded ODN (dsODN)	dGC_{16}	5'-GGG GGG GGG GGG GGG G-3' 3'-CCC CCC CCC CCC CCC C-5'
	FAM-dGC_{16}	5'-GGG GGG GGG GGG GGG G-3' 3'-CCC CCC CCC CCC CCC C-Fluorescein-5'
EAK16-II	EAK	n-AEAEAKAKAEAEAKAK-c
	FAM-EAK	n-AEAEAKAKAEAEAKAK-c-Fluorescein

UV-Vis Absorbance. UV-Vis absorption spectra were obtained on a Hewlett-Packard 8452A diode array spectrophotometer (California, USA) using a 50 μL quartz cuvette from Hellma (Müllheim, Germany).

Samples for the construction of binding isotherms were prepared at pH 4, 7, and 11. For each pH, three or four ODN concentrations of about 3 μM and 7 μM were used. At each ODN concentration, six to seven samples were prepared with EAK concentrations ranging from 0 to 0.2

mg/mL (equivalent to 0-120 μM) by mixing the ODN solution with different amounts of EAK powder. The resulting solutions were stirred vigorously for a few seconds with a vortex mixer and incubated at 25 ºC for 30 mins. The EAK-ODN aggregates formed in the solution were removed by centrifugation at 10,000 rpm for 2 minutes with a Centrifuge 5410 from Eppendorf (Hamburg, Germany). The supernatant was collected and its absorbance was measured on the spectrophotometer at wavelengths between 190 and 800 nm. Beer's Law was used to determine the total ODN concentration and the concentration of the ODN left in the supernatants from the absorbance of the ODN at 260 nm of the initial solution (OD_o) and the supernatant (OD_s), respectively. The term (OD_o-OD_s)/OD_o was defined as the relative UV-Vis absorbance change ΔOD_r. The obtained ΔOD_r were then analyzed using the ligand binding density function (23) to generate binding isotherms.

Polyacrylamide Gel Electrophoresis (PAGE). PAGE was applied to detect whether EAK-dsODN complexes/aggregates were present in the supernatant after centrifugation. Samples containing 3.6 μM of dGC_{16} with 0, 0.01, 0.1, or 0.2 mg/mL (0, 6, 60, or 120 μM) of EAK were prepared at pH 4 and 7. The supernatants obtained by centrifuging the samples were analyzed with non-denaturing 20 % PAGE. The polyacrylamide gels were 14 cm long × 15 cm wide × 0.5 mm thick. PAGE was performed in pH 4 or pH 7 buffer at 10 V/cm for 2 hrs. The gels were stained with a solution of 0.5 mg/mL ethidium bromide for 30 mins before being visualized with a Bio-Rad UV Transilluminator gel document system (California, USA).

Steady-State Fluorescence. Fluorescence spectra of dC_{16} labeled with carboxyfluorescein at the 5'-end (FAM-dC_{16}), dC_{16} labelled with carboxytetramethylrhodamine at the 3'-end (dC_{16}-Rh), and EAK labeled with carboxyfluorescein at the C-terminus (FAM-EAK) were acquired on a Photon Technology International steady-state fluorometer (New Jersey, USA) equipped with a Ushio UXL-75Xe Xenon arc lamp and PTI 814 photomultiplier detection system. The peak absorption wavelength of the solution was chosen as the excitation wavelength (λ_{ex}). For the FAM-dC_{16} and FAM-EAK solutions, λ_{ex} was 452 nm at pH 4 and 494 nm at pH 7, respectively; for the dC_{16}-Rh solutions, λ_{ex} was 560 nm at both pH 4 and pH 7.

Steady-State Fluorescence Anisotropy. Anisotropy of the supernatants obtained after centrifuging the solutions was measured using the steady-state fluorometer with polarizers fitted on the excitation and emission monochromators. Each sample was excited with vertically polarized light, and the fluorescence intensity was separately detected with the emission polarizer set in the vertical (I_{VV}) and horizontal (I_{VH}) orientations. In a fluorescence anisotropy experiment, the polarization dependence of the emission monochromator was corrected by the *G* factor (Lakowicz, 1999). To obtain the G factor, the excitation polarizer was set to the horizontal direction, and the fluorescence intensities were measured individually with vertical (I_{HV}) and horizontal (I_{HH}) emission polarization.

The G factor is given by the I_{HV}/I_{HH} ratio. The fluorescence anisotropy (r) was calculated using Equation 3-1 (Lakowicz, 1999)

$$r = \frac{I_{VV} - GI_{VH}}{I_{VV} + 2GI_{VH}} \tag{3-1}$$

The wavelength corresponding to the maximum absorption of FAM was chosen as the excitation wavelength (λ_{ex}). The fluorescence intensity was monitored at 514 nm, the peak wavelength of the emission spectra.

Time-Resolved Fluorescence Decays. Fluorescence decays were acquired by the time-correlated single photon counting technique on a time-resolved fluorometer (IBH system 2000, Glasgow, UK). Samples containing 3.6 μM of the chromophore-labeled dC_{16} were prepared in the presence and the absence of 0.2 mg/mL (120 μM) EAK at pH 4. The excitation wavelength (λ_{ex}) and emission wavelength (λ_{em}) were set to the wavelength corresponding to the absorption and emission maxima of the chromophores. For FAM-dC_{16}, λ_{ex} and λ_{em} were 452 nm and 514 nm, respectively; for dC_{16}-Rh, λ_{ex} and λ_{em} were 560 nm and 580 nm, respectively. A right angle configuration was used between the excitation and emission monochromators. All decay curves were collected over 512 channels with the rate of 59.3 ps/ch and with a total of 20,000 counts in the channel of maximum intensity. The analysis of the decay curves started by acquiring the instrument response function obtained with a scattering solution, which was then convoluted with a sum of exponentials shown in Equation 3-2 (Lakowicz, 1999)

$$I(\mathrm{t}) = \sum_{i=1}^{N} \alpha_i e^{-t/\tau_i} \tag{3-2}$$

where i=1, 2,… N; N is the minimum number of exponentials required to achieve a good fit (N<4). The fitting parameters were optimized using the Marquardt-Levenberg algorithm (Press, *et al*., 1992). The fits of the fluorescence decays were deemed satisfactory when the χ^2 value was smaller than 1.2 and the residuals and autocorrelation function of the residuals were randomly distributed around zero.

Static Light Scattering (SLS). SLS intensity of solutions of EAK, ODNs, and their mixtures was monitored at right angle with the steady-state fluorometer by irradiating the solution at 350 nm where the ODNs and EAK do not absorb or emit.

Dynamic Light Scattering (DLS). The hydrodynamic diameter of the EAK-ODN complexes/aggregates in the pH 4 buffer was obtained with a Zetasizer Nano ZS instrument equipped with a 4 mW He-Ne laser operating at 633 nm (Malvern, UK). All measurements were performed at 25 ºC at a measurement angle of 173º. Dust particles were found to be absent in the buffer solutions used to prepare the samples, as confirmed by dynamic light scattering. DLS experiments were performed 30 mins after sample preparation.

Atomic Force Microscopy (AFM). A Picoscan atomic force microscope (Molecular Imaging, Arizona, USA) was used to study the morphology of the EAK-ODN complexes/aggregates in solution. It was operated in magnetic AC (MAC) tapping mode in solution using magnetically coated cantilevers, Type II MAClevers (Molecular Imaging, Arizona, USA), with a spring constant of 0.5 N/m and a resonance frequency of ~27 kHz at room temperature. A volume of 400 μL of each solution was deposited on a freshly cleaved mica surface, inside a Teflon liquid chamber, where the AFM images were acquired.

3.3 Theoretical Background

As will be shown in the Results and Discussion section, interaction of EAK with ODN results in aggregates composed of EAK and ODN. The fraction of ODNs in the aggregates can be obtained from the relative change in absorbance, ΔOD_r, described in the Experimental Section. It has been shown (Teif, and Lando. 2001; Teif, 2005) that the fraction of ODN in aggregates is a unique function of binding density (ν), which is in turn a sole function of the free ligand concentration (P_f). The binding density, ν, is defined as (McGhee and von Hippel, 1974; Ballin, *et al*., 2004)

$$\nu = P_b / D_t \tag{3-3}$$

with P_b being the concentration of the total bound peptide and D_t the total ODN concentration expressed in terms of phosphate groups. Thus, ΔOD_r is a unique function of P_f. The ligand binding density function proposed by Bujalowski and Lohman (Bujalowski and Lohman, 1987; Bujalowski and Klonowaka, 1994) can be adopted to construct a binding isotherm by creating a data set (ν, P_f). This procedure is described in more detail in the Section 2.4 of Chapter 2. Briefly, for any given ΔOD_r, Equation 3-4 relates P_f to the total peptide concentration and the total ODN concentration:

$$P_{tx} = P_f + \nu D_{tx} \tag{3-4}$$

where P_{tx} and D_{tx} represent the total concentrations of peptide and ODN at the xth ODN concentration (there are four ODN concentrations for each system, see Figure 3.1), respectively. Since P_f and ν are constant values for a given ΔOD_r, the binding density ν can be obtained from the slope of the plot of P_t *vs*. D_t.

The procedure for building binding isotherms consists of using three or four ODN concentrations and plotting the fraction of ODN in the aggregates, i.e., ΔOD_r, as a function of the total peptide concentration (Figure 3.1). Each plot could be fitted reasonably well with the empirical equation $\Delta OD_r = A \times P_t/(1+B \times P_t)$, where A and B are regression parameters which are listed in Table 3.2. In this paper, sets of ν and P_f were obtained from the plot of P_t *vs*. D_t for a given ΔOD_r. Seven-to-ten ΔOD_r values were chosen. For each ΔOD_r value, the value of P_t was read from the fits of the curves shown in Figure 3.1 and plotted as a function of D_t. Then P_f and ν were obtained from the intercept and slope of the plot of P_t *vs*. D_t. Plotting ν/P_f versus ν generated the binding isotherms (Figure 3.2).

The interaction/binding between EAK and ODN molecules most likely starts with the formation of the EAK-ODN complexes as will be argued in the Results and Discussion section, which is followed by further association of the complexes into aggregates. This process is described in Scheme I

Scheme I

$$ODN + EAK \underset{}{\overset{K_c}{\rightleftharpoons}} [ODN, EAK]_{complexes} \overset{K_a}{\rightleftharpoons} [ODN, EAK]_{aggregates}$$

where K_c and K_a are the equilibrium constants for the formation of EAK-ODN complexes from unimolecular ODN and EAK and for the formation of EAK-ODN aggregates from the association of EAK-ODN complexes, respectively. One important aspect of the procedure described above is that, although ΔOD_r represents the fraction of ODNs present in the aggregates and does not account for the ODNs present in the supernatant as EAK-ODN complexes, ΔOD_r is still a unique function of P_f and ν as demonstrated by the work of Teif et al. (Teif, and Lando. 2001; Teif, 2005).

No suitable theoretical model could be found in the literature to describe the molecular binding (K_c) and aggregation (K_a) simultaneously unless the binding isotherm for each of the two steps has been constructed, which is not experimentally favored. To facilitate the analysis of the binding isotherms, i.e., the ν/P_f versus ν trends shown in Figure 3.2, the modified non-cooperative McGhee and von Hippel (MvH) model (McGhee and von Hippel, 1974; Tsodikov, *et al*., 2001) was used

$$\frac{\nu}{P_f} = K(1-n\nu)\left(\frac{1-n\nu}{1-(n-1)\nu}\right)^{(n-1)}\left(\frac{N-n+1}{N}\right) \qquad (3\text{-}5)$$

where K is the overall binding constant, accounting for both molecular binding and aggregation steps.

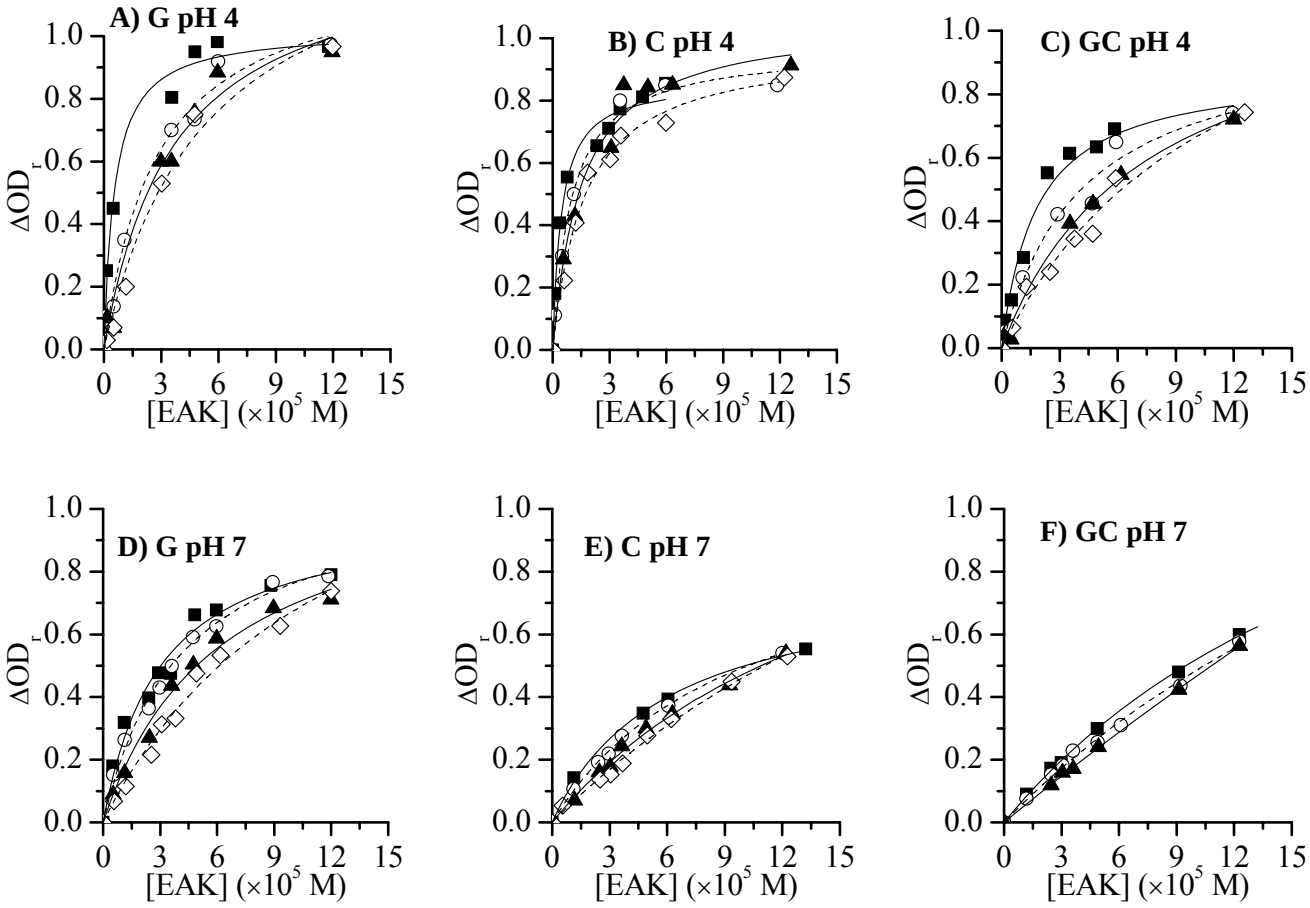

Figure 3.1. Plots of $\Delta\ OD_r$ as a function of the total EAK concentration. (A) pH 4, phosphate concentration of dG_{16} equals 32 μM (■), 64 μM (○), 94.4 μM (▲), and 152 μM (◇). (B) pH 4, phosphate concentration of dC_{16} equals 24 μM (■), 48 μM (○), 90 μM (▲), and 116.8 μM (◇). (C) pH 4, phosphate concentration of dGC_{16} equals 64 μM (■), 128 μM (○), 240 μM (▲), and 288 μM (◇). (D) pH 7, phosphate concentration of dG_{16} equals 16 μM (■), 32 μM (○), 64 μM (▲), and 96 μM (◇). (E) pH 7, phosphate concentration of dC_{16} equals 16 μM (■), 32 μM (○), 64 μM (▲), and 96 μM (◇). (F) pH 7, phosphate concentration of dGC_{16} equals 32 μM (■), 64 μM (○), and 128 μM (▲). The solid and dashed lines represent the best fits to the equation ΔOD_r = A×[EAK]/(1+B×[EAK]), but do not have any physical meaning. The A and B parameters have been listed in Table 3.2. Data in the range of 20-70 % of maximal ΔOD_r are used to obtain the ν and ν/P_f values reported in Figure 3.2.

Table 3.2. Parameters A and B retrieved from the fits of the ΔOD_r versus [EAK] plots shown in Figure 3.1 with the empirical equation: $\Delta OD_r = A \times [\text{EAK}] / (1 + B \times [\text{EAK}])$.

pH 4	dG_{16}			
Concentration	2.0 μM	4.0 μM	5.9 μM	9.5 μM
A (10^{-4})	18.454 ± 3.465	4.513 ± 0.507	3.574 ± 0.613	2.846 ± 0.248
B (10^{-4})	18.088 ± 3.853	3.645 ± 0.599	2.750 ± 0.751	2.053 ± 0.306

pH 4	dC_{16}			
Concentration	1.5 μM	3.0 μM	5.0 μM	7.3 μM
A (10^{-4})	19.262 ± 2.549	9.747 ± 0.981	6.954 ± 1.074	5.871 ± 0.583
B (10^{-4})	22.309 ± 3.481	10.073 ± 1.249	6.547 ± 1.328	5.996 ± 0.823

pH 4	dGC_{16}			
Concentration	2.0 μM	4.0 μM	7.5 μM	9.0 μM
A (10^{-4})	4.871 ± 0.671	2.436 ± 0.414	1.599 ± 0.153	1.247 ± 0.140
B (10^{-4})	5.539 ± 1.048	2.440 ± 0.670	1.367 ± 0.254	0.878 ± 0.236

pH 7	dG_{16}			
Concentration	1.0 μM	2.0 μM	4.0 μM	6.0 μM
A (10^{-4})	3.309 ± 0.387	2.612 ± 0.176	1.834 ± 0.163	1.237 ± 0.095
B (10^{-4})	3.318 ± 0.587	2.425 ± 0.269	1.636 ± 0.267	0.844 ± 0.160

pH 7	dC_{16}			
Concentration	1.0 μM	2.0 μM	4.0 μM	6.0 μM
A (10^{-4})	1.341 ± 0.082	1.001 ± 0.027	0.752 ± 0.036	0.621 ± 0.034
B (10^{-4})	1.686 ± 0.175	1.035 ±0.063	0.585 ± 0.085	0.339 ± 0.081

pH 7	dGC_{16}		
Concentration	1.0 μM	2.0 μM	4.0 μM
A (10^{-4})	0.748 ± 0.019	0.631 ± 0.035	0.503 ± 0.011
B (10^{-4})	0.442 ± 0.038	0.306 ± 0.077	0.082 ± 0.023

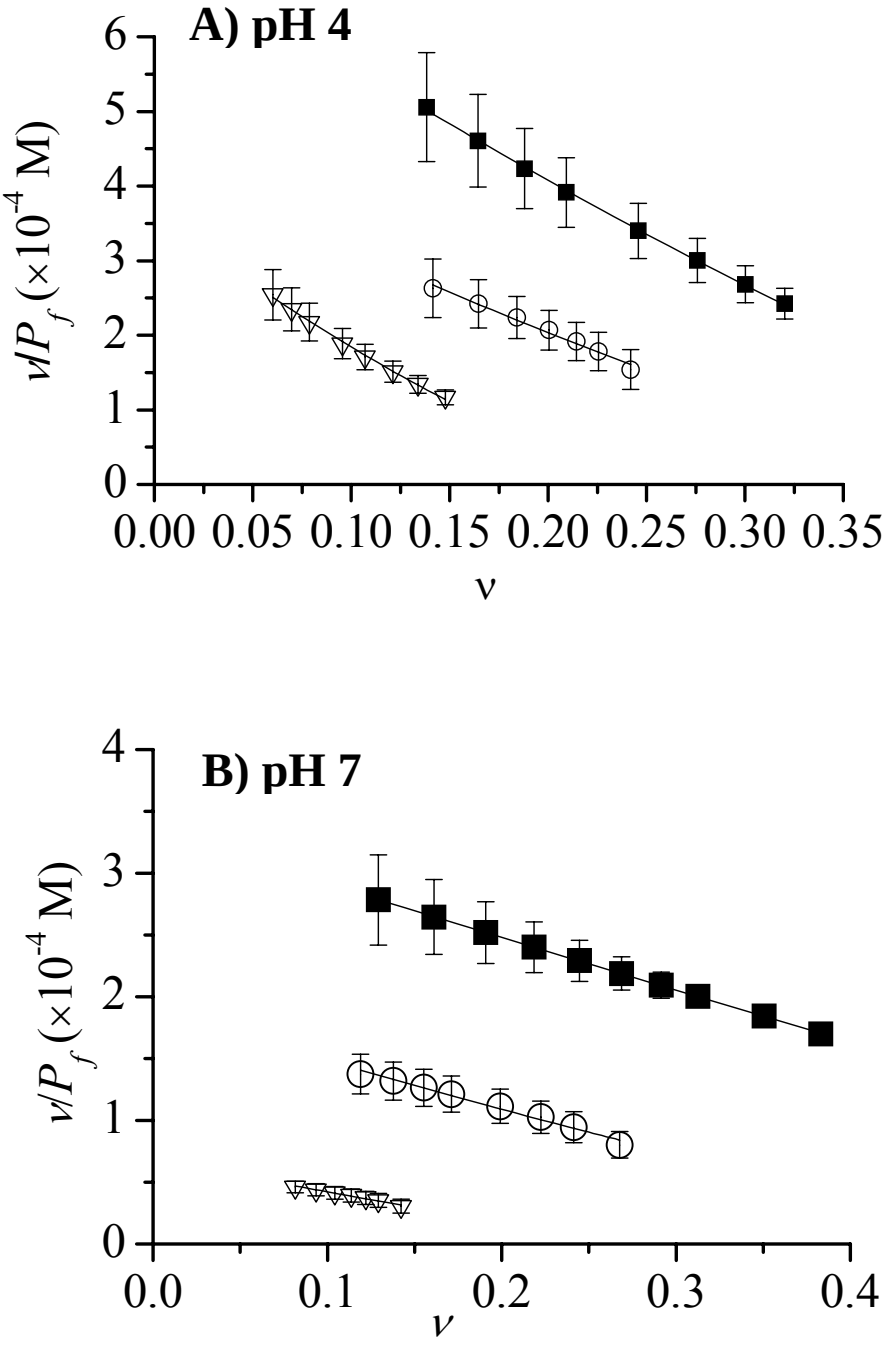

Figure 3.2. Plot of ν/P_f versus ν for the binding of EAK to dG_{16} (■), dC_{16} (Δ), and dGC_{16} (×) at (A) pH 4 and (B) pH 7. The solid lines represent the best fits to Equation 3-5. The parameters used in the fits are listed in Table 3.3.

It was noted that the MvH model describes the initial complexation process only, and does not take into account the second aggregation step. Nevertheless, we opted to use the MvH model for the following reasons: First, the main goal of the current study was to find differences or similarities in the process leading to the formation of EAK-ODN aggregates under different experimental conditions, e.g., pHs and nucleotide types; in other words, the MvH model is used for comparison purpose, as has been practiced before (Casas-Finet, *et al*., 1993). Second, the binding constant *K* calculated from the MvH model actually shows trends for the binding strength of EAK to different ODNs and under various solution conditions, which are also comparable with those reported for the binding of other DNA/peptide pairs. With these considerations, the binding isotherms shown in Figure 3.2 were fitted with Equation 3-5. Third, our experimental data are for equilibrium analyses. Although one can derive equilibrium equations for aggregation systems from the kinetic expressions of some aggregation models, such as the colloidal coagulation model, there are certain unique features in our systems that have not been dealt with in any of these coagulation models. The reasons are as follows: 1) our system starts with an initial complexation between peptide and oligo molecules, which we showed with the detection of dimers. It is then followed with aggregation of complexes, which we showed with the detection of aggregates. None of the current coagulation models actually describes this two-step event. It is reasonable to assume the kinetics is different between complexation and aggregation. It has been shown (von Hippel et al.) for the peptide-oligo complexation, the conventional kinetics, such as those based on the law of mass action, does not work. Thus, the conventional coagulation approaches will not be appropriate, even for dimer or oligomer formation. 2) if we were to use the McGhee and von Hippel (MvH) model for the first complexation and a coagulation model for our aggregation kinetics, the current coagulation model tends not to work as it has many limitations, e.g., the coagulates are from the association of spherical particles, the collisions are binary and that fluctuations in density are sufficiently small, and the clusters are considered to move due to free Brownian motion. One of these limitations is the assumption of spherical particles. From our experiments, we have fibrillar aggregates, which indicate the aggregation mechanisms in our case may be very different from other colloidal aggregation that the current coagulation models apply to. It is conceivable that the similar arguments used in the MvH model, related to the structure of the particles and arrangement probabilities, have to be implemented in the coagulation model. This however has not been considered yet in any of the current analyses. 3) we may try to develop a coagulation model by taking into account the detailed structural information and using a similar approach to that of von Hippel et al.; however, this will take tremendous effort and be beyond the scope of the current work.

3.4 Results and Discussion

This study aims at describing the interaction of EAK with ODNs. To reach this goal, several issues were addressed by carrying out a number of separate experiments. Each issue is treated in a separate part in this section. The structure of this section is briefly laid out here. First, proof of the binding of EAK to the ODNs was obtained by conducting absorption measurements on the supernatant of centrifuged solutions of the EAK-ODN mixtures. Second, PAGE, fluorescence anisotropy, and UV-Vis absorption measurements were conducted to confirm that the quantity ΔOD_r is an appropriate representation of the fraction of ODNs incorporated in the EAK-ODN aggregates. Third, fluorescence anisotropy and steady-state light scattering experiments established that the time scale over which the EAK-ODN aggregates form is much shorter than that over which the self-assembly of EAK occurs. Fourth, the size of the EAK-ODN aggregates was determined using AFM and dynamic light scattering. Fifth, the modified MvH model was used to compare the binding of EAK to the ODNs under different pHs and nucleotide types. Sixth, the accessibility of the ODNs to the solvent once encapsulated inside the EAK-ODN aggregates was investigated by performing fluorescence quenching experiments.

3.4.1 Effect of pH on Binding

EAK contains four glutamic acids (Glu, E) and four lysines (Lys, K) with pK_a values of 4.25 and 10.53, respectively (Lehninger, 1993). The carboxylic acid of Glu and the amine of Lys are negatively and positively charged at pH 7, respectively. Therefore, EAK exhibits alternating negative and positive charges along its backbone at pH 7. Since glutamic acid residues are mostly protonated under acidic conditions at pHs below 4.25, EAK molecules are expected to be positively charged at pH 4. Similarly Lys becomes neutral at pHs above 10.53, so that EAK molecules are expected to be negatively charged at pH 11. Since the binding of negatively charged ODNs to cationic molecules, such as lysine-rich peptides, is believed to be due to electrostatic attraction (Gottschalk, *et al*., 1996), the different charges born by EAK at different pHs should affect the binding of EAK to the ODNs, with a higher binding constant being expected at lower pHs. To check whether this prediction is correct, the binding of EAK to dC_{16}, dG_{16}, and dGC_{16} was monitored at pH 4, 7, and 11. Solutions were prepared with different EAK concentrations at two ODN concentrations. The absorbance of the solution supernatant was measured after the EAK-ODN aggregates had been centrifuged out. The relative change in absorbance, ΔOD_r, was calculated by following the procedure described in the Experimental Section. Plots of ΔOD_r as a function of the total EAK concentration were generated for each ODN concentration at pH 4 and 7 (Figure 3.1)).

In Figure 3.1, ΔOD_r is found to increase with increasing total EAK concentration, eventually leveling off for the single-stranded dG_{16} and dC_{16} at pH 4. This trend indicates that more EAK binds to the ODNs upon increasing the EAK concentration, until the ssODNs are saturated. ΔOD_r increases with increasing EAK concentration at pH 7 for both the ssODNs and the dsODN; however, it requires higher EAK concentration to reach the plateau. Furthermore at a given ODN concentration, the ΔOD_r values at pH 7 are significantly lower than those at pH 4. These results suggest that increasing the pH from 4 to 7 results in a much weaker binding between EAK and the ODNs. At pH 11, no binding of EAK to the ODNs could be detected as the EAK concentration was varied from 0 to 120 μM and ΔOD_r equaled zero. Considering that the charge of EAK is changed from positive to neutral, and then to negative when the pH is increased from 4 to 7, and then to 11, the trends shown in Figure 3.1 confirm the important role played by the electrostatic forces in the binding of EAK to the ODNs.

Figure 3.1 also shows the effect of the nucleotide type on binding. The ΔOD_r values for dG_{16} are higher than those for dC_{16} at a given EAK concentration, implying that more EAK binds to dG_{16} than to dC_{16}.

3.4.2 Nature of the ODNs Remaining in the Supernatant after Centrifugation

The fraction of the ODN in the EAK-ODN aggregates was determined from the relative UV absorbance change of the solution, ΔOD_r, by assuming that no EAK-ODN aggregates remained in the supernatant after centrifugation. The validity of this assumption was verified first by fluorescence anisotropy experiments.

Fluorescence anisotropy reflects changes in the rotational correlation time of a chromophore, which is related to the hydrodynamic volume of the species to which the chromophore is attached. Larger particles have a longer rotational correlation time, hence a larger anisotropy (Lakowicz, 1999). Solutions containing 3.6 μM of FAM-dGC_{16} or of FAM-dC_{16} were mixed at pH 4 and pH 7 with EAK concentrations ranging from 0 to 0.2 mg/mL (0-120 μM). The solutions were centrifuged and the fluorescence anisotropy of the supernatants was measured. The anisotropy of the supernatants was plotted in Figure 3.3 as a function of EAK concentration. The fluorescence anisotropy of FAM-labeled ODNs equals 0.11 ± 0.01 and 0.04 ± 0.01 at pH 4 and pH 7, respectively. It does not equal 0.02 or so as expected for a free chromorphore, because FAM cannot rotate freely and rapidly when it is covalently bound to ODNs. The lower anisotropy for FAM-ODN at pH 7 might be due to the decay time of FAM-ODN which increases from 3.3 ns to 4.1 ns when the pH of the solution is raised from 4 to 7. When the FAM-labeled ODN solution was mixed with increasing EAK concentrations, the anisotropy of the FAM-labeled ODN species left in the supernatants ranged from 0.08 to 0.12 and

0.03 to 0.04 at pH 4 and pH 7, respectively, which was very close to that of the FAM-labeled ODN. These experiments indicate that, within the limit of accuracy of fluorescence anisotropy, the hydrodynamic volume of the fluorescently labeled species present in the supernatant of the EAK-ODN solutions remains the same as that of FAM-ODN. The results demonstrate that unimers of ODN existed in the centrifuged solutions; no EAK-ODN aggregates were detected.

To estimate the resolution limit of the fluorescence anisotropy experiments, the anisotropy of a 1 μM solution of FAM-dC_{16} was measured as a function of EAK concentration at pH 4 and was plotted in Figure A in the Appendices. With the *K* and *n* values (Table 3.3) retrieved from the analysis of the binding isotherms (Figure 3.2) using Equation 3-5, the fraction of ODNs incorporated in the EAK-ODN aggregates could be calculated and is also plotted in Figure A. It was found that ~10 mol% of ODNs needs to be present in the EAK-ODN aggregates to induce a detectable change in fluorescence anisotropy. Consequently the small anisotropy found in Figure 3.3 suggests that if EAK-ODN aggregates are left in the supernatant, they account for less than 10 mol% of the total ODN population. In other words, ΔOD_r shown in Figure 3.1 is an accurate representation of the fraction of ODNs in the EAK-ODN aggregates within ± 10 mol%.

UV-Vis absorption experiments were performed to demonstrate the existence of EAK-ODN complexes in the supernatant that were not detected in the anisotropy experiments. The absorption spectra of the samples containing 3.9 μM of dC_{16}–Rh in the presence and absence of 60 μM EAK were acquired before and after centrifugation. As shown in Figure 3.4, the absorption spectrum of a mixture of dC_{16}-Rh and EAK is different from that of free dC_{16}-Rh. Mixing dC_{16}-Rh with EAK induced a decrease in the absorbance at the 563 nm band characteristic of dC_{16}-Rh, and the appearance of a new prominent absorption band at 524 nm. The ratio of absorbance at 524 and 563 nm (OD_{524}/OD_{563}) for dC_{16}-Rh is 0.50 ± 0.01 and is concentration-independent as shown in Figure 3.4B. This ratio changes to 0.89 and 0.78 after mixing with EAK, before and after centrifugation, respectively. Since EAK does not absorb where dC_{16}-Rh does, the spectra and ratio of OD_{524}/OD_{563} for the mixtures would not be different from that of dC_{16}-Rh alone if there were no complexation between EAK and dC_{16}-Rh. The increase in the ratio of OD_{524}/OD_{563} might be due to the dimer formation of rhodamine (Förster and König, 1957; Hamman, *et al*., 1996) after EAK complexed with dC_{16}-Rh. Since most aggregates are centrifuged out and the ratio of OD_{524}/OD_{563} after centrifugation is similar to that before centrifugation, what remains in the supernatant causing the higher OD_{524}/OD_{563} ratio must be complexes, which are too small to be centrifuged out.

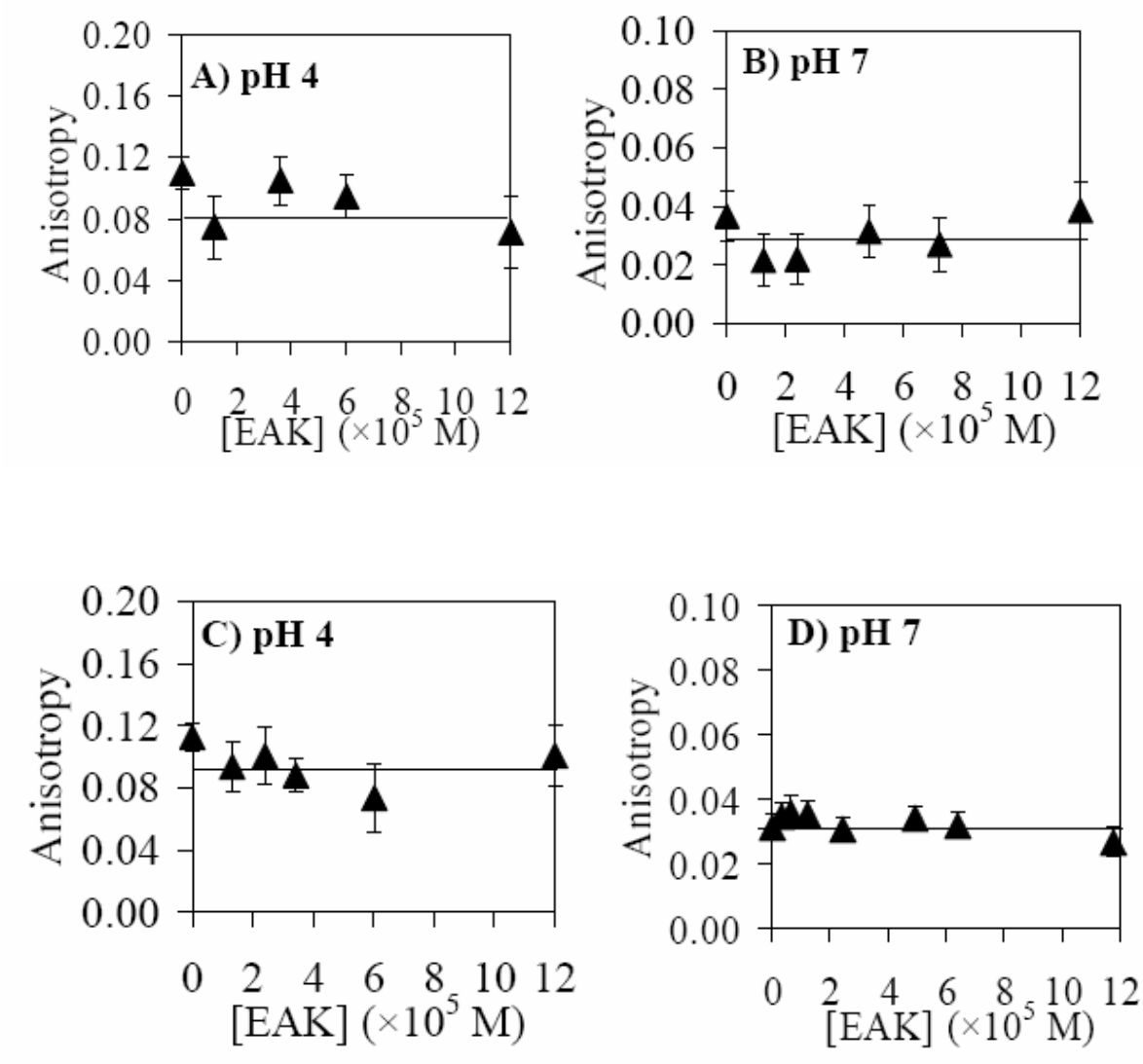

Figure 3.3. Fluorescence anisotropy of the supernatant of EAK solution mixed with 3.6 μM of (A) FAM-dGC$_{16}$ at pH 4 (λ_{ex}=452 nm, λ_{em}=514 nm), (B) FAM-dGC$_{16}$ at pH 7 (λ_{ex}=494 nm, λ_{em}=514 nm), (C) FAM-dC$_{16}$ at pH 4 (λ_{ex}=452 nm, λ_{em}=514 nm), and (D) FAM-dC$_{16}$ at pH 7 (λ_{ex}=494 nm, λ_{em}=514 nm).

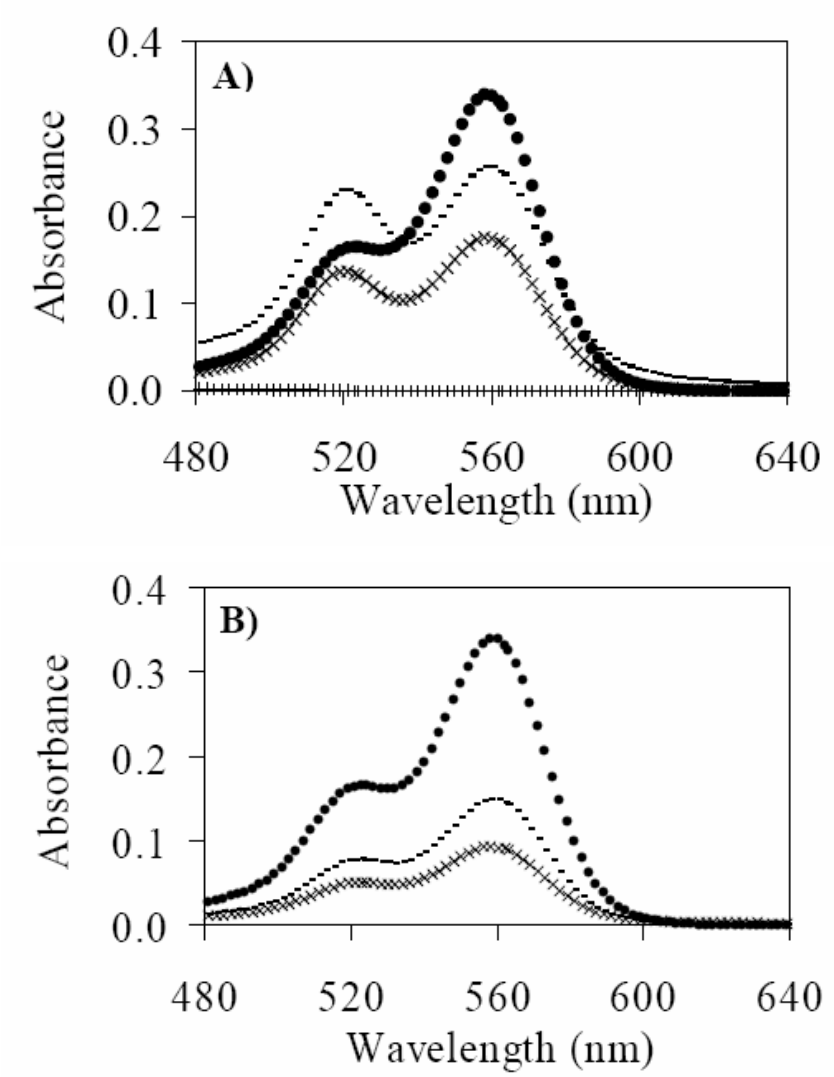

Figure 3.4. UV absorption spectra of dC_{16}-Rh in the presence and absence of EAK at pH 7. (A) 3.9 μM dC_{16}-Rh (●), 60 μM EAK(+), 3.9 μM dC_{16}-Rh and 60 μM EAK before centrifugation (−) and after centrifugation (×); (B) dC_{16}-Rh at concentration of 3.9 μM (●), 2.0 μM (−), and 1.3 μM (×).

Using the extinction coefficients of the rhodamine dimer reported in the literature (Hamman, *et al*., 1996), the data given in Figure 3.4A can be analyzed to estimate the concentrations of ODNs present in the solution as unimers (1.39 μM), complexes (1.63 μM), and aggregates (0.88 μM). In this situation, ΔOD_r would equal (0.88 μM)/(3.9 μM) = 0.23, close to the value of 0.28 obtained from the K and n values listed in Table 3.3. The agreement observed between the ΔOD_r values obtained through two different means supports the protocol discussed in the Theoretical Background for

analyzing the UV-Vis binding results (Figure 3.2). Despite the substantial amount of complexes remaining in the supernatant after centrifugation, no increase in anisotropy was observed in the supernatant (Figure 3.3C), whereas the presence of aggregates in the solution results in an observable increase in the anisotropy of the solution (Figure A). These observations suggest that the aggregates are much larger and more compact than the complexes, resulting in reduced mobility of the fluorescein label. More importantly, they highlight the structural difference between the flexible complexes and the large, compact and rigid aggregates.

Non-denaturing PAGE experiments were further conducted to investigate the nature of dsODN in the supernatant after centrifugation. Samples containing 3.6 μM of dGC_{16} mixed with 0, 6, 60, or 120 μM of EAK were centrifuged and their supernatants were run on a 20 % native gel at pH 4 and pH 7. As shown in Figure 3.5A, for the gel obtained at pH 4 and stained with ethidium bromide, the bands corresponding to the supernatants of EAK-dGC_{16} mixtures (Lanes 2-4) appear at the same position as the band corresponding to dGC_{16} (Lane 1). A similar observation was obtained for the gel run at pH 7 with the EAK-dGC_{16} mixtures (Figure 3.5B). These results suggest that no EAK-dGC_{16} aggregates of a size equivalent to 6-100 bp duplexes (Sambrook, *et al*., 1989) (i.e., the separation range of a 20 % polyacrylamide gel) remain in the supernatants after centrifugation.

The above three experiments have shown that the centrifugation has separated the EAK-ODN aggregates from the original EAK-ODN solution. In the supernatant, there exist free EAK and ODN molecules, as well as EAK-ODN complexes. The fact that the complexes were not detected in either PAGE or anisotropy experiments is due to the inherent resolution limits of the anisotropy and PAGE experiments.

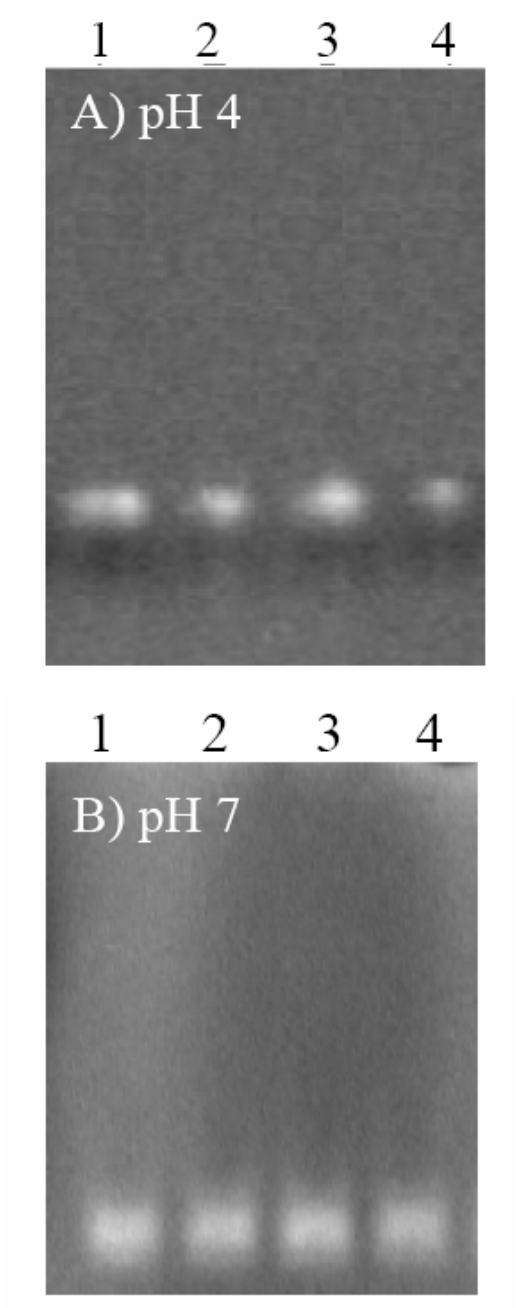

Figure 3.5. 20 % PAGE of 3.6 μM of dGC_{16} mixed with EAK at (A) pH 4 and (B) pH 7. The EAK concentrations are 0, 6, 60, 120 μM in lanes 1, 2, 3, and 4, respectively.

3.4.3 Pathway of the EAK-ODN Binding

Considering that EAK in solution has the potential to self-assemble and form aggregates, two most likely pathways can be proposed for the formation of EAK-ODN aggregates. In Pathway 1, EAK self-assembles into the aggregates onto which the ODNs bind to form the EAK-ODN aggregates. In

Pathway 2, the self-assembly of EAK occurs on a time scale which is much longer than the binding of molecular EAK onto ODNs. In this case, the complexation of molecular EAK with ODN molecules occurs first, and is followed by the association of these complexes into aggregates. To identify which pathway is leading to the formation of EAK-ODN aggregates, the time scale over which EAK self-assembles in solution was estimated. To this end, the fluorescence anisotropy of EAK and EAK-dG_{16} mixtures was measured at pH 4 and 7 over a one hour period immediately after sample preparation using carboxyfluorescein-labeled EAK (FAM-EAK). These experiments were performed with 0.1 mg/mL (60 μM) EAK solutions where 1 in 100 EAK molecules was fluorescently labeled. To these solutions, 5 μM of dG_{16} was added. The steady-state fluorescence anisotropy of EAK and the EAK-dG_{16} mixtures was measured at pH 4 and 7 as a function of time. The results are shown in Figure 3.6A and Figure 3.6B. Whether at pH 4 or 7, the fluorescence anisotropy of FAM-EAK alone remains constant as a function of time and equals 0.10 and 0.05, respectively. This trend indicates that EAK does not self-assemble in solution within a 1 hr period, at least to the resolution limit of the anisotropy measurements. On the other hand, addition of dG_{16} to the EAK solution results in a large increase in anisotropy, which reflects a large increase in the hydrodynamic volume of the species present in solution. These species are the EAK-ODN aggregates which may be centrifuged out.

The interaction between individual EAK and ODN molecules was further confirmed by SLS experiments on EAK and EAK-dG_{16} mixtures. The light scattered by the EAK solution remained constant within the first 20 mins at pH 4 and pH 7 as shown in Figure 3.7A and Figure 3.7B, respectively. As a control, the light scattered by dG_{16} in the buffer solution and by the buffer solution alone was also monitored for 20 mins. The SLS intensity of both solutions remained constant and close to the SLS intensity of the solution containing EAK only. These results indicate that the size of EAK remains constant during the first 20 mins after sample preparation. In comparison, the SLS intensity of the EAK-ODN mixtures increased initially and then leveled off within 30 mins at both pHs. Since an increase in SLS intensity reflects an increase in particle size, these results confirm that the size of the complexes/aggregates increases up to a plateau ~ 30 minutes after mixing, a conclusion similar to that drawn from the anisotropy experiments (Figure 3.6). It is noted that the time scales for the formation of EAK-ODN aggregates shown in Figures 3.6 and 3.7 are slightly different. This is due to experimental delays between the time the EAK-ODN mixture was prepared and the measurement was conducted, which resulted in inaccuracy for the first 5 minutes. However, one can still conclude that the time scale for the formation of EAK-ODN aggregates is much shorter than that needed for EAK to self-assemble.

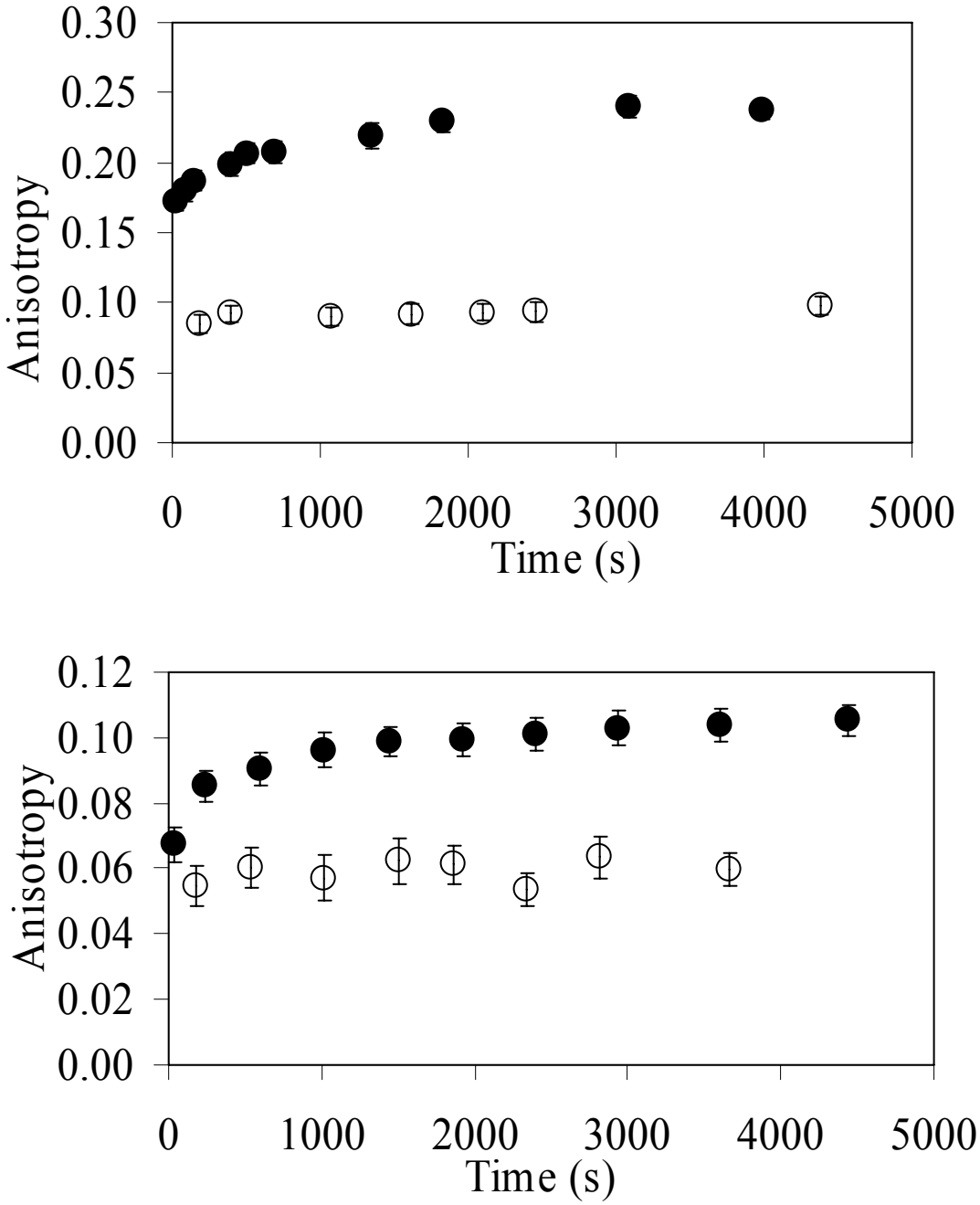

Figure 3.6. Fluorescence anisotropy of a 0.1 mg/mL EAK solution containing 1 mol % of FAM-EAK in the presence (●) and in the absence (○) of (A) 3.6 μM of dG_{16} at pH 4 (λ_{ex}=452 nm and λ_{em}=514 nm) and (B) 4.3 μM of dG_{16} at pH 7 (λ_{ex}=494 nm and λ_{em}=514 nm).

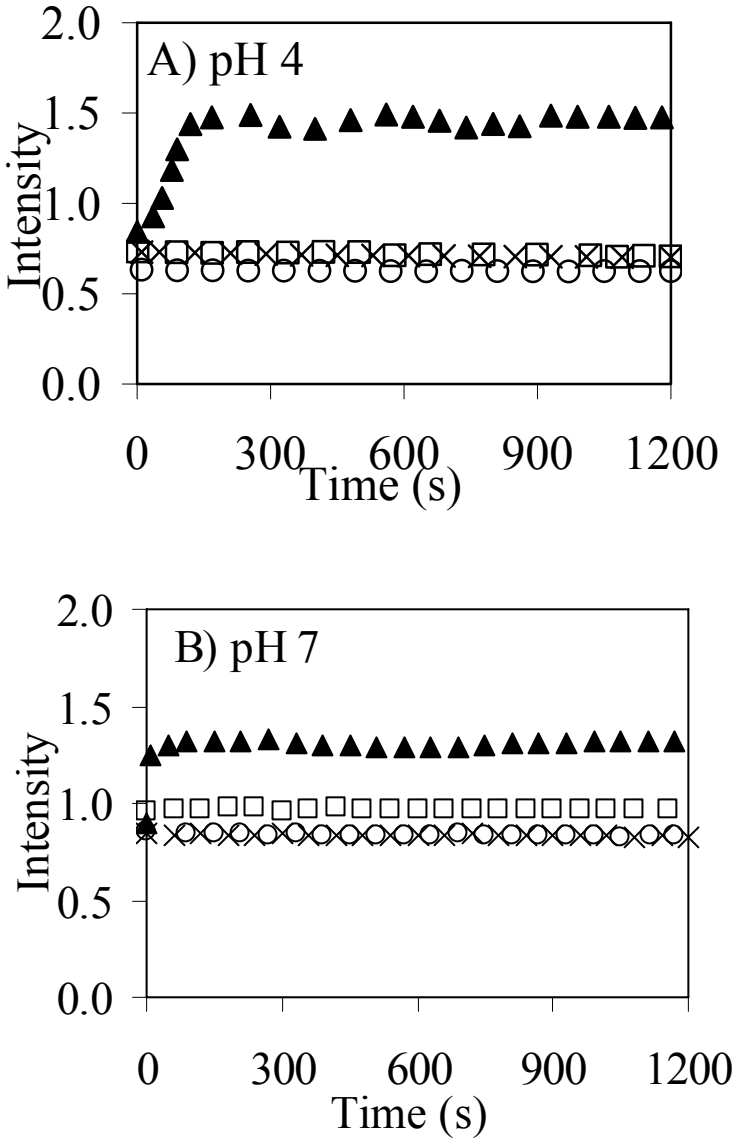

Figure 3.7. SLS experiments performed on (○) the buffer and on solutions containing (▲) 3.6 μM dG_{16} and 0.1 mg/mL EAK, (□) 0.1 mg/mL EAK, (×) 3.6 μM dG_{16} at (A) pH 4 and (B) pH 7. $\lambda_{ex}=\lambda_{em}$ =350 nm.

3.4.4 Size Characterization of EAK-ODN Aggregates by AFM and DLS

The size of the EAK-ODN aggregates was characterized using AFM and DLS. Images of the dG_{16}-EAK solution taken 8 and 60 mins after sample preparation are shown in Figure 3.8. Both small fibers and large aggregates were found after 8 and 60 mins and the sizes of these objects did not change during the 1 hr time period. The sizes of the smaller fibers are 36 nm wide, 5.2 nm tall and over 100 nm long. The large aggregates appear to be giant clusters of small fibers with lateral

dimensions of 650 nm and a height of 35 nm. Two control experiments were performed: No nanostructure could be detected when a 2 μM dG_{16} solution was imaged by AFM. Sparsely distributed globular structures with a diameter of 34 nm and a height of 1 nm were observed for the 0.1 mg/mL (60 μM) EAK solution 45 mins after solution preparation, which indicated that the majority of EAK molecules do not self-assemble into fibers (images shown in Section B of the Appendices). The small fibers and giant aggregates observed in the AFM images of the EAK-dG_{16} solution are likely due to the association of the EAK-ODN complexes into aggregates. Since the morphologies of the aggregates observed after 8 and 60 mins are very similar, it suggests that the entire complexation process between dG_{16} and EAK is completed within a short time period, less than 10 mins, which agrees with the conclusions drawn from the anisotropy (Figure 3.6) and SLS (Figure 3.7) results.

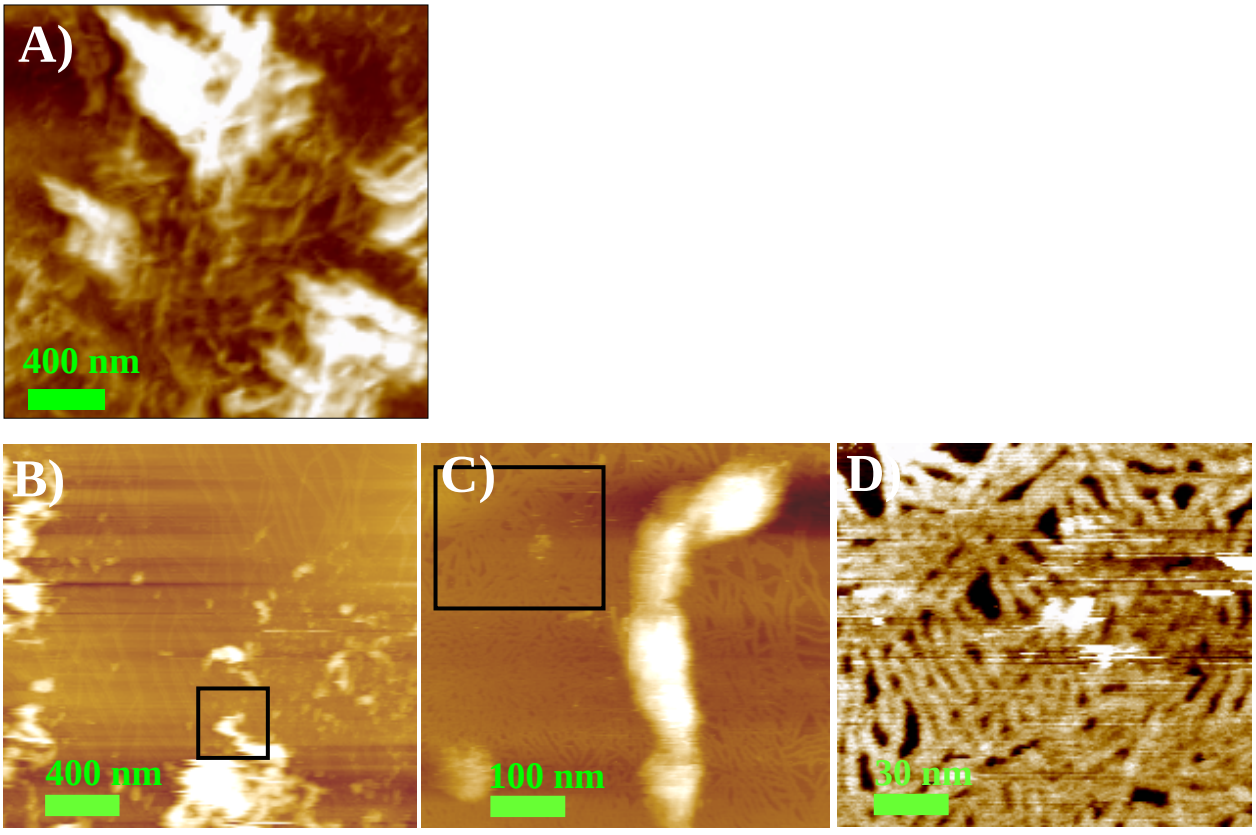

Figure 3.8. AFM images of the EAK-ODN complexes formed in a solution containing 3.6 μM dG_{16} and 0.1 mg/mL EAK. The complexes were imaged in solution at pH 4. (A) 8 mins, (B) 60 mins, (C) 70 mins, and (D) 75 mins. Images in C and D are zoomed in views of the marked areas in B and C, respectively.

In addition, the hydrodynamic diameter of the EAK-ODN aggregates in solution was obtained by DLS. The hydrodynamic diameter of the EAK-dG_{16} aggregates at pH 4 with varying concentrations of EAK was measured 30 min after sample preparation (Figure 3.9). The dG_{16} solutions at 7.2 μM exhibited a species with a hydrodynamic diameter of ~ 7.5 nm which was attributed to isolated ODNs in solution. The diameter of the species present in the dG_{16} solution increased to around 150 nm upon adding EAK and remained constant as the EAK concentration was increased from 0.01 to 0.04 mg/mL (6-24 μM). This result suggested that EAK binds first to ODN molecules, followed by aggregate formation. The hydrodynamic diameter increased to 1000 and 2000 nm when the EAK concentration was increased to 60 and 90 μM, respectively. This might be due to the excess EAK binding to preformed EAK-ODN complexes, resulting in a further increase in diameter. Under the condition used in Figure 3.9, dG_{16} is fully incorporated in the EAK-ODN aggregates for an EAK concentration of 60 μM, as shown in Figure 3.1 (empty square, Figure 3.1). Since 0.1 mg/mL (60 μM) of EAK exhibited a size of ~ 4 nm 40 minutes after preparation (Figure 3.9), it indicates that EAK does not self-assemble during that time and is present as single molecules. The observed large diameters in the EAK-ODN mixture solution are due to the aggregates of ODN and EAK in solution.

The results obtained by fluorescence anisotropy, SLS, and DLS all demonstrate that neither EAKs nor the ODNs self-assemble on their own within the first hour after sample preparation. Consequently the formation of EAK-ODN aggregates at pH 4 and pH 7 must result from the association of ODN and EAK unimers into complexes, which then self-assemble into aggregates (cf. Scheme I).

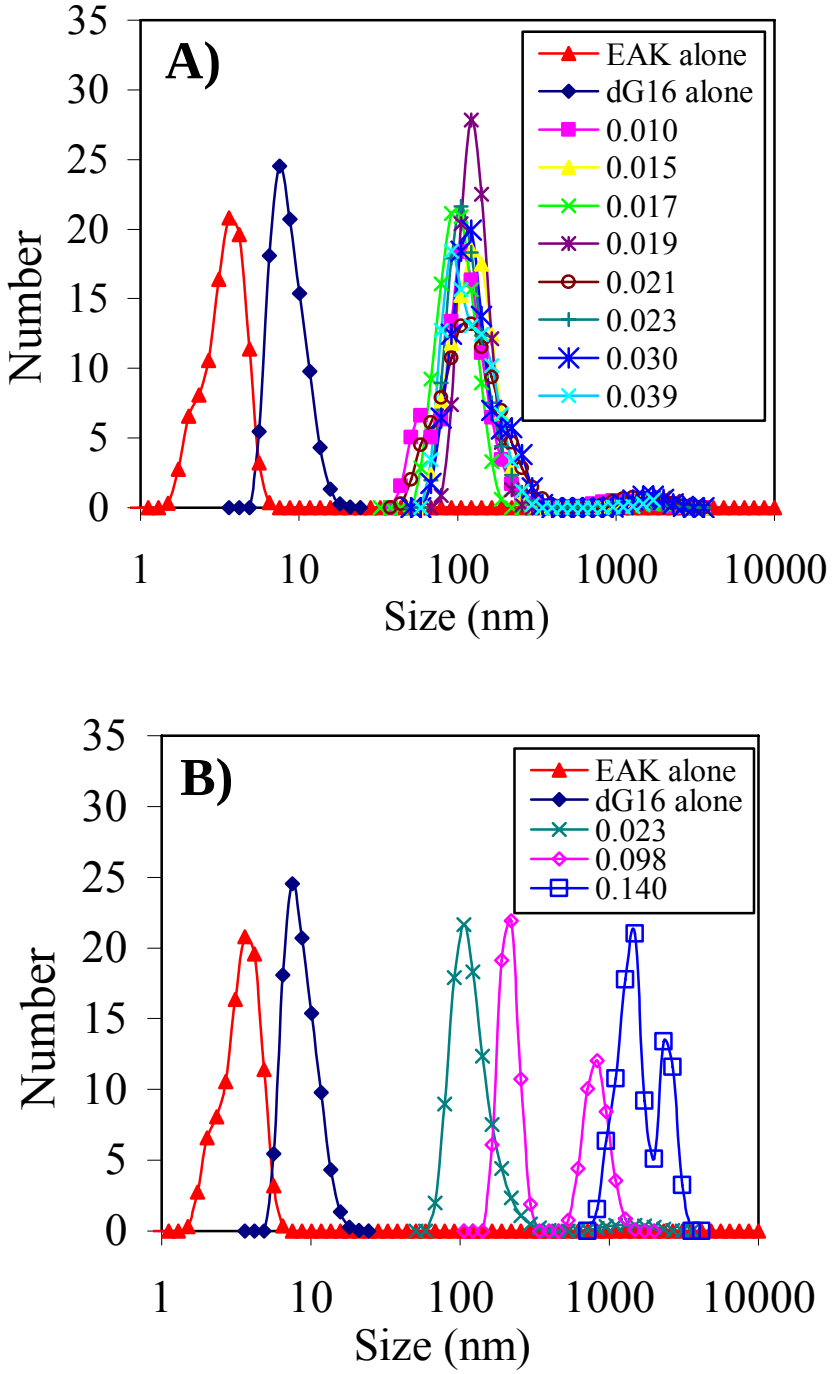

Figure 3.9. Population histogram of the EAK-ODN complexes as a function of particle diameter determined by dynamic light scattering. The EAK-ODN solutions contained 7.2 μM of dG_{16} with increasing EAK concentration at pH 4. The sample of EAK alone was 0.1 mg/mL (60 μM) and was measured 40 minutes after preparation. The concentration of dG_{16} alone was 7.2 μM.

3.4.5 Binding Parameters

The curves shown in Figure 3.1 were used to generate plots of ν/P_f as a function of ν (Figure 3.2). Equation 3-5 was used to obtain the binding constant, K, and the binding site size, n. The K and n values obtained for the binding of EAK to the ODNs at various pH values are listed in Table 3.3. As discussed in the Theoretical Background section, the association of the EAK-ODN complexes into aggregates is not accounted for by the MvH model. However the fits of ν/P_f versus ν with the MvH model shown in Figure 3.2 are rather good.

Table 3.3. Binding constant K and binding site size n retrieved from the fits of the data shown in Figure 3.2 with Equation 3-5.

ODNs	pH 4		pH 7		pH 11	
	n	K (10^4 M^{-1})	n	K (10^4 M^{-1})	N	K (M^{-1})
dG_{16}	1.66 ±0.05	7.6 ±1.2	1.16 ± 0.1	3.4 ± 0.5	No Interaction	
dC_{16}	1.96 ± 0.02	4.7 ± 0.6	1.63 ± 0.03	2.0 ± 0.2	No Interaction	
dGC_{16}	3.16 ± 0.2	4.2 ± 0.8	2.6 ± 0.3	0.7 ± 0.02	No Interaction	

* Each fit has $R^2 > 0.94$ with at least 5 data points. The error on the K and n values is estimated by generating three binding isotherms based on the trends shown in Figure 3.2. These binding isotherms were generated by taking arbitrarily the larger, intermediate, and smaller ν/P_f values obtained according to the error bars shown in Figure 3.2. The three binding isotherms were fitted with the McGhee and von Hippel model (Equation 3-5). And the spread in the K and n values retrieved from the fits provided an estimate of the errors on K and n, as reported in Table 3.3.

It is observed in Figure 3.1 that more EAK is required to form the same quantity of EAK-ODN aggregates when the pH is increased from 4 to 7, as a result of weaker electrostatic forces at pH 7. This observation is reflected quantitatively in Table 3.3, where the binding constant at pH 4 is 2.2-, 2.3-, and 6.0-fold larger than that at pH 7 for dG_{16}, dC_{16}, and dGC_{16}, respectively. The equilibrium constants obtained for the binding of EAK onto the ODNs range from 7.0×10^3 to 7.6×10^4 M^{-1}. In comparison, oligolysine and lysine-rich peptides such as KWKGK, KWK_6, K_4N_4, K_4N_6, and K_n (n=3-8) have been reported to bind to oligo- and polynucleotides with binding constants in the range of 1×10^3~1×10^5 M^{-1} (Latt and Sober, 1967; Roy, *et al*., 1992; Matsuno, *et al*., 2001; Ballin, *et al*., 2004). These values are comparable to those listed in Table 3.3.

The base composition of the ODN sequences, guanine in dG_{16} and cytosine in dC_{16}, appears to affect the binding of EAK to the ODNs since EAK binds more strongly to dG_{16} than to dC_{16} at both

pH 4 and 7 (Table 3.3). Statistical analysis of protein-DNA complexes has established that Lys binds more readily to guanine (G) than to cytosine (C) (Lejeune, *et al*., 2005). Binding of Lys to G occurs more effectively via hydrogen bonds to the two acceptors of the G base, whereas Lys binds preferentially to the phosphate oxygens of the C nucleotide. Furthermore, the study found that Lys has the highest propensity to interact with nucleotides, whereas Glu and Ala have the lowest (Lejeune, *et al*., 2005). Since the interactions between nucleotides and glutamic acid are poor and since the favorable electrostatic forces between the negatively charged backbone of the ODNs and EAK are expected to be similar for dG_{16} and dC_{16}, the observation that dG_{16} binds more strongly to EAK than dC_{16} is rationalized by the enhanced formation of hydrogen-bonds between the lysines of EAK and the guanines of dG_{16}.

The data listed in Table 3.3 indicate that EAK binds preferentially to ssODNs rather than to their duplex. This phenomenon has been observed for other peptides (Simeoni, *et al*., 2003). This might be caused by the formation of hydrogen bonds between the amino acids of EAK and the nucleotide bases of ssODNs. This favorable interaction disappears in the case of dsODNs, since each nucleotide base hydrogen-bonds with the opposite base in the complementary strand of the duplex.

3.4.6 Solvent Accessibility of ODNs in the EAK-ODN Aggregates

One important aspect of the structure of the EAK-ODN aggregates is whether the ODNs are located inside or outside the aggregates. ODNs located inside the aggregates will be less accessible to the solvent than those located on the surface, and hence be protected from the outside environment. The accessibility of the ODN to the solvent was measured by performing fluorescence dynamic quenching experiments. dC_{16} was labeled either at the 5'-end with fluorescein (FAM-dC_{16}, λ_{ex} = 452 nm, λ_{em} = 514 nm) or at the 3'-end with rhodamine (dC_{16}-Rh, λ_{ex} = 560 nm, λ_{em} = 580 nm) to investigate whether both ends of dC_{16} are protected from the solvent. The fluorescence emission of a solution containing 3.6 μM of the labeled dC_{16} was monitored as the quencher KI was added to the solution in the presence or absence of 0.2 mg/mL EAK. Throughout these experiments, the potassium ion concentration was maintained constant and equal to 0.3 M by addition of K_2SO_4 to the KI solution, ensuring constant ionic strength.

As the KI concentration increased, the fluorescence intensity of fluorescein or rhodamine decreased. The I_o/I ratio was plotted as a function of iodide concentration in Figure 3.10A and 3.10 B for fluorescein and rhodamine, respectively. The quantities I_o and I represent the fluorescence intensity of the chromophore without and with quencher, respectively. The I_o/I ratio was found to increase linearly with iodide concentration for both chromophores in the absence or presence of EAK. However the increase was stronger in the absence of EAK.

The fluorescence decays of FAM-dC_{16} and dC_{16}-Rh were acquired in the presence and absence of EAK. They were fitted with two exponentials according to Equation 3-2. The pre-exponential factors and decay times obtained from the fits are listed in Table 3.4. Although fluorescein itself displays a single lifetime of 4.1 ns (Sjoback, *et al*., 1995), the decay becomes more complex when fluorescein is covalently attached to an ODN where it shows two decay times. This phenomenon has been reported (Sjoback, *et al*., 1998) to be due to a change in the conformation of fluorescein when it is covalently linked to an ODN. The binding of EAK onto the labeled ODN does not change the lifetime of the chromophore significantly as shown in Table 3.4.

To ensure that the quenching is dynamic, the fluorescence decays of the FAM-dC_{16}-EAK mixture were acquired in the absence and presence of 0.2 M KI. The average lifetime of the decays was determined and the ratio of the average lifetime of the solution without KI (τ_o) over that of the solution with 0.2 M KI (τ) was found to be 1.8, i.e. τ_o/τ=1.8. The I_o/I ratio obtained from the steady-state fluorescence measurements equaled 1.9 for a concentration of 0.2 M KI, a value comparable to the τ_o/τ ratio. The agreement obtained between the I_o/I and τ_o/τ ratios strongly suggests that the quenching is dynamic (Lakowicz, 1999). Fitting the I_o/I vs. [I^-] trends shown in Figure 3.10 with the Stern-Volmer equation given in Equation 3-6 yields the bimolecular quenching rate constant, k_q, which reflects the accessibility of the chromophore to the solvent (Lakowicz, 1999).

$$I_o / I = 1 + K_{SV}[Q] = 1 + k_q \tau_o [Q] \qquad (3\text{-}6)$$

The slopes of the straight lines referred to as the Stern-Volmer constants, K_{SV}, are listed in Table 3.5. As indicated in Equation 3-6, k_q is determined from the ratio K_{SV}/τ_o where τ_o is the lifetime of the chromophore in the absence of quencher (Lakowicz, 1999).

Since the fluorescence decay of the choromophores without quencher is biexponential, the average lifetime $\overline{\tau_o}$ was used to calculate the bimolecular quenching rate constant k_q from the slope K_{SV} of the plots in Figure 3.10. The values of K_{SV}, $\overline{\tau_o}$, and k_q are listed in Table 3.5. In the absence of EAK, k_q for FAM-dC_{16} and dC_{16}-Rh equals 2.5×10^9 $M^{-1}s^{-1}$ and 3.5×10^9 $M^{-1}s^{-1}$, respectively. The bimolecular quenching rate constant is related to the quenching efficiency, size, and diffusion coefficient of the chromophore and quencher. Since the iodide ions have quenching efficiencies near unity (Lakowicz, 1999) and the overall sizes of the two labeled ODNs are comparable, the differences in k_q found for FAM-dC_{16} and dC_{16}-Rh (Table 3.5) must reflect differences in the efficiency of iodide at quenching the excited chromophores. Indeed, FAM and Rh are neutral and positively charged at

pH 4, respectively. Considering electrostatic forces alone, the negatively charged iodide ions are expected to quench Rh more efficiently than FAM. In addition, FAM is expected to be less mobile than Rh as an 8- and 12-atom linker connects the 5'-end and the 3'-end phosphate groups of dC_{16} to FAM and Rh, respectively. In the presence of EAK, k_q decreases for both FAM-dC_{16} and dC_{16}-Rh. For FAM-dC_{16}, k_q decreases from 2.5×10^9 $M^{-1}s^{-1}$ to 1.5×10^9 $M^{-1}s^{-1}$. Similarly, for dC_{16}-Rh, k_q decreases from 3.5×10^9 $M^{-1}s^{-1}$ to 2.0×10^9 $M^{-1}s^{-1}$. Considering that the diffusion coefficient of the fluorophore-labeled ODN of 16 bases would be around 1.3×10^{-6} cm^2/s (Gordan, 2005), which is 10-fold lower than that of iodide ion with 1.9×10^{-5} cm^2/s (Weast, 1971), k_q will be affected by at most 10 % by the diminution of the diffusion coefficient of the ODNs after incorporation in the EAK-ODN aggregates. Thus, the decrease in k_q observed in Table 5 (~ 40%) suggests that the accessibility of ODNs must be reduced after binding to EAK.

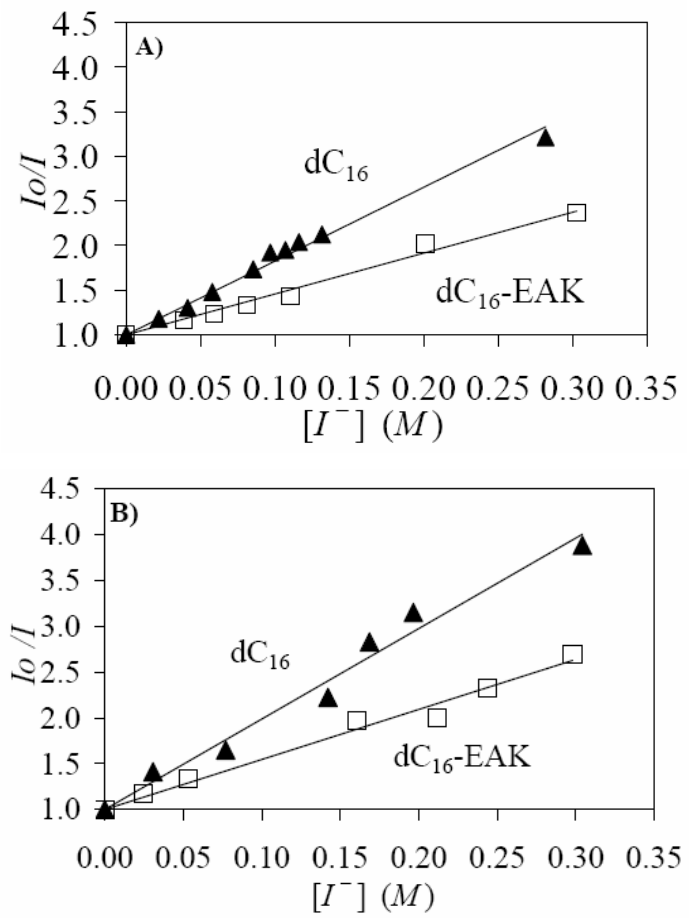

Figure 3.10. Stern-Volmer plots for a solution of 3.6 μM of fluorescently labeled dC_{16} free and bound to 0.2 mg/mL of EAK at pH 4 quenched by KI. Solid lines represent the fits to the Stern-

Volmer equation with parameters listed in Table 3.5. (A) FAM-dC_{16} (▲), FAM-dC_{16}-EAK (□), and (B) dC_{16}-Rh (▲), dC_{16}-Rh-EAK (□).

Table 3.4. Pre-exponential factors and decay times obtained from the analysis of the fluorescence decays of the fluorescent ODNs in the absence and presence of EAK in pH 4 buffer, respectively.

	τ_1 (ns)	α_1	τ_2 (ns)	α_2	$\bar{\tau}$ (ns)*	χ^2
FAM-dC_{16} (without KI)	3.9	0.67	2.0	0.33	3.3	1.12
EAK-FAM-dC_{16} (without KI)	3.7	0.63	1.7	0.37	3.0	1.00
EAK-FAM-dC_{16} (with KI)	2.8	0.43	1.0	0.57	1.7	1.15
dC_{16}-Rh (without KI)	3.9	0.60	1.5	0.40	2.9	1.13
EAK-dC_{16}-Rh (without KI)	3.8	0.58	1.3	0.42	2.8	1.37

* $\bar{\tau}$ is the number average lifetime, given by $\bar{\tau} = \frac{\sum \tau_i \alpha_i}{\sum \alpha_i}$

The change in accessibility of the ODNs upon EAK binding was quantified with the relative accessibility change, γ, defined by (Bujalowski and Klonowaka, 1994)

$$\gamma = k_q^b / k_q^f \qquad (3\text{-}7)$$

where k_q^b and k_q^f are the bimolecular quenching constants for the chromophore-labeled ODNs in the presence and absence of EAK, respectively. The values of γ for the two different labels are listed in Table 3.5. The relative accessibility changes of dC_{16} for both types of labels are similar and smaller

than unity, being 0.60 and 0.57 for the 5'-labeled FAM-dC_{16} and the 3'-labeled dC_{16}-Rh, respectively. Since γ is smaller than 1.0, the accessibility of the 5'– and 3'–ends of dC_{16} to the solvent is reduced after the binding of EAK to dC_{16}. Since the γ values corresponding to the two labels are similar, the accessibility of both ends of dC_{16} to the solvent is reduced by the same extent, about 40 %. The fact that different sections of the ODN exhibit a similar reduction in accessibility suggests that the entire ODN molecule is protected by the EAK molecules inside the EAK-ODN aggregates.

Table 3.5. Stern-Volmer quenching constants K_{SV}, bimolecular quenching rate constant, k_q, fluorescence lifetime τ_o, and relative accessibility change γ when dC_{16} is in the absence or presence of 0.2 mg/mL of EAK in pH 4 buffer.

ODNs	5' end fluorescein labeling				3' end rhodamine labeling			
	K_{SV} (M^{-1})	τ_o (ns)	k_q ($10^9\ M^{-1}S^{-1}$)	γ	K_{SV} (M^{-1})	τ_o (ns)	k_q ($10^9\ M^{-1}S^{-1}$)	γ
Fluorescently labeled dC_{16} (free)	8.3 ± 0.2	3.3	2.5 ± 0.1		9.9 ± 0.4	2.8	3.5 ± 0.1	
Fluorescently labeled EAK-dC_{16} (bound)	4.6 ± 0.1	3.0	1.5 ± 0.1	0.60	5.5 ± 0.2	2.7	2.0 ± 0.1	0.57

It is worth noting that while the negatively charged ODNs should repel the quencher (I^-), the negative charges on the ODNs are, at least partially, neutralized by the positively charged EAK in the EAK-ODN aggregates. Consequently the iodide ions would be expected to be more efficient at colliding with the ODNs in the presence of EAK. Interestingly the opposite is observed, which strengthens the claim that EAK protects the ODN from its environment.

Unprotected ODNs are rapidly degraded *in vitro* and *in vivo* due to the presence of nucleases. The reduction of accessibility to the solvent experienced by the ODNs upon assembly with EAK suggests that the degradation of the complexed ODN will be reduced when used in biological systems. Further investigations are underway to verify the stability of the EAK-ODN aggregates and the potential of ODN encapsulation by EAK for oligonucleotide delivery.

3.5 Summary

In this work the molecular interaction of EAK with ODNs in solution was studied by a number of physicochemical methods. UV-Vis absorption experiments show that the binding between EAK and ODNs results in the formation of EAK-ODN aggregates which could be centrifuged out. Fluorescence anisotropy, PAGE, and UV-Vis experiments demonstrate that EAK-ODN complexes, as well as EAK and ODN unimers, exist in the supernatant of the centrifuged EAK-ODN mixtures. The binding isotherms between EAK and ODNs are established from the UV-Vis absorption results through a binding density function analysis. Fluorescence anisotropy and static light scattering experiments show that the process of EAK binding to ODNs starts with EAK-ODN molecular complexation, followed by association of the complexes into aggregates. For comparison purpose, the binding isotherm was fitted with the modified non-cooperative MvH model to extract the equilibrium "binding constants". The binding is found to be strongest at pH 4. No binding is observed at pH 11. The equilibrium binding constant decreases 2-6 folds when the pH changes from 4 to 7. Since the equilibrium binding constant decreases as EAK becomes less positively charged, the interaction between EAK and ODNs must occur mainly via electrostatic interactions, but hydrogen bonding between EAK and the nucleotides of the ODNs may also be involved. Hydrogen bonds are believed to promote the binding of EAK to dG_{16} to a greater extent than to dC_{16}. Furthermore, EAK has a slight preference to bind with the ssODNs than to the dsODN.

The size of EAK-ODN aggregates was determined by AFM and DLS, and found to equal ~ 150 nm at low EAK concentrations. Fluorescence quenching experiments showed that the accessibility of ODNs to the solvent was reduced upon EAK binding. EAK-ODN aggregates can protect the ODNs from encountering the quencher in the surrounding solvent.

References

Aggeli, A., N. Boden, and S. Zhang. 1999. Self-assembly of peptides in medicine: two sides of the coin. *Mol. Med. Today* **5:** 512-513.

Agou, F., S. Raveh, S. Mesnildrey, and M. Veron. 1999. Single Strand DNA Specificity Analysis of Human Nucleoside Diphosphate Kinase B. *J. Biol. Chem.* **274:** 19630-19638.

Akinrimisi, E. O., C. Sander, and P. O. P. Ts'o. 1963. Properties of helical polycytidylic acid. *Biochemistry* **2:** 340-344.

Ballin, J. D., I. A. Shkel, and M. T. Record. 2004. Interactions of the KWK6 Cationic Peptide with Short Nucleic Acid Oligomers: Demonstration of Large Coulombic End Effects on Binding at 0.1-02 M Salt. *Nucl. Acids Res.* **32:** 3271-3281.

Bergen, J. M., and S. H. Pun. 2005. Peptide-enhanced gene delivery. *MRS Bulletin* **30:** 663-667.

Bolumar, T., T. Y. Sanz, M. C. Aristoy, and F. Toldra. 2003. Purification and Characterization of a Prolyl Aminopeptidase from Debaryomyces hansenii. *Appl. Environ. Microbio.* **69:** 227-232.

Boraston, A. B., P. Chiu, R. A. J. Warren, and D. G. Kilburn. 2000. Specificity and affinity of substrate binding by a family 17 carbohydrate-binding module from Clostridium cellulovorans cellulase 5A. *Biochemistry* **39:** 11129-11136.

Bujalowski, W., and T. M. Lohman. 1987. A General Method of Analysis of Ligand-Macromolecule Equilibria Using a Spectroscopic Signal from the Ligand to Monitor Binding. Application to E. coli SSB Protein-Nucleic Acid Interactions. *Biochemistry* **26:** 3099-3106.

Bujalowski, W., and M. M. Klonowaka. 1994. Structural Characteristics of the Nucleotide-Binding Site of Escherichia coli Primary Replicative Helicase DnaB Protein. Studies with Ribose and Base-Modified Fluorescent Nucleotide Analogs. *Biochemistry* **33:** 4682-4694.

Casas-Finet, J. R., J. D. Smith, A. Kumar, J. G. Kim, S. H. Wilson, and R. L. Karpel. 1993. Mammalian heterogeneous ribonucleoprotein A1 and its constituent domains: Nucleic acid interaction, structural stability and self-association. *J. Mol. Biol.* **229:** 873-889.

Chen, P. 2005. Self-assembly of Ionic-complementary Peptides: a Physicochemical Viewpoint. *Colloids Surf. A* **261:** 3-24.

Creagh, A. L., E. Ong, E. Jervis, D. G. Kilburn, and C. A. Haynes. 1996. Binding of the cellulose-binding domain of exoglucanase Cex from *Cellulomonas fimi* to insoluble microcrystalline cellulose is entropically driven. *Proc. Natl. Aca. Sci.* **93:** 12229-12234.

Crothers, D. M. 1968. Calculation of binding isotherms for heterogeneous polymers. *Biopoly.* **6:** 575-584.

Endoh, T., H. Funabashi, M. Mie, and E. Kobatake. 2005. Method for detection of specific nucleic acids by recombinant protein with fluorescent resonance energy transfer. *Anal. Chem.* **77:** 4308-4314.

Epstein, I. R. 1978. Cooperative and non-cooperative binding of large ligands to a finite one-dimensional lattice. A model for ligand-oligonucleotide interactions. *Biophy. J.* **8:** 327-339.

Förster, T., and E. König. 1957. Absorptionsspektren und Fluoreszeneigenschaften konzentrierter Lösungen organischer Farbstoffe. *Z. Elektrochem.* **61:** 344-348.

Fung, S.Y., C. Keyes, J. Duhamel, and P. Chen. 2003. Concentration Effect on the Aggregation of a Self-Assembling Oligopeptide. *Biophys. J.* **85:** 537-548.

Galletto, R., M. J. Jezewska, and W. Bujalowski. 2003. Interactions of the Escherichia coli DnaB helicase hexamer with the replication factor the DnaC protein. Effect of nucleotide cofactors and the ssDNA on protein-protein interactions and the topology of the complex. *J. Mol. Biol.* **329:** 441-465.

Gordan, S.P., S. Berezhna, D. Scherfeld, N. Kahya, and P. Schwille. 2005. Characterization of Interaction between Cationic Lipid-Oligonucleotide Complexes and Cellular Membrane Lipids Using Confocal Imaging and Fluorescence Correlation Spectroscopy. *Biophys. J.* 88: 305-316.

Gottschalk, S., J. T. Sparrow, J. Hauer, M. P. Mims, F. E. Leland, and S. Woo. 1996. A Novel DNA-peptide Complex for Efficient Gene Transfer and Expression in Mammalian Cells. *Gene Ther.* **3:** 448-457.

Hamman, B. D., A. V. Oleinikov, G. G. Jokhadze, D. E. Bochkariov, R. R. Traut, and D. M. Jameson. 1996. Tetramethylrhodamine Dimer Formation as a Spectroscopic Probe of the Conformation of *Escherichia coli* Ribosomal Protein L7/L12 Dimers. *J. Biol. Chem.* **271:** 7568-7573.

Holmes, T. C., S. D. Lacelle, X. Su, G. Liu, A. Rich and S. Zhang. 2000. Extensive neurite outgrowth and active synapse formation on self-assembling peptide scaffolds. *Proc. Natl. Acad. Sci. USA* **97:** 6728-6733.

Hong, Y., R. L. Legge, S. Zhang, and P. Chen. 2003. Effect of Amino Acid Sequence and pH on Nanofiber Formation of Self-Assembling Peptides EAK16-II and EAK16-IV. *Biomacromol.* **4:** 1433-1442.

Jensen, D. E., and P. H. von Hippel. 1977. A boundary sedimentation velocity method for determining nonspecific nucleic acid-protein interaction binding parameters. *Anal. Biochem.* **80:** 267-281.

Keyes-Bag, C., S. Y. Fung, J. Bezaire, and P. Chen. 2004. Self-Assembling Peptide as a Potential Carrier of Hydrophobic Compounds. *J. Am. Chem. Soc.* **126:** 7522-7532.

Lakowicz, J. R. 1999. *Principles of Fluorescence Spectroscopy*. Plenum Publisher, New York.

Latt, S. A., and H. A. Sober. 1967. Protein-nucleic acid interactions. II. Oligopeptide-polyribonucleotide binding studies. *Biochemistry* **6:** 3293-3306.

Lehninger, A. L. 1993. *Principles of Biochemistry*. Worth Publishers.

Lejeune, D., N. Delsaux, B. Charloteaux, A. Thomas, and R. Brasseur. 2005. Protein–Nucleic Acid Recognition: Statistical Analysis of Atomic Interactions and Influence of DNA Structure. *Proteins* **61:** 258-271.

Matsuno, H., K. Niikura, and Y. Okahata. 2001. Design and Characterization of Asparagine- and Lysine-Containing Alanine-Based Helical Peptides That Bind Selectively to A·T Base Pairs of Oligonucleotides Immobilized on a 27 MHz Quartz Crystal Microbalance. *Biochemistry* **40:** 3615-3622.

McGhee, J. D., and P. H. von Hippel. 1974. Theoretical Aspects of DNA-Protein Interactions: Co-operatice and Non-co-operative Binding of Large Ligands to a One-dimensional Homogeneous Lattice. *J. Mol. Biol.* **86:** 469-489.

Michel, S. L., A. L. Guerrerio, and J. M. Berg. 2003. Selective RNA binding by a single CCCH zinc-binding domain from Nup475 (Tristetraprolin). *Biochemistry* **42:** 4626-4630.

Morii, T., J. Yamane, Y. Aizawa, K. Makino, and Y. Sugiura. 1996. Cooperative Oligomerization Enhances Sequence-Selective DNA Binding by a Short Peptide. *J. Am. Chem. Soc.* **116:** 10011-10017.

Muller, R., T. Restle, J. Reinstein, and R. S. Goody. 1991. Interaction of Fluorescently Labeled Dideoxynucleotides with HIV-1 Reverse Transcriptase. *Biochemistry* **30:** 3709-3715.

Plank, C., M. X. Tang, A. R. Wolfe, and F. C. Szoka. 1999. Branched cationic peptides for gene delivery: Role of type and number of cationic residues in formation and *in vitro* activity of DNA polyplexes. *Human Gene Ther.* **10:** 319-332.

Press, W. H., B. P. Flannery, S. A. Teukolsky, and W. T. Vetterling. 1992. *Numerical Recipes. The Art of Scientific Computing*. Cambridge University Press, Cambridge.

Roy, K. B., S. Kukreti, H. S. Bose, V. S. Chauhan, and M. R. Rajeswari. 1992. Hairpin and duplex forms of a self-complementary dodecamer, d-AGATCTAGATCT, and interaction of the duplex form with the peptide KGWGK: can a pentapeptide destabilize DNA? *Biochemistry* **31:** 6241-6245.

Scatchard, G. 1949. The attractions of proteins for small molecules and ions. *Ann. N. Y. Acad. Sci.* **51:** 660-672.

Schwarz, G. 1970. Cooperative Binding to Linear Biopolymers. 1. Fundamental Static and Dynamic Properties. *Eur. J. Biochem.* **12:** 442-453.

Schwarz, G., and F. Watanabe. 1983. Thermodynamics and Kinetics of Co-operative Protein-Nucleic Acid Binding I.General Aspects of Analysis of Data. *J. Mol .Biol.* **163:** 467-484.

Seimiya, M., and Y. Kurosawa. 1996. Kinetics of binding of Antp homeodomain to DNA analyzed by measurements of surface plasmon resonance. *FEBS Lett.* **398:** 279-284.

Simeoni, F., M. C. Morris, F. Heitz, and G. Divita. 2003. Insight into the mechanism of the peptide-based gene delivery system MPG: implications for delivery of siRNA into Mammalian Cells. *Nucl. Acids Res.* **31:** 2717-2724.

Sjoback, R., J. Nygren, and M. Kubista. 1995. Absorption and Fluorescence Properties of Fluorescein. *Spectrochim. Acta Part A*, **51:** L7-L21.

Sjoback, R., J. Nygren, and M. Kubista. 1998. Characterization of fluorescein-oligonucleotide conjugates and measurement of local electrostatic potential. *Biopoly.* **46:** 445-453.

Stierle, V., J. Couprie, C. Ostlund, I. Krimm, S. Zinn-Justin, P. Hossenlopp, H. J. Worman, J. C. Courvalin, and I. Duband-Goulet. 2003. The carboxyl-terminal region common to lamins A and C contains a DNA binding domain. *Biochemistry* **42:** 4819- 4828.

Tsodikov, O. V., J. A. Holbrook, I. A. Shkel, and M. T. Record. 2001. Analytic Binding Isotherms Describing Competitive Interactions of a Protein Ligand with Specific and Nonspecific Sites on the Same DNA Oligomer. *Biophy. J.* **81:** 1960-1969.

Teif, V.B., and D. Y. Lando. 2001. Calculations of DNA Condensation Caused by Ligand Adsorption. *Mol. Biol.* **35:** 106-107.

Teif, V.B. 2005. Ligand-Induced DNA Condensation: Choosing the Model *Biophys. J.* **89:** 2574-2587.

Sambrook, J., E. F. Fritsch, and T. Maniatis. 1989. *Molecular Cloning: A Laboratory Manual*, *2nd Edition*, P 6.37. Cold Spring Harbor Laboratory Press.

Weast, R.C. 1971. *Handbook of Chemistry and Physics.* P. F47. The Chemical Rubber Co. Cleveland, Ohio.

Zhang, S., T. C. Holmes, C. Lockshin, and A. Rich. 1993. Spontaneous Assembly of a Self-Complementary Oligopeptide to Form a Stable Macroscopic Membrane. *Proc. Natl. Acad. Sci. USA* **90**: 3334-3338.

Zhang, S., C. Lockshin, R. Cook, and A. Rich. 1994. Unusually stable beta-sheet formation in an ionic self-complementary oligopeptide. *Biopoly.* **34:** 663-672.

Zhang, S., T. C. Holmes, M. Dipersio, R. O. Hynes, X. Su, and A. Rich. 1995. Self-complementary Oligopeptide Matrices Support Mammalian Cell Attachment. *Biomater.* **16:** 1385-1393.

Zhang, S. 2002. Emerging biological materials through molecular self-assembly. *Biotechnol. Adv.* **20:** 321-339.

Chapter 4
Binding of the Self-Assembling Peptide EAK16IV to Oligodeoxynucleotides: Effect of Charge Distribution

4.1 Introduction

Self-assembling peptides have recently drawn intense interests following their use in various biomedical engineering applications, including scaffolding for tissue engineering (Zhang, *et al*., 1995; Holmes, *et al*., 2000), biological surface patterning (Zhang, 2002), and drug delivery (Keyes-Bag, *et al*., 2004). In the application of oligonucleotide (ODN) delivery, self-assembling peptides offer several advantages over many other natural and synthetic peptides. The self-assembling peptides can not only be made cationic to enhance associations with ODNs via electrostatic interactions, but also possess unique distributions of charges and hydrophobic residues along their backbone that enable them to self-assemble into stable nanostructures.

Among the self-assembling peptides is a class of ionic-complementary peptides, e.g., EAK peptides, which are made of glutamic acid (E), alanine (A), and lysine (K) residues (Zhang, *et al*., 1993). EAK originates from zuotin, a yeast protein that preferentially binds to left-handed Z-DNA (Zhang, *et al*., 1993). It has alternating hydrophobic (A) and hydrophilic (E and K) amino acids. The pK_a values of E and K are 4.25 and 10.53, respectively. Therefore, E and K are negatively and positively charged at pH 7, which enables ionic-complementarity. The electrostatic and hydrophobic interactions, together with hydrogen bonding lead to the self-assembly of the peptides into highly stable structures in solution (Fung, *et al*., 2003; Hong, *et al*., 2003; Jun, *et al.*, 2004). In a previous study with EAK16II, an EAK peptide, this feature was taken advantage of to embed ODNs in an EAK matrix and protect the ODNs from the surrounding medium (Wang, *et al*., 2006). The binding of EAK16II to ODNs was controlled by adjusting the pH of the solution (Wang, *et al*., 2006). The dependence of the binding upon the solution pH demonstrated that electrostatic interactions play an important role in the binding. This observation could be rationalized by considering how the charge status of E and K in EAK16II is being affected by pH (Wang, *et al*., 2006).

Since electrostatic interaction has been found to be the main driving force for the binding of EAK16II to the ODNs, it is important to investigate the effect that the distribution of charges along the EAK peptides has on the binding of EAK onto ODNs. Thus, the binding of EAK16IV, another EAK peptide, to ODNs was studied. EAK16IV and EAK16II have the same amino acid composition but a different charge distribution, given by the sequence − − − − + + + + and − − + + − − + + for

EAK16IV and EAK16II at neutral pH, respectively. As reported by Hong et al (2003), EAK16IV and EAK16II self-assemble into distinct nano/microstructures as a result of their different charge distribution. EAK16IV forms globular assemblies at neutral pH, but fibrillar assemblies at other pH values. EAK16II forms fibrillar assemblies regardless of pH. The substantial changes observed with the structures of the assemblies generated by EAK16II and EAK16IV suggested that the different charge distribution of the peptide would also affect its binding to ODNs. To determine whether this would be the case, the binding of EAK16IV to ODNs was investigated at different pHs.

The effect of charge distribution on EAK16IV-ODN binding was investigated by characterizing the binding of EAK16IV to ODNs in terms of the binding strength, the size of the EAK16IV-ODN aggregates, and the accessibility of the ODNs in the aggregates to the solvent. These results were then compared to those obtained with EAK16II. The fraction of ODNs in the EAK16IV-ODN aggregates formed upon the addition of EAK16IV to ODN solutions was determined from the UV-Vis absorption of the supernatant obtained after centrifuging the EAK16IV-ODN solutions. The binding isotherms were generated by analyzing the data obtained from the absorption measurements with a binding density function (Bujalowski and Lohman, 1987; Lohaman and Bujalowski, 1991; Bujalowski and Klonowaka, 1994). The binding constant was obtained by applying the modified non-cooperative McGhee and von Hippel (MvH) model to the binding isotherms (McGhee and von Hippel, 1974; Tsodikov, *et al*., 2001). In addition, the existence of the main species present in the peptide-ODN solutions was established by the combination of fluorescence anisotropy, Polyacrylamide Gel Electrophoresis (PAGE), Dynamic Light Scattering (DLS), Atomic Force Microscopy (AFM), and UV-Vis absorption. The time scale over which aggregation occurs was determined by Static Light Scattering (SLS). The size of the resulting EAK16IV-ODN aggregates was investigated with AFM and DLS. The accessibility of the ODNs to the solvent was evaluated by fluorescence quenching experiments, as this property is critically important to assess the stability and potency of ODNs during their delivery both *in vitro* and *in vivo* (Plank, *et al*., 1999; Simeoni, *et al*., 2003).

4.2 Experimental Section

4.2.1 Materials

All materials, including reagents, buffers (Akinrimisi, *et al*., 1963; Bolumar, *et al*., 2003), and oligonucleotides were the same as those reported in an earlier study (Wang, *et al*., 2006). The peptide EAK16IV, whose sequence is n-AEAEAEAEAKAKAKAK-c, was purchased from Research Genetics (Alabama, USA) and used without further purification.

4.2.2 Methods

The physicochemical methods applied in this work have been described in details in an earlier publication (Wang, *et al*., 2006). The following is the brief description for each of the methods.

UV-Vis Absorption Spectroscopy. UV-Vis absorbance measurements were conducted on a Biochrom ultrospec 4300 pro UV-Vis spectrophotometer (Cambridge, England).

Samples used to construct the binding isotherms were prepared at pH 4, 7, and 11. For each pH, two ODN concentrations were used. At each ODN concentration, six to eight samples were prepared with EAK concentrations ranging from 0 to 0.1 mg/mL (equivalent to 0-60 μM). The EAK-ODN aggregates formed spontaneously upon mixing and 30 minutes after sample preparation these aggregates were removed by centrifuging the solutions at 10,000 rpm for 2 min. UV-Vis absorption spectra of the supernatants were recorded. The fraction of ODNs in the aggregates was then calculated from the relative UV-Vis absorbance change ΔOD_r equal to $(OD_o\text{-}OD_s)/OD_o$, where OD_o is the absorbance at 260 nm of the initial solution and OD_s is the absorbance at 260 nm of the supernatant. The obtained ΔOD_r was then analyzed using the ligand binding density function (Bujalowski and Lohman, 1987; Lohaman and Bujalowski, 1991) to generate the binding isotherms.

Polyacrylamide Gel Electrophoresis (PAGE). Non-denaturing 20 % PAGE was used to determine the composition of the supernatant of the EAK16-IV-ODN solutions.

Steady-State Fluorescence Anisotropy. Fluorescence anisotropy was measured to demonstrate that a negligible amount of EAK16IV-ODN aggregates remained in the supernatant after centrifugation. Experiments were conducted on a Photon Technology International steady-state fluorometer (New Jersey, USA) equipped with a LPS 220-B xenon arc lamp and PTI 814 photomultiplier.

Static Light Scattering (SLS). SLS was monitored with the steady-state fluorometer to investigate the binding pathway of EAK16-IV to ODNs.

Dynamic Light Scattering (DLS). The ODN and EAK16IV solutions were separately filtered through a polycarbonate membrane with a pore size of 200 nm before mixing. The size of the EAK-ODN aggregates was measured by DLS on a Zetasizer Nano ZS instrument.

Atomic Force Microscopy (AFM). A Picoscan AFM from Molecular Imaging was used to characterize the nanostructure of the EAK-ODN complexes/aggregates.

Steady-State Fluorescence. Steady-state fluorescence was utilized to study the solvent accessibility of the ODNs in the EAK-ODN aggregates. Fluorescence spectra were acquired on the steady-state fluorometer.

Time-Resolved Fluorescence Decays. The decay time of the fluorophore-labeled ODN with or without EAK peptide was obtained from fluorescence decay measurements on an IBH model 2000 time-resolved fluorometer. The principle and analysis (Press, *et al*., 1992; Lakowicz, 1999) was described in an earlier work (Wang, *et al*., 2006).

4.2.3 Binding Assay

The procedure which was applied to construct the isotherms for the binding of EAK16IV to ODNs is the same as the one described in in the Section 2.4 of Chapter 2. Briefly, the relative change in absorbance (ΔOD_r), which equals the fraction of ODNs in the aggregates, was plotted as a function of the EAK concentration for three or four ODN concentrations in Figure 4.1. It has shown that the fraction of ODN in aggregates is a unique function of binding density (Teif, and Lando. 2001; Teif, 2005) ($\nu = P_b/D_t$), which is in turn a sole function of free ligand concentration (P_f). Based on the ligand binding density function proposed by Bujalowski and Lohman (Bujalowski and Lohman, 1987; Lohaman and Bujalowski, 1991; Bujalowski and Klonowaka, 1994), Equation 4-1 relates ν and P_f to the total peptide concentration and the total ODN concentration for a given ΔOD_r.

$$P_{tx} = P_f + \nu D_{tx} \tag{4-1}$$

In Equation 4-1, P_{tx} and D_{tx} represent, respectively, the total concentrations of peptide and ODN at the xth ODN concentration. For a given ΔOD_r, the binding density (ν) and free peptide concentration (P_f) can be obtained from the slope and y-intercept of the plot of P_t *vs*. D_t, respectively. One important aspect of the procedure described above is that, although ΔOD_r represents the fraction of ODN present in the aggregates and does not account for the ODN present in the supernatant as EAK16IV-ODN complexes, ΔOD_r can still be used to find out P_f and ν.

Each curve shown in Figure 4.1 could be fitted reasonably well with empirical equations of the form $\Delta OD_r = A \times P_t^C/(B^C + P_t^C)$ or $\Delta OD_r = A \times P_t/(1+B \times P_t)$, where A, B and C are regression parameters listed in Table 4.1. Seven-to-ten ΔOD_r values were chosen. For each ΔOD_r value, the value of P_t was read from the fits of the curves shown in Figure 4.1 and plotted as a function of D_t. Then P_f and ν were obtained from the intercept and slope of the plot of P_t *versus* D_t. The P_f and ν values enable the construction of the binding isotherms as the ν/P_f versus ν plots given in Figure 4.2.

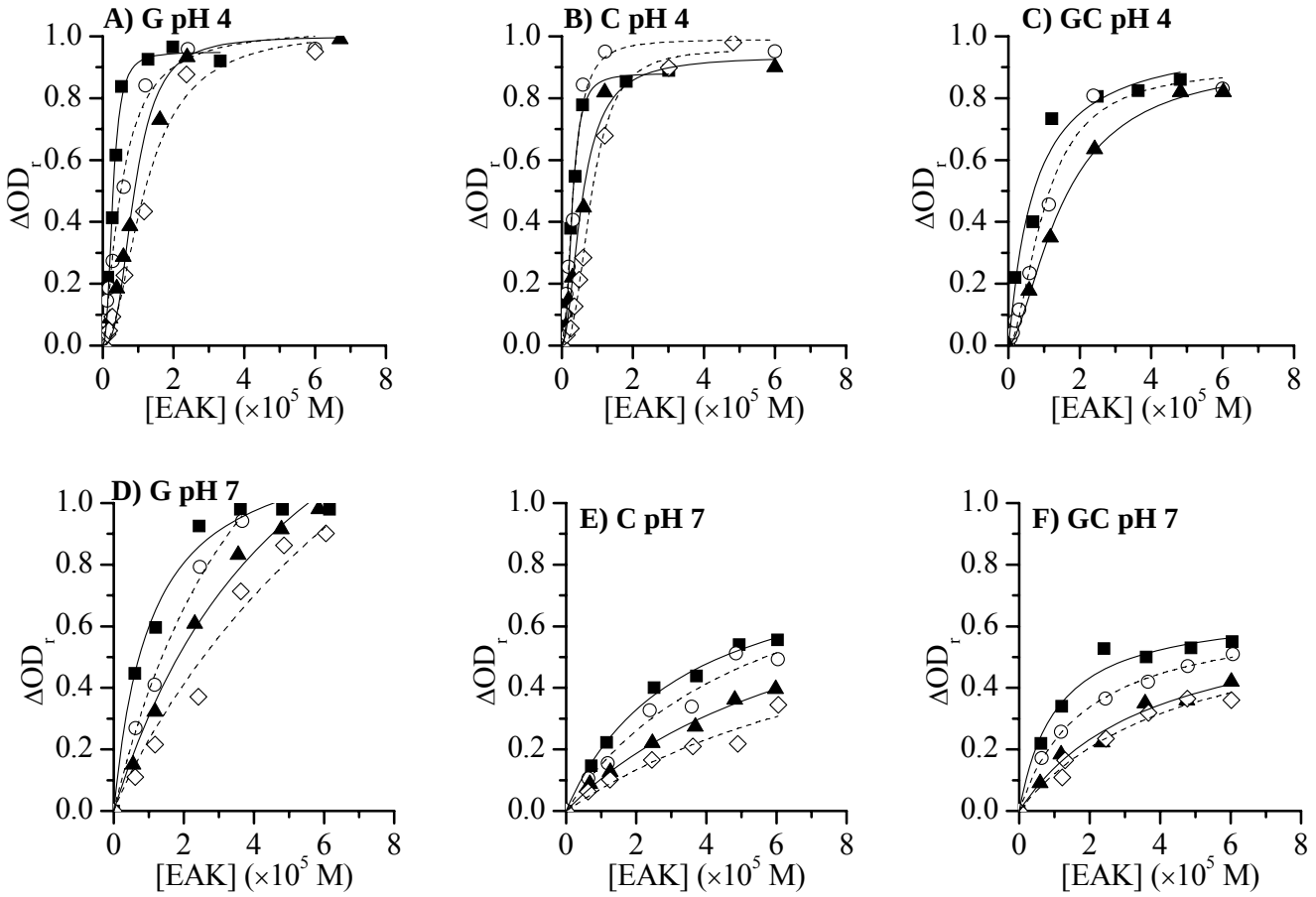

Figure 4.1. Plots of ΔOD_r as a function of the total EAK concentration. (A) pH 4, phosphate concentration of dG_{16} equals 23.2 μM (■), 64 μM (○), 89.6 μM (▲), and 152 μM (◇). (B) pH 4, phosphate concentration of dC_{16} equals 29.6 μM (■), 48 μM (○), 80 μM (▲), and 110 μM (◇). (C) pH 4, phosphate concentration of dGC_{16} equals 44.8 μM (■), 128 μM (○), and 185.6 μM (▲). (D) pH 7, phosphate concentration of dG_{16} equals 16 μM (■), 50.2 μM (○), 64 μM (▲), and 107 μM (◇). (E) pH 7, phosphate concentration of dC_{16} equals 16 μM (■), 36.8 μM (○), 64 μM (▲), and 118.4 μM (◇). (F) pH 7, phosphate concentration of dGC_{16} equals 32 μM (■), 57.6 μM (○), 128 μM (▲), and 182.4 μM (◇). The solid and dashed lines represent the best fits to the equation $\Delta OD_r = A\times[\mathrm{EAK}]^C/(B^C+[\mathrm{EAK}]^C)$ or $\Delta OD_r = A\times[EAK]/(1+B\times[EAK])$, but they do not have physical meaning. The *A, B* and *C* parameters have been listed in Table 4.1. Data in the range of 20-70% of maximal ΔOD_r are used to obtain the ν and ν/P_f values reported in Figure 4.2.

Table 4.1. Parameters A, B or C retrieved from the fits of the ΔOD_r versus [EAK] plots shown in Figure 4.1 with the empirical equation: $\Delta OD_r = A \times [EAK]^C / (B^C + [EAK]^C)$ or $\Delta OD_r = A \times [EAK] / (1 + B \times [EAK])$.

pH 4		dG_{16}		
Concentration	1.45 μM	4 μM	5.6 μM	9.5 μM
A	0.95	1.19	1.00	3.88
B	2.81×10^{-6}	6.90×10^{-6}	8.98×10^{-6}	6.78×10^{-5}
C	2.59	1.25	2.70	1.17

pH 4		dC_{16}		
Concentration	1.85 μM	3.0 μM	5.0 μM	6.88 μM
A	0.93	1.09	2.91	0.99
B	2.75×10^{-6}	3.59×10^{-6}	3×10^{-5}	7.94×10^{-6}
C	2.59	1.79	1.14	2.59

pH 4		dGC_{16}	
Concentration	1.4 μM	4.0 μM	5.8 μM
A	1	2.04	1
	7.35×10^{-6}	3×10^{-5}	1.75×10^{-5}
B	1.05	1.14	1.41

pH 7		dG_{16}		
Concentration	1.0 μM	3.14 μM	4.0 μM	6.69 μM
A	1.16×10^{4}	4.75×10^{4}	3.65×10^{4}	2.89
B	9.42×10^{4}	2.23×10^{4}	1.85×10^{4}	1.35×10^{-4}
C	N/A	N/A	N/A	0.94

pH 7		dC_{16}		
Concentration	1.0 μM	2.3 μM	4.0 μM	7.4 μM
A	3.03×10^{4}	1.77×10^{4}	1.18×10^{4}	0.79×10^{4}
B	4.29×10^{4}	1.78×10^{4}	1.31×10^{4}	0.92×10^{4}

pH 7		dGC_{16}		
Concentration	1.0 μM	1.8 μM	4.0 μM	5.7 μM
A	6.18×10^{4}	3.49×10^{4}	1.77×10^{4}	1.48×10^{4}
B	9.33×10^{4}	5.33×10^{4}	2.64×10^{4}	2.19×10^{4}

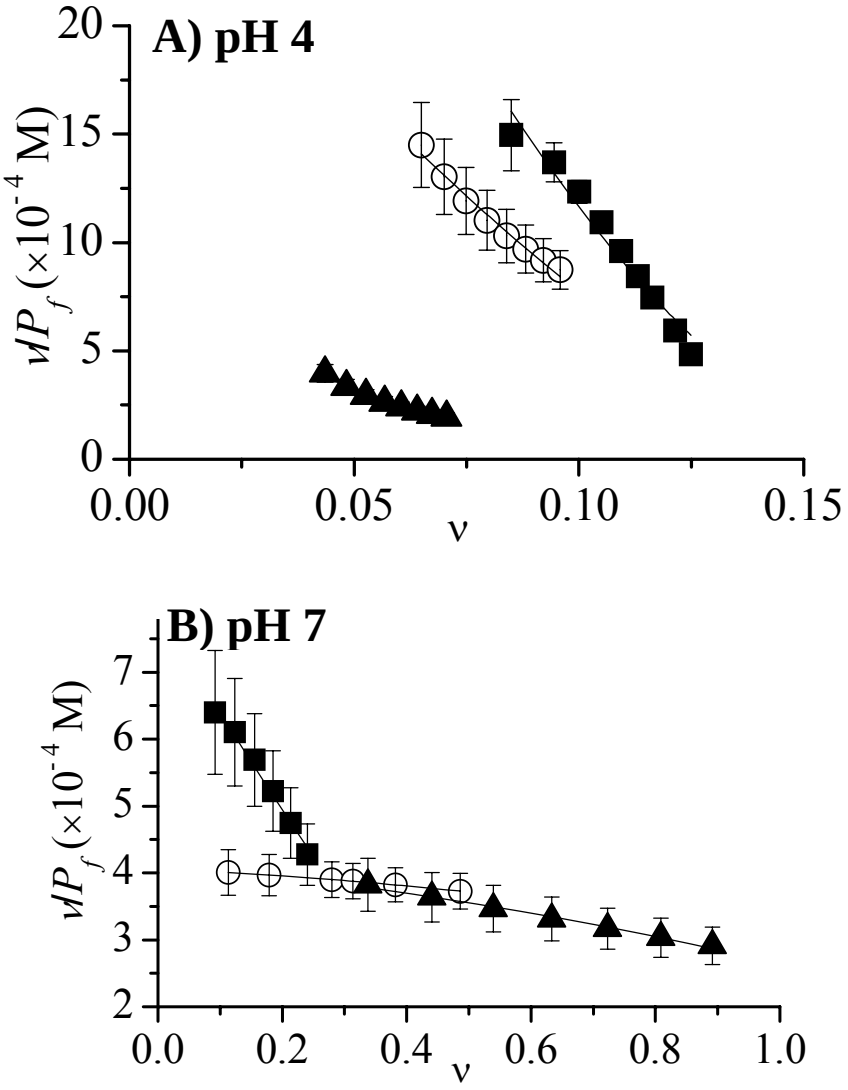

Figure 4.2. Plot of ν/P_f versus ν for the binding of EAK16-IV to dG_{16} (■), dC_{16} (○), and dGC_{16} (▲) at (A) pH 4, and (B) pH 7. The solid lines represent the best fits to Equation 4-2. The parameters used in the fits are listed in Table 4.2.

The binding isotherms in Figure 4.2 were fitted with Equation 4-2 derived by McGhee and von Hippel (MvH) (McGhee and von Hippel, 1974; Tsodikov, *et al*., 2001).

$$\frac{\nu}{P_f} = K(1-n\nu)\left(\frac{1-n\nu}{1-(n-1)\nu}\right)^{(n-1)}\left(\frac{N-n+1}{N}\right) \qquad (4\text{-}2)$$

In Equation 4-2, K and n are the binding constant and binding site size, respectively. N is the total number of phosphate groups of ODN molecules equal to 16 and 32 for ssODN and dsODN molecules, respectively.

The applicability of the MvH model to the binding of a peptide onto ODNs has been discussed earlier. In the present study, the parameters K and n retrieved from the fit of the binding isotherms obtained for EAK16IV with Equation 4-2 are compared to the K and n values reported for the binding of EAK16-II to the same ODNs (Wang, *et al*., 2006). In so doing, the effect of charge distribution on the binding strength of the peptide to ODNs can be characterized.

4.3 Results and Discussion

The description of the effect that the charge distribution of peptides has on their binding to ODNs began with the characterization of the binding of EAK16IV to ODNS in terms of binding strength, size of EAK16IV-ODN aggregates, and accessibility of the ODNs to the solvent. These results were then compared to those obtained with EAK16II. The clear differences observed between the trends obtained with EAK16II and EAK16IV enable one to assess the effect that the peptide charge distribution of EAK16II and EAK16IV has on its binding onto ODNs.

4.3.1 Binding of EAK16IV to ODNs

The earlier study on the binding of EAK16II onto ODNs showed that the binding was strongest at pH 4, weaker at pH 7, and inexistent at pH 11 (Wang, *et al*., 2006). The pK_a values of the four glutamic acids and four lysines in all EAK16-type peptides equal 4.25 and 10.53 (Lehninger, 1993), respectively. Therefore, earlier results suggested that, at pH 4, the positively charged EAK16II associates strongly with the negatively charged ODNs, whereas at pH 11, negatively charged EAK16II does not bind to the ODNs. An intermediate binding strength is observed at pH 7. Such a pH effect on binding would be expected to be similar for EAK16IV. The binding of EAK16IV to dC_{16}, dG_{16}, and dGC_{16} at pH 4, 7, and 11 was thus investigated and was compared with the results obtained with EAK16II to study the charge distribution effect on the binding.

Plots of ΔOD_r, which represents the fraction of ODNs in the EAK16IV-ODN aggregates, as a function of the total EAK16IV concentration are shown in Figure 4.1 for three or four ODN concentrations. ΔOD_r increases with increasing total EAK16IV concentration at both pH 4 and 7. ΔOD_r eventually levels off for the single-stranded dG_{16} and dC_{16} (ssODNs) at pH 4, as the ssODNs become saturated with the peptides. EAK concentrations larger than 60 μM are required to reach saturation at pH 7. The increase of ΔOD_r with EAK concentration in the low EAK16IV concentration range is much less pronounced at pH 7 than at pH 4. Furthermore at a given ODN and EAK

concentration, the ΔOD_r values at pH 7 are significantly lower than those at pH 4. These results suggest that the binding between EAK16IV and the ODNs at pH 4 is stronger than at pH 7. At pH 11, no binding of EAK16IV to the ODNs could be detected. Considering that EAK16IV is positively charged at pH 4, neutral at pH 7, and negatively charged at pH 11, the trends shown in Figure 1 indicate that electrostatic interactions are the main driving force for the binding of EAK16IV to the ODNs. Figure 4.1 also shows that the strength of the binding of EAK16IV to different ODN sequences follows the trend $dG_{16} \geq dC_{16} > dGC_{16}$ at pH 4 and dG_{16} is higher than both dC_{16} and dGC_{16} at pH 7, which is similar to what was observed with EAK16II (Wang, *et al*., 2006).

The formation of large aggregates between EAK16IV and the ODNs can be demonstrated not only by centrifuging out the aggregates from the solution and confirming the reduction in ODN concentration by conducting UV-Vis absorption measurements (Figure 4.1), but also by monitoring the fluorescence anisotropy of a fluorescently labeled ODN as EAK is added to the solution (Figure 4.3). The fluorescence anisotropy of the labeled ODNs increases with increasing EAK concentration as they are incorporated into the aggregates of ODN and EAK16IV. The increase in fluorescence anisotropy is less pronounced at pH 7 than at pH 4, reflecting the weaker binding of EAK16IV to the ODNs at pH 7.

Both UV and anisotropy results showed that the different charge distribution of different EAK peptides does not affect the electrostatic interaction as a main driving force for EAK peptides binding to ODNs.

4.3.2 Composition of the EAK16IV-ODN Solutions

Solutions containing 3.6 μM of FAM-dC_{16} or 1.8 μM of FAM-dGC_{16} were mixed with increasing concentrations of EAK at pH 4 and pH 7. The solutions were centrifuged and the fluorescence anisotropy of the supernatant is shown in Figure 4.3 (solid symbol). The anisotropy of the FAM-labeled ODN species left in the supernatants of the EAK16IV-ODN solutions ranges from 0.08 to 0.12 at pH 4 and 0.03 to 0.04 at pH 7, very close to that of the free labeled ODNs. It demonstrates that the majority of species that lead to the anisotropy increase shown in Figure 4.3 before centrifugation (empty symbols) have been efficiently removed by centrifugation. The EAK16IV-ODN aggregates are large and rigid, certainly resulting from the interaction of the negatively charged ODNs with the peptides. The composition of what remained in the supernatant after centrifugation is investigated.

A 5.7 μM dGC_{16} solution was mixed with 0, 12, and 24 μM of EAK16IV. The solutions were centrifuged and their supernatants were run on a 20 % native gel at pH 4 (Figure 4.4). The bands corresponding to the supernatants of the EAK16IV-dGC_{16} mixtures (Lanes 2-3) appear at the same position as the band corresponding to dGC_{16} (Lane 1). These results suggest that no EAK-dGC_{16}

aggregate of size in the 6-100 bp range (i.e., the bp range of a 20% polyacrylamide gel)[24] remains in the supernatants after centrifugation.

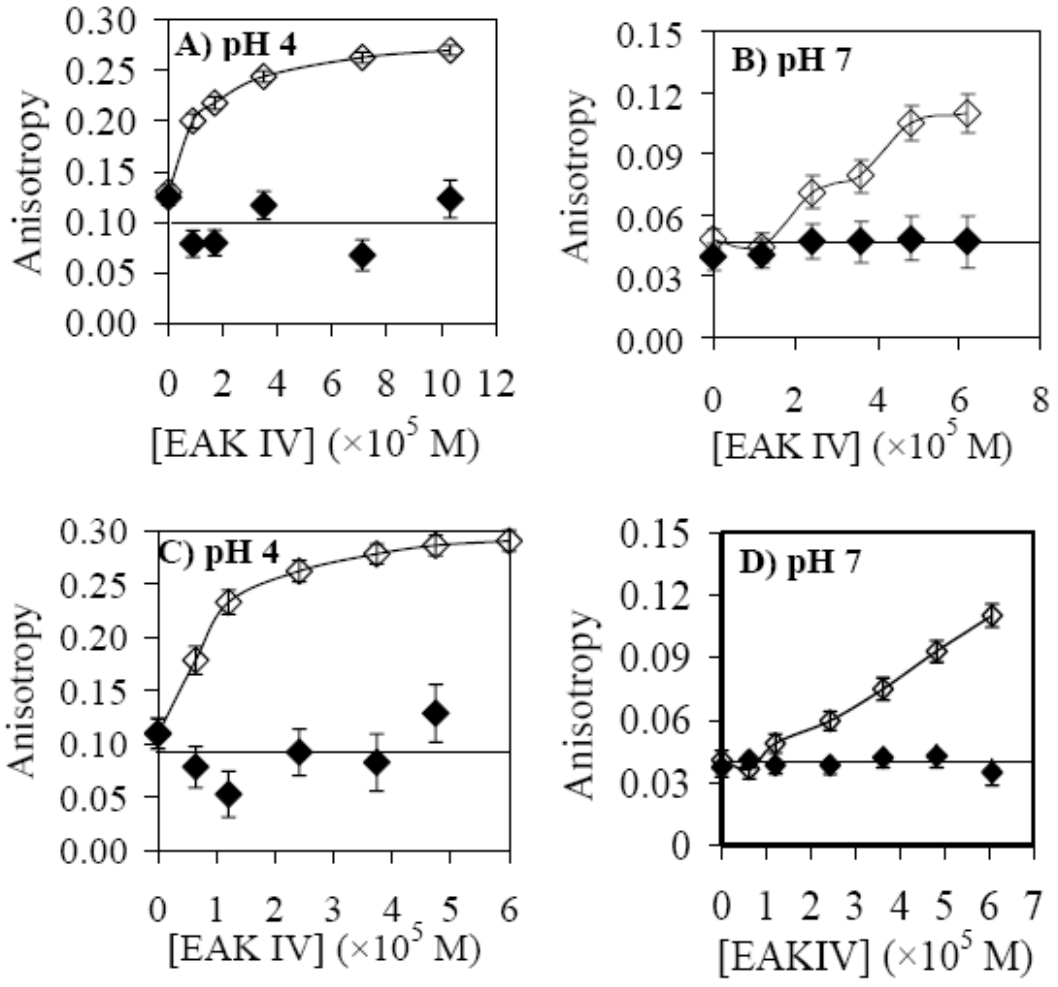

Figure 4.3. Fluorescence anisotropy of the supernatant of EAK16-IV solution mixed with (A) 3.6 μM of FAM-dC_{16} at pH 4 (λ_{ex}=452, λ_{em}=514 nm), (B) 3.6 μM of FAM-dC_{16} at pH 7 (λ_{ex}=494, λ_{em}=514 nm), (C) 1.8 μM of FAM-dGC_{16} at pH 4 (λ_{ex}=452, λ_{em}=514 nm), and (D) 1.8 μM of FAM-dGC_{16} at pH 7 (λ_{ex}=494, λ_{em}=514 nm) before (○) and after centrifugation (●).

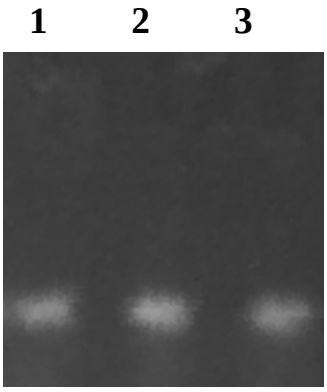

Figure 4.4. 20 % PAGE of 5.7 μM of dGC_{16} mixed with EAK16-IV peptide at pH 4. The peptide concentrations are 0, 12, 24 μM in lanes 1, 2 and 3, respectively.

Absorption measurements were conducted on a mixture of Rh-dC_{16} and EAK16IV to investigate whether some EAK16IV-ODN aggregates larger than a 100 bp duplex but too small to be centrifuged out would remain in the supernatant. Two samples containing 3.9 μM of dC_{16}-Rh in the absence and presence of 60 μM EAK16IV were prepared at pH 7. The absorption spectra of the resulting solution were acquired 30 minutes after sample preparation. As shown in Figure 4.5, the absorbance band at 563 nm characteristic of the rhodamine monomer decreases upon the addition of EAK16IV and a new prominent absorption band at 524 nm appears. The spectrum of the supernatant after centrifugation remains similar to that of the solution before centrifugation. The ratio of the absorbance at 524 and 563 nm (OD_{524}/OD_{563}) of dC_{16}-Rh increases from 0.50 ± 0.01 to 1.01 and 0.96 upon the addition of EAK16IV before and after centrifugation, respectively. Such an increase in the OD_{524}/OD_{563} ratio is due to the formation of rhodamine dimmers (Hamman, *et al*., 1996) induced by the complexation of EAK16IV with dC_{16}-Rh. Since the OD_{524}/OD_{563} ratio of the supernatants is similar to that of the solution before centrifugation, it suggests that the supernantant contains some intermediate EAK16IV-ODN complexes which are too small to be centrifuged out.

The concentration of each species in the supernatant can be calculated using the reported extinction coefficients of the rhodamine dimmer (Hamman, *et al*., 1996) as was done in the EAK16II study (Wang, *et al*., 2006). The supernatant contained 0.50 μM of unimers and 1.54 μM of EAK16IV-ODN complexes. Since the total ODN concentration equals 3.9 μM, the concentration of ODNs in the aggregates which are centrifuged out equals 1.86 μM. These concentrations result in a ΔOD_r value of (1.86 μM)/(3.9 μM) = 0.47, close to the value of 0.52 obtained from the K and n values listed in Table 4.2. The agreement observed between the ΔOD_r values obtained through two

different means supports the procedure used to generate the binding isotherms shown in Figure 4.2 and their analysis with the MvH model to retrieve the *K* and *n* values.

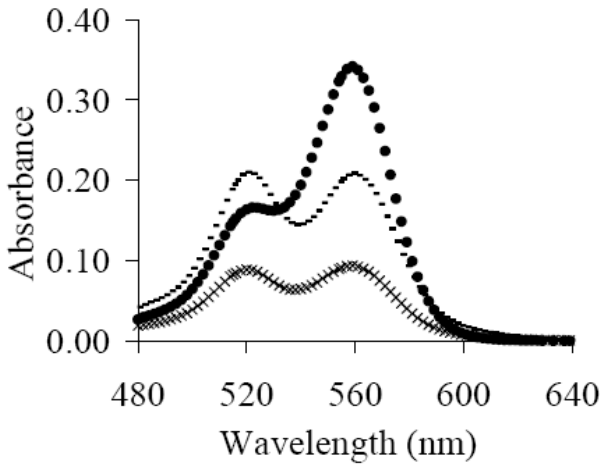

Figure 4.5. UV absorption spectra of dC_{16}-Rh in the presence and absence of EAK16-IV at pH 7. (A) 3.9 μM dC_{16}-Rh (●), (B) 3.9 μM dC_{16}-Rh and 60 μM EAK16-IV before centrifugation (−) and after centrifugation (×).

It is worth noting that the anisotropy of the supernatant after centrifugation is close to that of the free ODNs (Figure 4.3B, solid symbol), even though there are around 75 % of complexes in the supernatant. In contrast, the anisotropy increases substantially when more than 10 % of the ODNs are incorporated into EAK16II-ODN aggregates that can be centrifuged out (Wang, *et al*., 2006). These observations indicate that the aggregates formed between EAK16IV and the ODNs are larger and more rigid than the corresponding intermediate complexes remaining in the supernatant after centrifugation. A similar conclusion was also reached with EAK16II.

The experiments conducted in this section have established that the EAK16IV-ODN solutions contain four species which are the free ODN and EAK16IV molecules, EAK16IV-ODN complexes larger than a 100 bp duplex but too small to be centrifuged out, and large and compact EAK16IV-ODN aggregates.

4.3.3 Binding Pathway

Due to its self-assembly capability, the peptide can form aggregates by itself. Thus, it becomes essential to establish whether the peptide-ODN aggregates result from the complexation of the ODNs with pre-existing EAK16IV aggregates, or from the association between individual ODN and EAK16IV molecules into complexes which further assemble into large, rigid EAK16IV-ODN aggregates. Static Light Scattering (SLS) was used to monitor the formation of the large ODN-EAK aggregates in solution as a function of time. The results are shown in Figure 4.6.

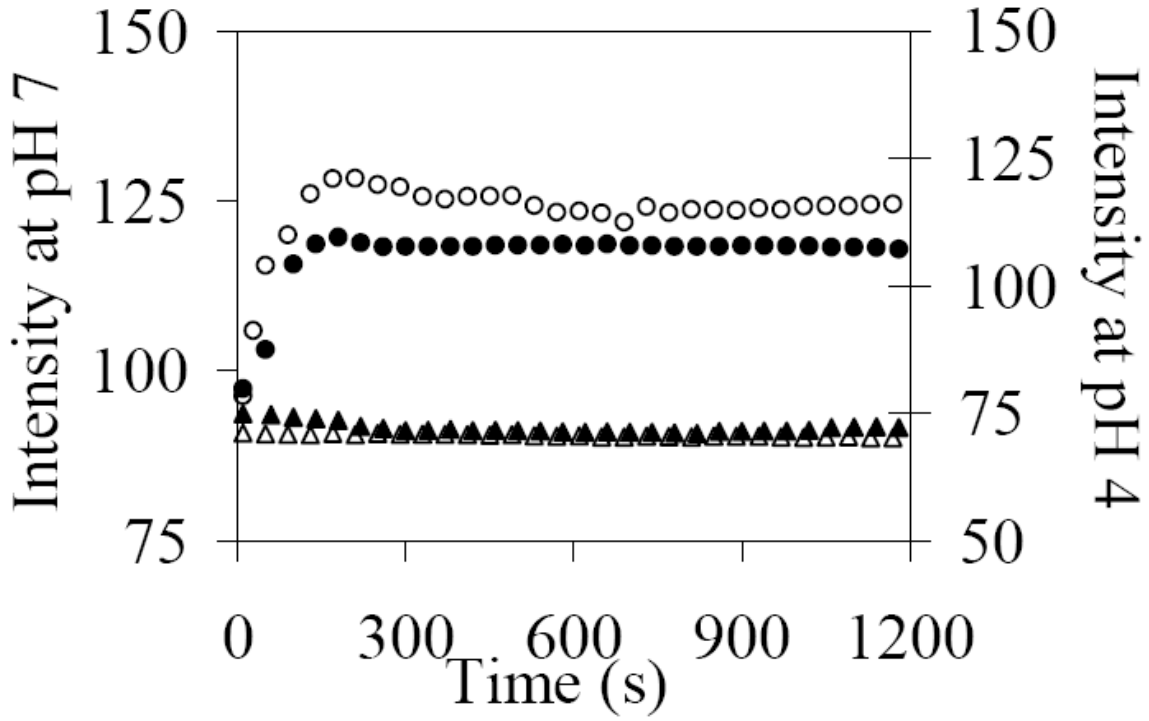

Figure 4.6. SLS experiments performed for 60 μM EAK solution without (triangle) and with the presence of 3.6 μM dG_{16} (circle) at pH 4 (empty symbol) and pH 7 (solid symbol), respectively. $\lambda_{ex} = \lambda_{em} = 350$ nm.

The light scattering intensity of the buffer and EAK16IV solutions remain constant for the first 20 mins at pH 4 and 7 as shown in Figures 4.6. It indicates that the size of EAK remains constant during the first 20 mins after sample preparation. In comparison, the SLS intensity of the EAK-dG_{16} mixtures increases initially and then levels off after the first few minutes at both pHs. Since an increase in SLS intensity reflects an increase in particle size, these results confirm that the formation of EAK16IV-ODN aggregates is complete within a few minutes after mixing.

Theoretically the increase in LS intensity observed at the early time in Figure 4.6 should provide a means to estimate the time scale over which the aggregates form. Unfortunately, the LS measurements were conducted a few minutes after the solution had been prepared and brought to the instrument. Consequently, it was estimated that the time required for the LS intensity to reach a signal in Figure 4.6 could be off by as much as five minutes. Nevertheless, the trends shown in Figure 4.6 allowed one to conclude that the time scale for the formation of EAK16IV-ODN aggregates is shorter than 20 mins. During the same period of time, EAK16IV alone does not self-assemble. This result suggests that EAK16IV binds first to the ODNs in the molecular form to generate intermediate complexes, which further associate into the large aggregates that can be centrifuged out. Thus, the charge distribution did not change the pathway suggested for the formation of peptide-ODN aggregates obtained with EAK16II (Wang, *et al*., 2006).

4.3.4 Size of EAK16IV-ODN Aggregates

AFM and DLS were used to characterize the morphology and size of the EAK16IV-ODN aggregates. Images of the EAK16IV-ODN aggregates formed by mixing a 0.02 mg/mL (12 μM) EAK16IV solution with a 8.6 μM dG_{16} solution, equivalent to an EAK-to-dG_{16} molar ratio of 1.4:1 were taken 5 and 20 mins after sample preparation. The images are shown in Figure 4.7A and B. In average, the aggregates are 36 nm wide, 5.2 nm tall, and over 100 nm long. Their morphology and size do not change after 20 mins. Since the dG_{16} or EAK16IV solutions do not generate any nanostructure on their own over one hour as imaged by AFM (images not shown), the aggregates seen in the AFM images of the EAK-dG_{16} solution must be due to EAK16IV-ODN aggregates. Since the morphologies of the aggregates observed after 5 and 20 mins are very similar, it suggests that the entire aggregation process between dG_{16} and EAK is completed within the first 5 min, which agrees with the conclusion drawn from the SLS experiments shown in Figure 4.6.

The AFM images obtained by mixing a 0.1 mg/mL (60 μM) EAK solution with a 1.8 μM dG_{16} solution in an EAK-to-dG_{16} molar ratio of 33.5:1 at pH 4 at time of 5 and 20 mins are shown in Figures 4.7C and D. Figure 4.7C shows that at this molar ratio, the EAK-dG_{16} solution has two major populations of globular aggregates. One is mainly around 250 nm wide, 15 nm high, and 250 nm long. The other one is around 250 nm wide, 15 nm high, and over 800 nm long, much larger than those obtained at the lower EAK-to-dG_{16} molar ratio. This result suggests that the size of the EAK16IV-ODN aggregates can be affected by adjusting the EAK-to-ODN molar ratio.

The hydrodynamic diameter of the EAK16IV-ODN aggregates in solution was obtained by DLS. The hydrodynamic diameter of a 1.8 μM dG_{16} solution at pH 4 mixed with varying concentrations of EAK16IV was measured 30 min after sample preparation (Figure 4.8). The dG_{16}

solutions exhibit a species with a ~7.5 nm hydrodynamic diameter which is attributed to isolated dG_{16} molecules in solution. The diameter of the species present in the solution increases to around 100 nm while the EAK16IV concentration increases from 0.002 to 0.010 mg/mL (1.2-6 μM). The hydrodynamic diameter increases further as the EAK16IV concentration increases from 0.02 to 0.10 mg/mL (12-60 μM). At EAK16IV concentration of 0.10 mg/mL, two major sizes are around 250 nm and 1000 nm, respectively. The size of the aggregates generated at different EAK-to-ODN molar ratios is compatible with that obtained by AFM. Since the steady-state light scattering results (Figure 4.6) suggest that EAK is present as a single molecule 30 mins after sample preparation, its size is expected to be much smaller than the large diameters observed by DLS. These large diameters characterize the aggregates of ODN and EAK16IV in solution.

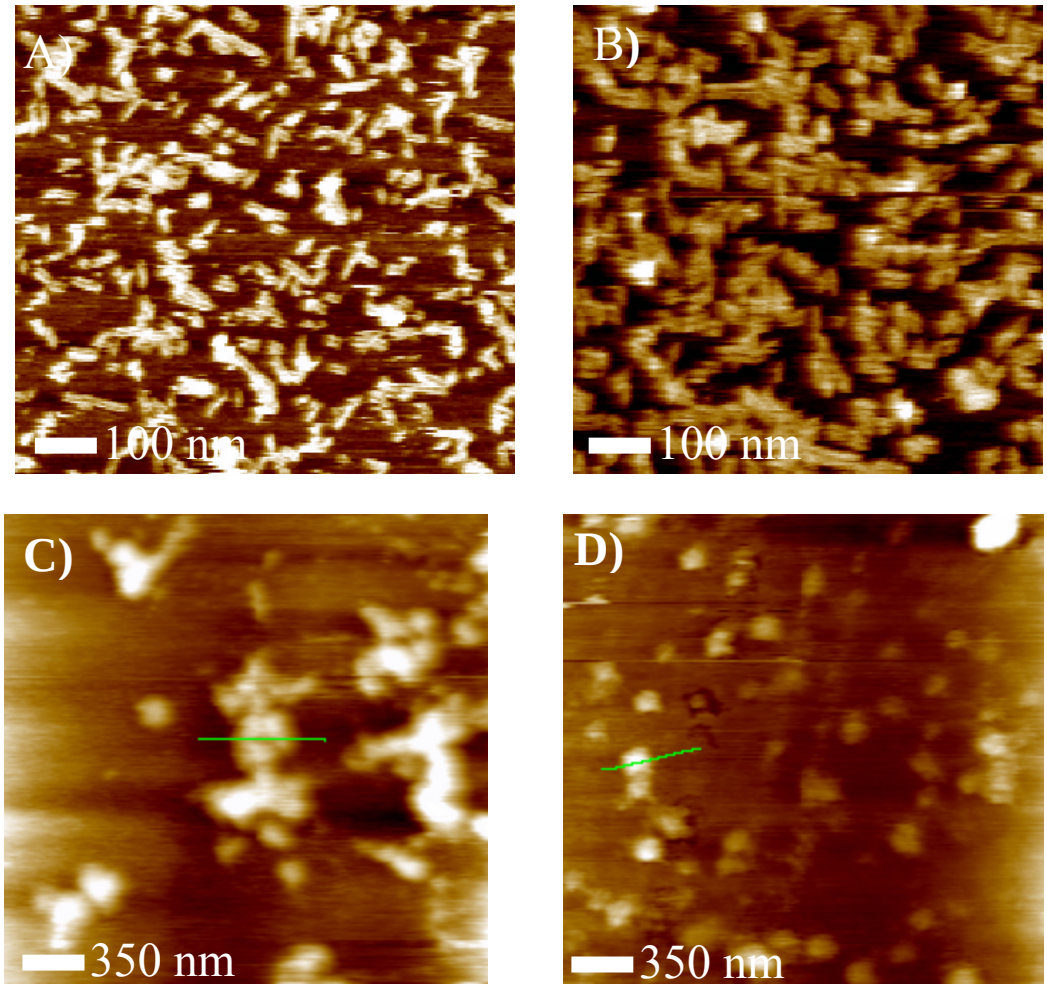

Figure 4.7. AFM images of the EAK16IV-dG_{16} complexes formed at pH 4. The solution containing 8.6 μM dG_{16} and 60 μM EAK16IV imaged after (A) 5 mins, (B) 20 mins. Scale bar = 100 nm. The solution of 1.8 μM dG_{16} and 60 μM EAK16-IV imaged after (C) 5 mins, (D) 20 mins. Scale bar = 350 nm.

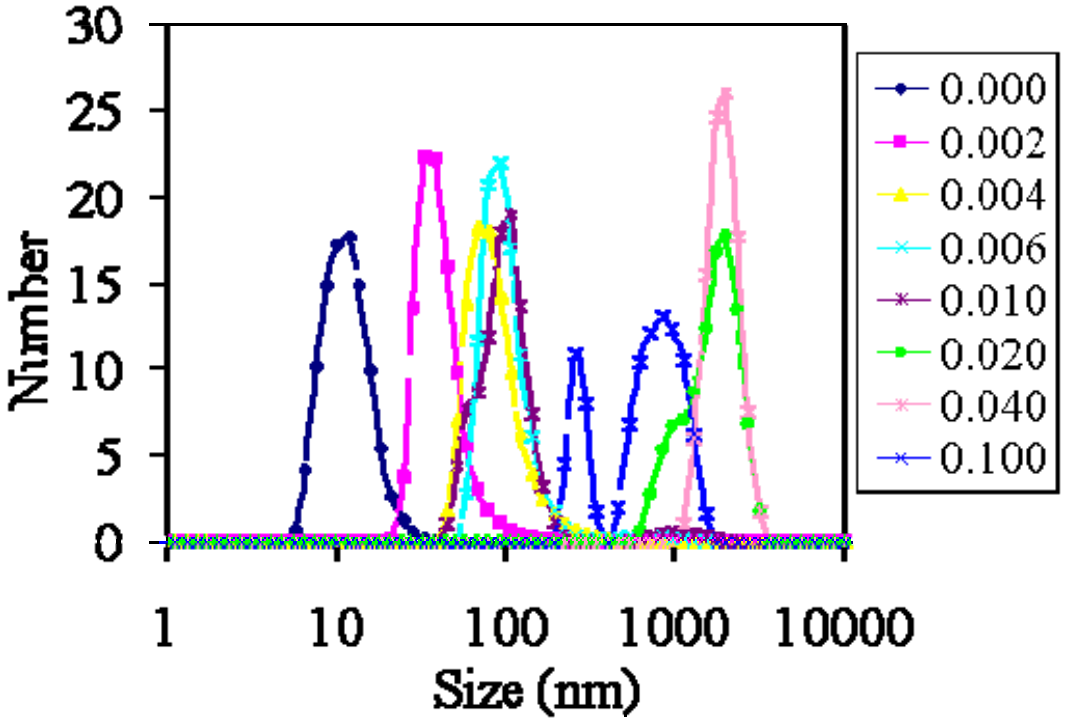

Figure 4.8. Population histogram of the EAK16IV-ODN aggregates as a function of particle diameter determined by dynamic light scattering. The solutions contained 1.8 μM of dG_{16} with increasing EAK16IV concentration (mg/mL) at pH 4.

4.3.5 Binding Parameters

The binding isotherms obtained by plotting v/P_f as a function of v were generated from the curves shown in Figure 4.1 following the procedure outlined in the Binding Assay section. The resulting binding isotherms (Figure 4.2) were fitted with Equation 4-2 according to the McGhee and von-Hippel (MvH) model to obtain the binding constant, K, and the binding site size, n, at two pH values. The K and n values are listed in Table 4.2. Although the MvH model does not account for the formation of the EAK16IV-ODN aggregates, the fits of the binding isotherms with Equation 4-2 were rather good, as shown in Figure 4.2.

The effect of pH on the binding of EAK16IV to the ODNs can be seen from Table 4.2. The binding constant for EAK16IV binding to a given ODN increases when the pH is decreased from 7 to 4. This result indicates that electrostatic interactions play an important role in the binding of EAK16IV to the ODNs.

Table 4.2. Binding constant *K* and binding site size *n* retrieved from the fits of the data shown in Figure 4.2 with Equation 4-2.

ODNs	pH 4		pH 7		pH 11	
	n	K (10^4 M^{-1})	n	K (10^4 M^{-1})	N	K (M^{-1})
dG_{16}	4.99 ±0.30	45.1 ± 4.4	1.50 ± 0.1	8.2 ± 1.4	No Interaction	
dC_{16}	4.76 ± 0.13	37.4 ± 5.7	0.55 ± 0.02	4.0 ± 0.3	No Interaction	
dGC_{16}	7.05 ± 0.24	9.7 ± 1.0	0.62 ± 0.04	4.1 ± 0.4	No Interaction	

* Each fit has $R^2 > 0.94$ with at least 5 data points. The error on the *K* and *n* values is estimated by generating three binding isotherms based on the trends shown in Figure 4.2. These binding isotherms were generated by taking arbitrarily the larger, intermediate, and smaller ν/P_f values obtained according to the error bars shown in Figure 4-2. The three binding isotherms were fitted with the McGhee and von Hippel model (Equation 4-2). And the spread in the *K* and *n* values retrieved from the fits provided an estimate of the errors on *K* and *n*, as reported in Table 4.2.

The binding parameters listed in Table 4.2 allow one to compare the binding strength of EAK16IV to a given ODN at a specific pH. At pH 4, *K* decreases according to the trend $dG_{16} \geq dC_{16} > dGC_{16}$. Thus, the binding strength of EAK16IV to dG_{16}, dC_{16}, and dGC_{16} follows the same trend observed for EAK16II. Similarly one finds the trend $dG_{16} > dC_{16} \approx dGC_{16}$ for the binding of EAK16IV at pH 7. These trends are similar to those obtained with EAK16II. As has been argued earlier, the slight stronger binding of the EAK peptides with dG_{16} might be a result of the stronger hydrogen bonds being generated between lysine and guanine (Wang, *et al*, 2006).

The effect of charge distribution of the peptides on the binding of EAKs to the ODNs can be investigated in a straightforward manner from the binding parameters listed in Table 4.2. The equilibrium constants obtained for the binding of EAK16IV to the ODNs range from 4.1×10^4 to 45.1×10^4 M^{-1}. In comparison, EAK16II has been reported to bind to these ODNs with binding constants in the range of 0.7×10^4 to 7.6×10^4 M^{-1}. At a same pH and for a given ODN sequence, EAK16IV displays a larger *K* value than EAK16II. It suggests that EAK16IV binds to the ODNs more strongly than EAK16II. Considering that the charge distribution is − − + + − − + + for EAK16II and − − − − + + + + + for EAK16IV at neutral pH and that those negatively charged amino acid are protonated at pH 4, all positively charged lysines accumulate at one end of the EAK16IV peptide, but are more evenly distributed along the EAK16II backbone. Thus concentrating the binding sites of a peptide at one position of the peptide backbone appears to be beneficial to enhance the binding strength of that peptide to an ODN.

4.3.6 Reduced Accessibility to Solvent of ODNs Embedded in an EAK16-IV Matrix

A successful peptide-based ODN delivery system must ensure that the ODNs incorporated inside the peptidic matrix are protected against the nucleases present in vivo. Consequently the location of the ODNs within the EAK16IV-ODN aggregates must be established. ODNs located inside EAK16IV-ODN aggregates will be less accessible to the solvent than those located on the surface, and hence be better protected from the surroundings. Fluorescence dynamic quenching experiments were carried out to assess the accessibility of the ODNs to the solvent. dC_{16} was labeled at the 5'-end with fluorescein. KI was used as the quencher because it can dynamically quench fluorescein via diffusive encounters (Wang, *et al*, 2006). The K^+ concentration was maintained constant at 0.6 M by addition of K_2SO_4 to the KI solution. The fluorescence emission of a 1.2 μM solution of the labeled dC_{16} was monitored as a function of KI concentration in the absence or presence of 120 μM EAK (0.2 mg/mL).

The fluorescence intensity of fluorescein decreases upon addition of KI to the solution. The Stern-Volmer plot is given in Figure 4.9 where the I_o/I ratio is represented as a function of iodide concentration. The quantities I_o and I represent the fluorescence intensity of the chromophore without and with quencher, respectively. The I_o/I ratio increases linearly with iodide concentration in the absence or presence of EAK. However the increase is stronger in the absence of EAK.

The fluorescence decays of FAM-dC_{16} were acquired in the presence and absence of EAK. The pre-exponential factors and decay times obtained from the analysis of the fluorescence decays with a sum of exponentials are listed in Table 4.3. As for EAK16II, the lifetime of the chromophore is not affected by the presence of EAK.

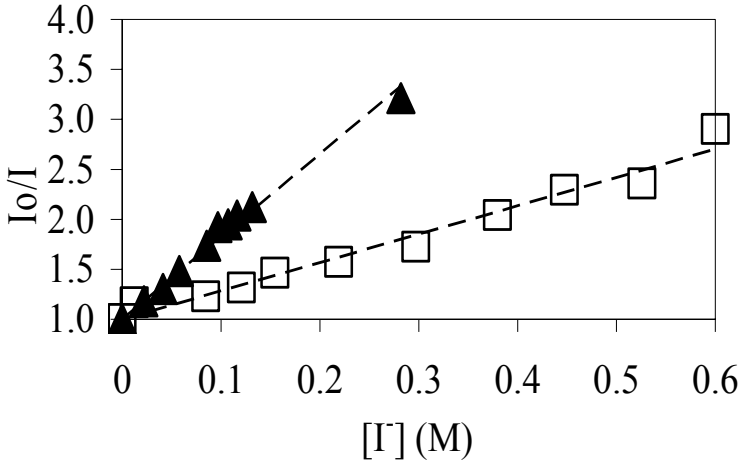

Figure 4.9. Stern-Volmer plots for a solution of 1.2 μM of fluorescently labeled dC_{16} free and bound to 120 μM of EAK16IV at pH 4 quenched by KI. Solid lines represent the fits to the Stern-Volmer equation with parameters listed in Table 4.4. FAM-dC_{16} (▲), FAM-dC_{16}-EAK (□) with λ_{ex} = 452 nm, λ_{em} = 514 nm.

Table 4.3. Pre-exponential factors and decay times obtained from the analysis of the fluorescence decays of the fluorescent ODNs in the absence and presence of 120 μM EAK16-IV in pH 4 buffer, respectively.

	τ_1 (ns)	α_1	τ_2 (ns)	α_2	$\bar{\tau}$ (ns)[a]	χ^2
FAM-dC$_{16}$	3.9	0.67	2.0	0.33	3.3	1.12
EAK-FAM-dC$_{16}$	4.1	0.67	1.6	0.33	3.3	1.01

[a] $\bar{\tau}$ is the number average lifetime, given by $\bar{\tau} = \frac{\sum \tau_i \alpha_i}{\sum \alpha_i}$

To evaluate the effect that the presence of EAK1-IV has on the accessibility of the ODNs to the solvent, the I_o/I vs. [I^-] plots in Figure 4.9 were fitted with the Stern-Volmer equation given in Equation 4-3 (Lakowicz, 1999):

$$I_o / I = 1 + K_{SV}[Q] = 1 + k_q \tau_o [Q] \qquad (4\text{-}3)$$

where, K_{SV} is the Stern-Volmer constant, and k_q is the bimolecular quenching rate constant, which reflects the accessibility of the chromophore to the solvent (Lakowicz, 1999). It is determined from the ratio K_{SV}/τ_o where τ_o is the lifetime of the chromophore in the absence of quencher (Lakowicz, 1999). Since the fluorescence decays of FAM-dC$_{16}$ were not monoexponential, the number-average lifetime $\overline{\tau_o}$ of the decays was used instead of τ_o. The values of K_{SV}, $\overline{\tau_o}$, and k_q are listed in Table 4.4 In the absence of EAK, k_q for FAM-dC$_{16}$ equals 2.5 $\times$ 10^9 $M^{-1}s^{-1}$. The presence of EAK reduces k_q to 0.9 $\times$ 10^9 $M^{-1}s^{-1}$. There might be two causes for the decrease of k_q after incorporation of FAM-dC$_{16}$ into the EAK16IV-ODN aggregates: the diminution of the diffusion coefficient of FAM-dC$_{16}$ or the reduced accessibility of FAM-dC$_{16}$. Considering that the diffusion coefficient of the fluorophore-labeled ODN with 16 bases is about 10-fold lower than that of the iodide ion (Gordan, 2005; Weast, 1971), the diminution of the diffusion coefficient of the ODNs after binding to EAK16IV will be

expected to affect k_q by no more than 10 %. Thus, the decrease in k_q observed above (~ 64 %) suggests that the accessibility of ODNs must be reduced in the presence of EAK.

Table 4.4. Stern-Volmer quenching constants K_{SV}, bimolecular quenching rate constant k_q, fluorescence lifetime τ_o, and relative accessibility change γ when dC_{16} is in the absence or presence of 120 μM of EAK16-IV in pH 4 buffer.

ODNs	5' end fluorescein labeling			
	K_{SV} (M^{-1})	τ_o (ns)	k_q ($10^9 M^{-1}S^{-1}$)	γ
Fluorescently labeled dC_{16} (free)	8.3 ± 0.2	3.3	2.5 ± 0.1	
Fluorescently labeled EAK-dC_{16} (bound)	2.8 ± 0.1	3.3	0.85 ± 0.0	0.34

The relative change in accessibility of the ODNs to the solvent upon EAK binding was quantified from the ratio of the k_q values obtained in the presence and absence of the peptides (Bujalowski and Klonowaka, 1994; Wang, *et al*., 2006). This ratio is referred to as γ. The value of γ is found to be 0.36 suggesting that the accessibility of dC_{16} to the solvent is reduced by about 64 % inside the EAK16IV-ODN aggregates.

In addition, the quenching events which were monitored took place between the negatively charged quencher (I^-) and either the negatively charged ODNs or the partially neutralized EAK16IV-ODN aggregates. Consequently, the quencher would be expected to quench more efficiently the EAK16IV-ODN aggregates due to the reduction in electrostatic repulsion. The opposite is observed, which strengthens the claim that EAK protects the ODN from its environment (Wang, *et al*., 2006).

Compared to EAK16II, the binding of EAK16IV to ODNs appears to induce a more efficient protection of the ODN by reducing the accessibility of FAM-dC_{16} to the solvent from 40 % for EAK16II to 64 % for EAK16IV (Wang, *et al*., 2006). It suggests that the stronger binding afforded by EAK16IV provides a better protection against small molecules or anions present in the solution, and consequently against large nucleases. This feature should help prevent ODN degradation. This property is desired for any oligonucleotide delivery candidate since the rapid degradation of ODNs in a biological system by nucleases is one of the major hurdles that must be overcome for a successful

antisense delivery. The stability of the EAK16IV-ODN aggregates in the presence of the nuclease is the topic of next chapter.

4.4 Summary

This study has investigated the binding of EAK16IV to ODNs. UV-Vis absorption and fluorescence anisotropy experiments demonstrated the formation of large EAK16IV-ODN aggregates which could be centrifuged out of solution. The binding isotherms constructed from the UV-Vis absorption data were fitted with the modified non-cooperative MvH model to extract the equilibrium binding constants and binding site sizes. The results showed that EAK16IV, whose positively charged residues are clustered at one end of the peptide, binds to ODNs more strongly than EAK16II whose positively charged residues are distributed throughout the peptide. Static light scattering experiments demonstrated that EAK16IV binds to ODNs in a similar manner as EAK16II. Peptide and ODNs complex first in the molecular form followed by the association of the complexes into large aggregates.

The size of the EAK16IV-ODN aggregates was determined by AFM and DLS. It ranged from a few hundreds of nanometers to several micrometers, depending on the molecular ratio of EAK16IV to ODNs. Fluorescence quenching experiments showed that the accessibility of the ODNs to the solvent is reduced by 64 % upon the addition of EAK16IV, a much higher reduction than the value of 40% caused by EAK16II. In view of these results, EAK16IV might be a better peptide candidate for the protection of an ODN against degradation by nucleases.

References

Akinrimisi, E. O., C. Sander, and P. O. P. Ts'o. 1963. Properties of helical polycytidylic acid. *Biochemistry* **2:** 340-344.

Bolumar, T., T. Y. Sanz, M. C. Aristoy, and F. Toldra. 2003. Purification and Characterization of a Prolyl Aminopeptidase from Debaryomyces hansenii. *Appl. Environ. Microbio.* **69:** 227-232.

Bujalowski, W., and T. M. Lohman. 1987. A General Method of Analysis of Ligand-Macromolecule Equilibria Using a Spectroscopic Signal from the Ligand to Monitor Binding. Application to E. coli SSB Protein-Nucleic Acid Interactions. *Biochemistry* **26:** 3099-3106.

Bujalowski, W., and M. M. Klonowaka. 1994. Structural Characteristics of the Nucleotide-Binding Site of Escherichia coli Primary Replicative Helicase DnaB Protein. Studies with Ribose and Base-Modified Fluorescent Nucleotide Analogs. *Biochemistry* **33:** 4682-4694.

Fung, S.Y., C. Keyes, J. Duhamel, and P. Chen. 2003. Concentration Effect on the Aggregation of a Self-Assembling Oligopeptide. *Biophys. J.* **85:** 537-548.

Gordan, S.P., S. Berezhna, D. Scherfeld, N. Kahya, and P. Schwille. 2005. Characterization of Interaction between Cationic Lipid-Oligonucleotide Complexes and Cellular Membrane Lipids Using Confocal Imaging and Fluorescence Correlation Spectroscopy. *Biophys. J.* 88: 305-316.

Hamman, B. D., A. V. Oleinikov, G. G. Jokhadze, D. E. Bochkariov, R. R. Traut, and D. M. Jameson. 1996. Tetramethylrhodamine Dimer Formation as a Spectroscopic Probe of the Conformation of *Escherichia coli* Ribosomal Protein L7/L12 Dimers. *J. Biol. Chem.* **271:** 7568-7573.

Holmes, T. C., S. D. Lacelle, X. Su, G. Liu, A. Rich and S. Zhang. 2000. Extensive neurite outgrowth and active synapse formation on self-assembling peptide scaffolds. *Proc. Natl. Acad. Sci. USA* **97:** 6728-6733.

Hong, Y., R. L. Legge, S. Zhang, and P. Chen. 2003. Effect of Amino Acid Sequence and pH on Nanofiber Formation of Self-Assembling Peptides EAK16-II and EAK16-IV. *Biomacromol.* **4:** 1433-1442.

Jun, S., Y. Hong, H. Imamura, B. Y. Ha, J. Bechhoefer, and P. Chen. 2004. Self-assembly of the ionic peptide EAK16: The effect of charge distributions on self-assembly. *Biophy. J.* **87:** 1249-1259.

Keyes-Bag, C., S. Y. Fung, J. Bezaire, and P. Chen. 2004. Self-Assembling Peptide as a Potential Carrier of Hydrophobic Compounds. *J. Am. Chem. Soc.* **126:** 7522-7532.

Lakowicz, J. R. 1999. *Principles of Fluorescence Spectroscopy*. Plenum Publisher, New York.

Lehninger, A. L. 1993. *Principles of Biochemistry*. Worth Publishers.

Lohaman, T.M., and W. Bujalowski. 1991. Thermodynamic methods for model-independent determination of equilibrium binding isotherms for protein-DNA interactions-Spectroscopic approaches to monitor binding. *Methods Enzymol.* **208:** 258-290.

McGhee, J. D., and P. H. von Hippel. 1974. Theoretical Aspects of DNA-Protein Interactions: Co-operatice and Non-co-operative Binding of Large Ligands to a One-dimensional Homogeneous Lattice. *J. Mol. Biol.* **86:** 469-489.

Plank, C., M. X. Tang, A. R. Wolfe, and F. C. Szoka. 1999. Branched cationic peptides for gene delivery: Role of type and number of cationic residues in formation and *in vitro* activity of DNA polyplexes. *Human Gene Ther.* **10:** 319-332.

Press, W. H., B. P. Flannery, S. A. Teukolsky, and W. T. Vetterling. 1992. *Numerical Recipes. The Art of Scientific Computing*. Cambridge University Press, Cambridge.

Sambrook, J., E. F. Fritsch, and T. Maniatis 1989. *Molecular Cloning: A Laboratory Manual*, *2nd Edition*, P 6.37. Cold Spring Harbor Laboratory Press.

Simeoni, F., M. C. Morris, F. Heitz, and G. Divita. 2003. Insight into the mechanism of the peptide-based gene delivery system MPG: implications for delivery of siRNA into Mammalian Cells. *Nucl. Acids Res.* **31:** 2717-2724.

Smith, L. C., J. Duguid, M. S. Wadhwa, M. J. Logan, C. H. Tung, V. Edwards, and J. T. Sparrow.1998. Synthetic peptide-based DNA complexes for nonviral gene delivery. *Adv. Drug Deliv. Rev.* **30:** 115-131.

Tsodikov, O. V., J. A. Holbrook, I. A. Shkel, and M. T. Record. 2001. Analytic Binding Isotherms Describing Competitive Interactions of a Protein Ligand with Specific and Nonspecific Sites on the Same DNA Oligomer. *Biophy. J.* **81:** 1960-1969.

Wang, M., M. Law, J. Duhamel, and P. Chen. 2006. Interaction of a Self-Assembling Peptide with Oligonucleotides: Complexation and Aggregation. *Biophys. J.* In Press

Weast, R.C. 1971. *Handbook of Chemistry and Physics.* P. F47. The Chemical Rubber Co. Cleveland, Ohio.

Zhang, S., T. C. Holmes, C. Lockshin, and A. Rich. 1993. Spontaneous Assembly of a Self-Complementary Oligopeptide to Form a Stable Macroscopic Membrane. *Proc. Natl. Acad. Sci. USA* **90**: 3334-3338.

Zhang, S., T. C. Holmes, M. Dipersio, R. O. Hynes, X. Su, and A. Rich. 1995. Self-complementary Oligopeptide Matrices Support Mammalian Cell Attachment. *Biomater.* **16:** 1385-1393.

Zhang, S. 2002. Emerging biological materials through molecular self-assembly. *Biotechnol. Adv.* **20:** 321-339.

Chapter 5
Aggregates of Oligonucletides and Self-Assembling Peptides. Nuclease Resistance of Oligonucleotides and Stability of the Aggregates

5.1 Introduction

Antisense oligodeoxynucleotides (ODNs) are being widely investigated to downregulate gene expression (Crooke, 1992; Dias and Stein, 2002). To inhibit the production of faulty proteins, antisense ODNs have to reach the cytoplasm or nucleus of cells where they act by specific binding to the target mRNA or DNA. An important challenge in antisense technology remains the lack of efficient delivery systems. Before the ODNs can reach their target site, they have to cross the cellular membrane, escape from the endosomal compartment, leave their carriers and hybridize with the target sequence (Garcia-Chaumont, *et al*., 2000). During these multiple steps of trafficking, rapid degradation of the ODNs results in shorter ODN segments, which are more likely to base pair with parasite mRNA sequence other than the target sequences (Crooke, 2000). Thus, the sequence specificity and efficacy of the ODNs are compromised and their success in therapeutic applications is limited.

One approach to improve the stability of antisense ODNs against nucleases is through chemical modification of the ODN phosphodiester backbone. However, the modified ODNs often have low transfection efficiency resulting in lowered biological activity (Ghosh, *et al*., 1993; Pavid, 2000), non-specific protein binding, or poor solubility (Hogrefe, 1999). The other common approach to improving antisense activity is the development of suitable delivery systems. The delivery system, often composed of cationic lipids, polymers, or peptides, is designed to improve the cellular uptake of ODNs and facilitate their escape from the endosomes. Protection of the ODNs against nucleases is an important aspect in the design of delivery systems. Ideally, a delivery system should protect the ODNs during all the different steps involved in the trafficking of the ODNs from outside a cell to its target inside the cell. In general, cationic carriers are believed to protect the ODNs against degradation. Indeed, some carriers have been reported to enhance efficacy of antisense ODNs, while others have failed (Remaut, *et al*., 2005).

Previous work from our laboratory has established that ODNs can complex with a class of self-assembling peptides of the EAK family (Wang, *et al*., 2006). These self-assembling peptides have an amphiphilic structure consisting of alternating negatively and positively charged amino acids on one

side, and hydrophobic amino acids on the other side. The ionic complementarity, together with hydrogen bonding and hydrophobic and van der Waals interactions promote the self-assembly of the peptides into highly stable aggregates over time. The positively charged amino acids facilitate the complexation of the peptide with the ODNs through electrostatic interaction. The inherent self-assembling capability of EAK further enables the association of the resulting complexes into aggregates. The ODNs incorporated inside the aggregates exhibit reduced accessibility to the surrounding solvent, which may also reduce their accessibility to nuclease, and prevent their degradation. These peptides do not cause cytotoxicity, arouse minimal immune response and inflammation in the host, and are biocompatible (Zhang, *et al*., 1994; Zhang, 2002). They can be easily modified to incorporate cell targeting compounds to improve specific cellular uptake. These combined features make them promising carriers for gene delivery.

The present study focuses on the stability of the ODN-EAK aggregates and the nuclease resistance of the ODNs embedded in the EAK matrix. Fluorescence resonance energy transfer (FRET) is a common tool used to monitor the degradation of ODNs (Uchiyama, *et al*., 1996). In FRET, the excited donor (D) transfers its excess energy to the acceptor (A) in a radiationless process, which causes a decrease in the fluorescence intensity of the donor. The FRET efficiency is extremely sensitive to the distance between the donor and the acceptor. FRET can be used to study the degradation of ODNs doubly-labeled with a donor and acceptor fluorophore at each end since degradation of the ODNs results in a longer donor-acceptor distance and a substantial decrease in FRET efficiency (Uchiyama, *et al*., 1996).

In this study, the nuclease resistance of doubly-labeled ODNs in the EAK-ODN aggregates prepared at different pHs was evaluated using FRET. The percentage of degraded ODNs was determined from the ratio of fluorescence intensity of the donor to that of the acceptor, the I_D/I_A ratio, which is a measure of FRET efficiency. Intact ODNs where the donor and acceptor are held at short distances undergo efficient FRET and have small I_D/I_A ratios. Degraded ODNs have donors and acceptors that are no longer held in close proximity and the I_D/I_A ratio is large. The dissociation of the EAK-ODN aggregates generated at pH 4 and pH 7 after they were incubated with nuclease solution was investigated by UV-Vis absorption measurements to ensure that a reduced nuclease resistance of the ODNs was due to a break up of the EAK-ODN aggregates.

The stability of the EAK-ODN aggregates upon dilution of the solution was also studied to predict the effect of dilution on the protection provided by the EAK matrix to the ODNs. The stability after dilution of an assembly resulting from the association between an ODN and its carrier is an important parameter to assess as the assembly is being diluted many folds after the delivery system

has been injected in the body. A break up of the ODN-carrier assembly exposes the ODNs to the surrounding medium which leads to their degradation by nucleases.

5.2 Materials and Methods

5.2.1 Materials

The reagents, buffers, peptides, and oligonucleotides are the same as those reported in Chapter 2. *E.coli* exonuclease I (20 U/μL) and its 10× degradation buffer (670 mM glycine-KOH (pH 9.5 at 25°C), 67 mM $MgCl_2$, 10 mM DTT) were purchased from Fermentas Canada Inc. (Burlington, Canada).

A cytosine hexadecamer doubly-labeled with fluorescein at the 5'-end and rhodamine at the 3'-end, namely Fl-dC_{16}-Rh, was used for the nuclease resistance study. Two unlabeled guanine and cytosine hexadecamers, namely dG_{16} and dC_{16}, were used for the stability study. The ODNs obtained were 95 % purity after HPLC purification and were purchased from Eurogentec North America (San Diego, USA).

5.2.2 Preparation of the EAK-ODN Aggregates for Nuclease Resistance Studies

The evaluation of the protection afforded to the oligonucleotides by the EAK matrix against nuclease degradation was conducted as follows. First, 100 μL of 2.3 μM Fl-dC_{16}-Rh alone or encapsulated with 60 μM of EAK was prepared by mixing an ODN stock solution with binding buffer or with an EAK stock solution, respectively. The resulting solutions were vortexed vigorously for a few seconds and kept at 25 ºC for 30 mins prior to use. Second, 100 μL of the EAK-ODN solution was centrifuged at 10,000 rpm for 2 minutes in an Eppendorf Centrifuge 5410. The pellets, corresponding to the EAK-ODN aggregates, were collected and incubated with 500 μL of 0.7 U/μL exonuclease I in 1× degradation buffer (pH 9.5) at 25 ºC.

To ensure that degradation of the ODNs was occurring in the absence of EAK, 100 μL of a 2.3 μM ODN solution was diluted 5-fold by adding the appropriate amount of stock exonuclease I solution (20 U/μL), 10× degradation buffer, and water to obtain a solution with 0.46 μM ODN, 0.7 U/μL exonuclease I in 1× degradation buffer (pH 9.5) at 25ºC. Further controls included incubating the EAK-ODN mixture or ODN solutions with 1× degradation buffer under the same conditions as those treated with exonuclease I. For all these solutions, 55 μL of solution was removed at different points in time and inactivated by the addition of 2 μL of 40 % sodium dodecyl sulfate (SDS) (Moyer and Rothe, 1977). The resulting samples were lyophilized with the Savant Model ISS110 DNA SpeedVac system (Minnesota, USA) and redissolved in 55 μL of pH 11 buffer to completely release

the ODNs from the EAK-ODN aggregates. This releasing procedure was also applied to the ODN samples that contained no EAK to ensure that comparisons were drawn from results obtained with samples that had undergone the same experimental protocol. In the end, each sample was centrifuged at 10,000 rpm for 2 mins and the supernatant was collected for the FRET measurements.

5.2.3 Fluorescence Resonance Energy Transfer (FRET) Measurement

The fluorescence spectra of the supernatant were acquired using a Photon Technology International steady-state fluorometer (New Jersey, USA) equipped with a LPS 220-B xenon arc lamp and PTI 814 photomultiplier. The fluorescein donor was excited at its peak absorption wavelength (λ_{ex} = 494 nm). The ratio of the donor to the acceptor fluorescence intensity (I_D/I_A ratio) was determined by monitoring the fluorescein and rhodamine fluorescence at 517 and 583 nm, respectively.

5.2.4 Stability Assay of the EAK-ODN Aggregates

Samples containing 8.6 μM of ODNs and different amounts of the EAK peptides were prepared at pH 4 and pH 7. Half an hour after mixing, each sample was treated in two different ways. In one procedure, the EAK-ODN mixtures were diluted 5- and 10-fold with the corresponding buffer. The resulting samples are referred to as “dilute-5” and “dilute-10” sample, respectively. In the other procedure, the EAK-ODN mixture was centrifuged at 10,000 rpm for 2 mins. Its supernatant was discarded and the carefully collected pellets of the EAK-ODN aggregates were resuspended in the same volume of buffer solution used to prepare the mixture solutions. The samples obtained from this treatment are referred to as “refill” samples. UV-Vis spectroscopy was utilized to measure the relative UV absorbance change (ΔOD_r) over time for these samples following a procedure outlined in an earlier study (Wang, *et al*., 2006).

5.3 Results and Discussion

5.3.1 Releasing the ODNs from the EAK-ODN Aggregates

The stability of antisense oligonucleotides against degradation by nucleases is an important pre-requisite for a successful antisense oligonucleotide delivery *in vivo*. In this study, fluorescence resonance energy transfer (FRET) was used to monitor the time-dependent degradation of the ODNs by a nuclease. The ODNs were labelled at one end with a fluorescence donor (fluorescein) and at the other end with a fluorescence acceptor (rhodamine). The FRET phenomenon is sensitive to the distance separating the donor from the acceptor. The distance between the two labels increases if the doubly-labeled ODNs are degraded and the degraded ODNs can diffuse freely away. Under such conditions, degradation of the doubly-labeled ODNs is accompanied by a decrease in FRET

efficiency. However, since the ODNs are initially encapsulated inside the EAK-ODN aggregates, the degraded ODNs might not be allowed to diffuse out of the EAK-ODN aggregates, holding the donor and acceptor at the same position in the EAK matrix. In order for FRET to reflect the true degradation profiles of the ODNs, it becomes important to ensure that the ODNs can be extracted from the EAK matrix.

EAK contains four glutamic acids (Glu, E) and four lysines (Lys, K) with pKa values of 4.25 and 10.53, respectively (Lehninger, 1993). According to these pKa values, the EAK molecules are expected to be negatively charged at pH 11 and not to interact with the ODNs due to electrostatic repulsion between the negatively charged amino acid residues of EAK and the phosphate groups of the ODNs (Wang, *et al*., 2006). Thus, adjusting the solution pH to 11 should provide a means to release the ODNs from the EAK matrix of the EAK-ODN aggregates.

UV-Vis experiments were carried out to confirm this expectation. First, the EAK-ODN aggregates were formed by mixing 5.0 μM of dC_{16} with 120 μM of EAK16-II at pH 4. The UV-Vis absorbance at the peak wavelength at 276 nm of this solution was 0.75 and dropped to about zero after centrifugation (Figure 5.1). This indicates that in this solution, all ODNs were incorporated in the aggregates, which were centrifuged out (Wang, *et al*., 2006). This solution was then dried and resuspended in pH 11 buffer. The UV absorbance of the resulting solution at 276 nm before and after centrifugation was 0.73 and 0.71 (Figure 5.1). Since centrifugation has been shown to be very efficient at removing the EAK-ODN aggregates from the solution, the constant absorption before and after centrifugation demonstrates that when the solution pH is brought from 4 to 11, most ODNs are either successfully extracted from the aggregates or present in much smaller EAK-ODN aggregates, too small to be centrifuged out. This extraction method was applied in the next series of experiments to determine the nuclease resistance of the ODNs encapsulated in the EAK matix.

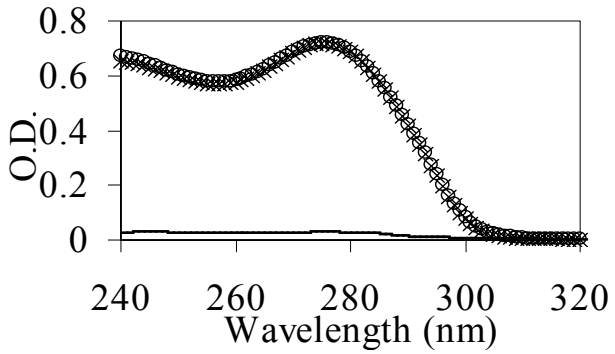

Figure 5.1. UV-Vis absorption spectra of the supernatant of 5.0 μM dC_{16} mixed with 0.2 mg/mL EAK16-II at pH 4 after centrifugation (-); The above EAK-dC_{16} mixture was dried and resuspended in pH 11 buffer. UV-Vis absorption spectra of the new solution before centrifugation (○), and after centrifugation (×).

5.3.2 Nuclease Resistance of the ODNs Encapsulated in the EAK Matrix

The extent of ODN protection against the nuclease when the ODNs are incorporated in the EAK-ODN aggregates made of either EAK16-II or EAK16-IV at different pHs was investigated by performing fluorescence resonance energy transfer (FRET) experiments. Fl-dC_{16}-Rh doubly-labelled with fluorescein at the 5'-end and rhodamine at the 3'-end was used as probe. The emission spectra were acquired from 500 to 700 nm while exciting the solution at the absorbance peak wavelength of the fluorescein donor (λ_{ex} = 494 nm).

Control solutions of the doubly-labeled ODNs prepared in the presence or absence of EAK16-IV at pH 4 were incubated in 1× degradation buffer solution at pH 9.5 without exonuclease I for 1 hr. FRET took place as seen from the two emission peaks at 517 and 583 nm corresponding to the fluorescein donor and the rhodamine acceptor, respectively (Figure 5.2). The ratio of the donor to the acceptor fluorescence intensity at the peak wavelengths (I_D/I_A) for the ODNs decreases from 1.4 (control in Figure 5.2A) to 1.2 (control in Figure 5.2B) upon addition of EAK16-IV. Smaller I_D/I_A ratio indicates that association of Fl-dC_{16}-Rh with EAK16-IV results in strong FRET, which might be due to the ODN adopting a more compact conformation in the EAK-ODN aggregates.

The emission spectra were also taken at different points in time after adding exonuclease I to the ODN or EAK-ODN solutions at pH 4 (Figure 5.2). For the ODNs alone (Figure 5.2A), the donor fluorescein fluorescence immediately increased 2.6-fold as that of rhodamine decreased, indicating a lower extent of FRET and demonstrating the degradation of the ODNs. Figure 5.2A also indicates that a substantial percentage of the ODNs are degraded within 20 minutes, a result consistent with the expectation that the unprotected ODNs are rapidly degraded by nucleases (Agrawal, 1999). In contrast, the EAK-ODN aggregates generated with EAK16-IV at pH 4 are not degraded by exonuclease I even after 100 minutes, as indicated by the similarity of the emission spectra before and after nuclease treatment (Figure 5.2B). This result is consistent with the fluorescence quenching experiments, which showed that ODNs incorporated in an EAK matrix were less accessible to the solvent than naked ODNs were (Wang, *et al*., 2006).

The ODN solutions with and without EAK were incubated with exonuclease I and aliquots were removed from the solution as a function of time. After applying the protocol described in the experimental section, the normalized I_D/I_A ratio was determined and the percentage of degraded ODNs was established as a function of time by applying the calibration curve shown in Figure 5.3.

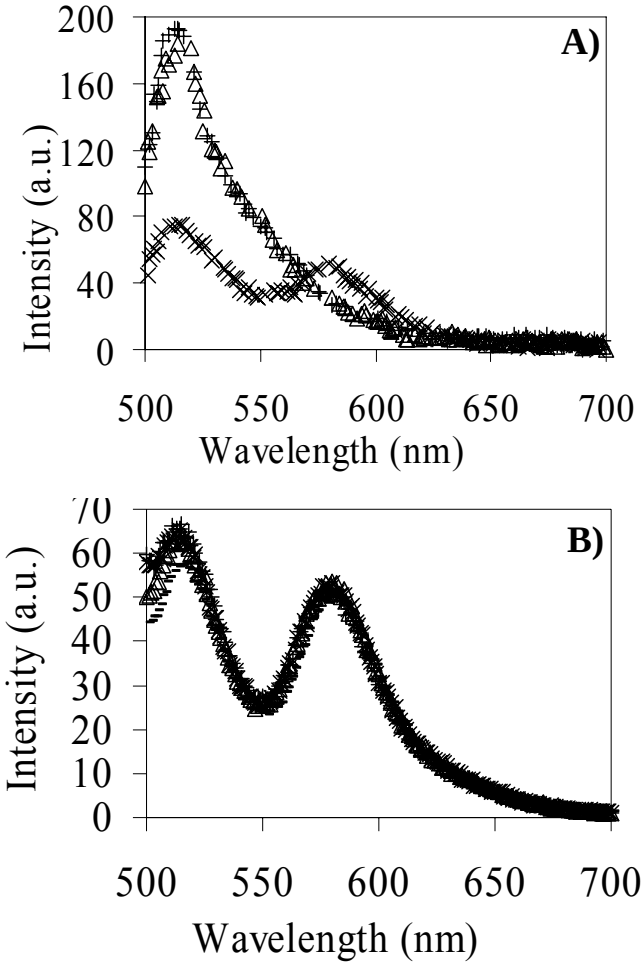

Figure 5.2. FRET of Fl-dC_{16}-Rh incubated with exonuclease I at pH 9 in the absence (A) or presence (B) of 0.1 mg/mL EAK16-IV at pH 4; A) without EAK16-IV: control (×), 20 min (Δ), and 30 min (+); B) with EAK16-IV: control (×), 20 (+), 60 (Δ), and 104 min (-).

To monitor the degradation of the ODNs in a quantitative manner, the I_D/I_A ratio was determined for solutions containing different amounts of the intact and completely degraded ODNs (Figure 5.3). In these experiments, a 0.46 μM solution of the intact doubly-labeled dC_{16} was prepared and its fluorescence spectrum was acquired. It was mixed in different proportions with a solution containing 0.46 μM of fluorescein-labeled dC_{16} and 0.46 μM of rhodamine-labeled dC_{16}. The equimolar solution of fluorescein- and rhodamine-labeled dC_{16} was used as a mimic of the fully degraded ODNs. The I_D/I_A ratios of the mixtures were normalized to the I_D/I_A ratio of the intact ODNs. Figure 5.3 shows that the normalized I_D/I_A ratio increases linearly with the percentage of singly-labeled ODNs present in solution. The plot in Figure 5.3 was used as a calibration curve to determine quantitatively the percentage of ODNs which were degraded by the nuclease.

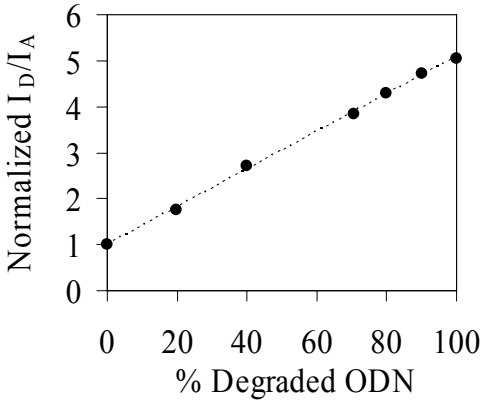

Figure 5.3. Calibration curve correlating the normalized I_D/I_A ratio to the percentage of degraded ODNs. The dashed line represents the best fit to the equation: *normalized* $I_D/I_A = A \times$ % *degraded ODN* + 1 with A = 0.0409 and $R^2 = 0.999$.

Figure 5.4A shows the percentage of degraded ODNs in the presence or absence of EAK after the aggregates generated at pH 4 were incubated with exonuclease I at pH 9.5. The profile obtained for the naked ODNs with no EAK present indicates that 85 % of the ODNs are degraded within 20 minutes. Ideally, 100 % of the ODNs should have been degraded. The fact that this was not observed might reflect some discrepancies between the calibration curve determined under ideal condition and the samples having undergone nuclease degradation. Nevertheless, the data shown in Figure 5.4A demonstrate that the naked ODNs are degraded efficiently by the nuclease. In contrast, the ODNs complexed with either EAK16-IV or EAK16-II at pH 4 did not exhibit any degradation even after being incubated for 100 mins with exonuclease I. These results suggest that the ODNs are located inside the EAK-ODN aggregates where they remain inaccessible to the nuclease. It is worth pointing out that in these experiments, the EAK-ODN aggregates are prepared at a pH which is much more acidic than the pH of 9.5 of the degradation buffer. The observation that the EAK matrix protects the ODNs against nuclease degradation at pH 9.5 demonstrates that the EAK-ODN aggregates prepared at pH 4 are stable even after being incubated at a more basic pH. These are promising properties for using EAK as a carrier for gene delivery.

The degradation of the free ODNs and the ODNs encapsulated with EAK at pH 7 are shown in Figure 5.4B. The free ODNs prepared in a pH 7 buffer and incubated with the nuclease solution at pH 9.5 are strongly degraded within a few minutes, as was observed for the free ODNs prepared in a pH 4 buffer. The ODNs which were allowed to form aggregates with EAK16-II at pH 7 show a degradation profile in Figure 5.4B which is similar to that of the free ODNs. This indicates that the EAK-ODN aggregates prepared with EAK16-II at pH 7 do not offer any protection to the ODNs

against nuclease. On the other hand, the ODNs which were allowed to form aggregates with EAK16-IV at pH 7 are also degraded over time (Figure 5.4B), but to a lesser extent than those prepared with EAK16-II at pH 7. The reason for EAK16-IV offering a slightly better protection than EAK16-II might be due to EAK16-IV binding more strongly to the ODNs (Chapter 4), and thus generating more stable aggregates.

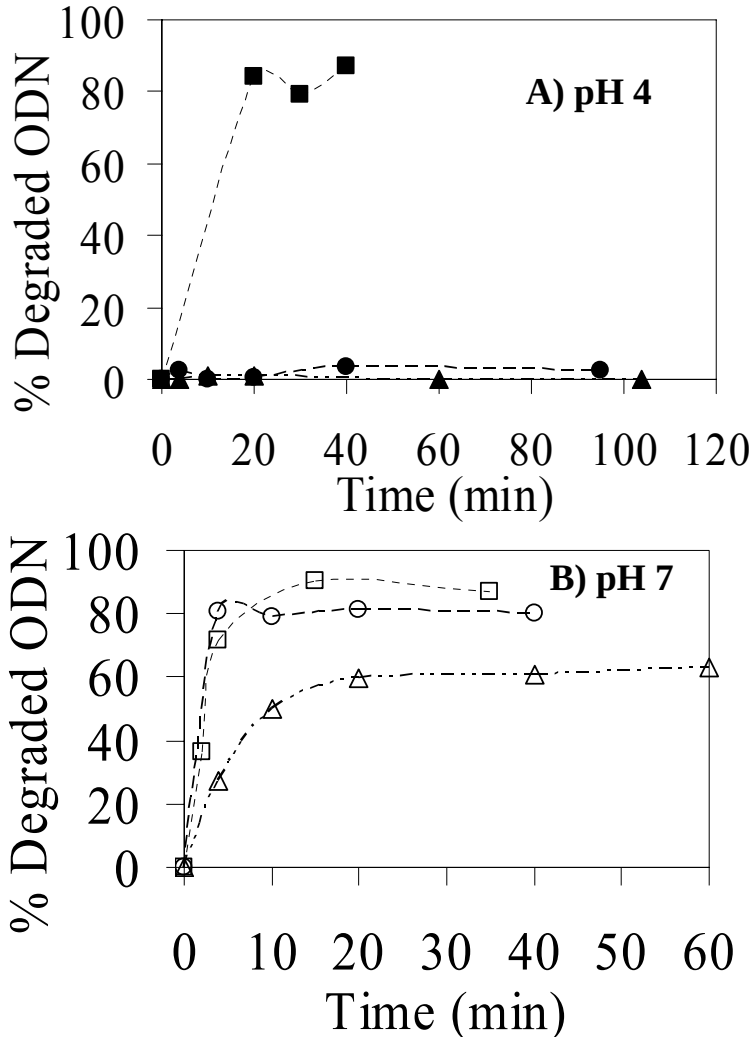

Figure 5.4. The percentage of degraded ODNs in the samples prepared at A) pH 4, and B) pH 7, as a function of incubation time with exonuclease I. Free ODNs (square), EAK16-IV-ODN (triangle), and EAK16-II-ODN (circle).

The apparently weaker protection provided by the EAK-ODN aggregates prepared at pH 7 could be due to the breakup of the EAK-ODN aggregates under basic conditions. Indeed both EAKs bind to the ODNs much more strongly at pH 4 than at pH 7, and EAK16-IV binds more strongly to the ODNs than EAK16-II does. To investigate whether the nuclease protection experiments shown in

Figure 5.4B could be rationalized according to the binding strength of EAK to the ODNs, the following experiments were performed. 8.6 μM of dC_{16} was mixed with 0.1 mg/mL EAK16-IV at pH 4 and pH 7. The resulting solutions were centrifuged 30 mins after preparation. The EAK-dC_{16} aggregates were collected and resuspended in the pH 9.5 degradation buffer with no exonuclease I. The relative UV absorbance change (ΔOD_r) representing the fraction of ODNs in the aggregates was monitored over time (Figure 5.5).

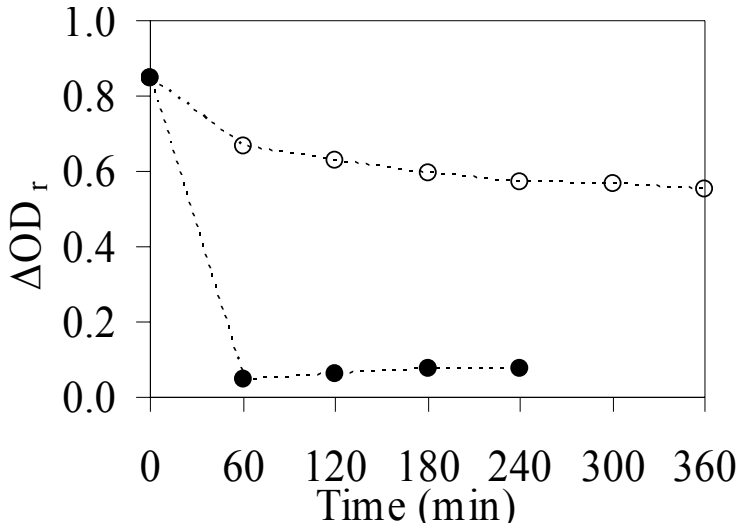

Figure 5.5. Relative UV-Vis absorbance change (ΔOD_r) as a function of time for the sample obtained by resuspending preformed aggregates prepared with 8.6 μM dC_{16} and 0.1 mg/mL EAK16-IV at pH 4 (○) and pH 7 (●) in the pH 9.5 buffer used for the nuclease degradation experiments.

Ideally, ΔOD_r is expected to equal 1.0 at t = 0 since all ODNs should be in the EAK-ODN aggregates (pellets). In practice, this was difficult to achieve and the EAK-ODN aggregates were recovered with an 85 % yield. Regardless of these experimental errors, the fraction of ODNs incorporated inside the EAK-ODN aggregates prepared at pH 7 decreased to 0.05 in one hour. In contrast, ΔOD_r decreased gradually over time for the aggregates prepared at pH 4. Since the decrease in ΔOD_r indicates a breakup of the EAK-ODN aggregates over time, the results shown in Figure 5.5 demonstrate that the EAK-ODN aggregates prepared at pH 7 dissociate much more easily than those prepared at pH 4 when the pH is increased to 9.5. Since the EAK-ODN aggregates prepared with EAK16-IV at pH 7 dissociate at pH 9.5, their degradation profile is expected to be similar to that of the free ODNs. However, they still provide some protection against nuclease (Figure 5.4B). This might be due to the existence of some small EAK-ODN complexes in the solution. These small

complexes have been shown to contain a few ODN strands and are too small to be centrifuged out (Wang, *et al*., 2006).

To obtain the data shown in Figure 5.4, the nuclease added to the solutions of EAK-ODN aggregates was inactivated by SDS and the ODNs were released from the EAK matrix by increasing the solution pH to 11. Theoretically, the remaining intact ODNs in these solutions should be susceptible to nuclease degradation. To confirm this point, the solutions used in Figure 5.4 were mixed with 1-octanol to extract SDS. Then exonuclease I was added to the EAK-ODN samples that still had some intact ODNs such as those prepared with EAK16-IV at pH 4 and pH 7 and EAK16-II at pH 4. The degradation of the ODNs was monitored over time and the results are shown in Figure 5.6. Almost all ODNs were degraded in 25 mins, even though the degradation occurred more slowly than for the naked ODNs. The slow initial degradation rate may be caused by traces of SDS left in the solution which could decrease the activity of the nuclease. Nevertheless, the fact that most ODNs are degraded indicates that the ODNs are released from the EAK-ODN aggregates when the pH is increased to 11, in agreement with the conclusions drawn from the UV-Vis absorption measurements shown in Figure 5.1. Furthermore, the results shown in Figure 5.6 indicate that no EAK-ODN complexes remain at pH 11. This is reasonable since EAK is negatively charged at pH 11, which prevents its binding to the ODNs due to electrostatic repulsion. This result is different from what happens at pH 9.5, where the EAK-ODN aggregates prepared at pH 4 are stable enough to protect the ODNs against nuclease degradation.

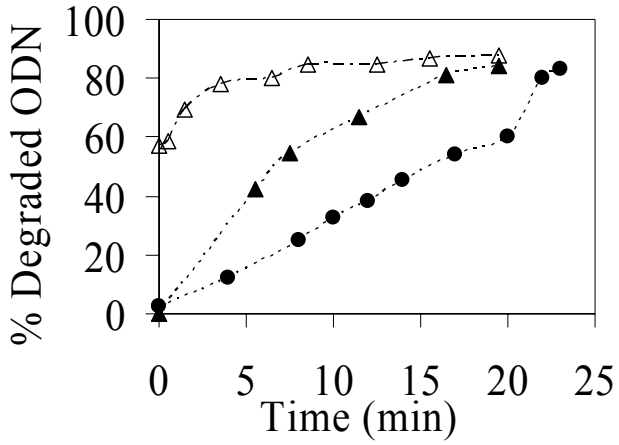

Figure 5.6. Degradation profiles of the ODNs treated with exonuclease I after having been released from the EAK-ODN aggregates prepared with Fl-dC_{16}-Rh and: EAK16-IV at pH 4 (▲),EAK16-II at pH 4 (●), and EAK16-IV at pH 7 (Δ).

5.3.3 Stability of the EAK-ODN Aggregates

The stability of the EAK-ODN aggregates was investigated to determine whether the EAK-ODN aggregates retain their structural integrity after being diluted several folds. The ODNs would be most likely unprotected and undergo nuclease degradation if dilution of the EAK-ODN solution induces the dissociation of the EAK-ODN aggregates. The EAK-ODN mixtures were prepared at pH 4 and pH 7. The relative UV-Vis absorbance change ΔOD_r of these mixtures, which reflects the percentage of ODNs in the aggregates, was measured 30 mins after sample preparation. The mixtures were then diluted 5 or 10 times with the corresponding buffer solution. The resulting samples were referred to as "dilute-5" and "dilute-10", respectively. The ΔOD_r values of these diluted samples were monitored over time. ΔOD_r is expected to decrease over time after dilution of the EAK-ODN solutions if the EAK-ODN aggregates dissociate.

A plot of ΔOD_r as a function of time is given in Figure 5.7A for the "dilute-5" and "dilute-10" samples obtained from the dilution of the solution containing 0.017 mg/mL EAK16-IV and 8.6 μM dG_{16} at pH 4. The ΔOD_r value of this solution before dilution equaled 0.46 ± 0.01. As evident from Figure 5.7A, ΔOD_r does not change much over time whether the original EAK-ODN solution is diluted 5 or 10 times. This experiment demonstrates that the EAK-dG_{16} aggregates prepared at pH 4 do not dissociate after dilution.

The EAK-ODN aggregates were also prepared at pH 7 by mixing 0.08 mg/mL EAK16-IV and 8.6 μM dG_{16} at pH 7. The aggregates were prepared with more peptide since the binding of EAK to the ODNs at pH 7 is weaker (Chapter 4). ΔOD_r of the original EAK-dG_{16} solution equalled 0.72 ± 0.01. ΔOD_r did not change after the solutions were diluted 5 or 10-fold with pH 7 buffer, as shown in Figure 5.7B. The data shown in Figures 5.7A and 5.7B suggest that dissociation of the EAK-ODN aggregates prepared with EAK16-IV and dG_{16} at pH 4 or pH 7 is rather small upon dilution of the solutions.

The weak dissociation of the EAK-ODN aggregates is observed not only with EAK16-IV, but also with EAK16-II. Figures 5.8A and 5.8B present the ΔOD_r vs. time for the "dilute-5" and "dilute-10" EAK-ODN solutions prepared by mixing 8.6 μM dG_{16} with either 0.04 mg/mL EAK16-II at pH 4 (Figure 5.8A) or 0.1 mg/mL EAK16-II at pH 7 (Figure 5.8B), respectively. No decrease in the ΔOD_r value over time is observed regardless of the pH at which the solutions were prepared. This result demonstrates that the EAK-ODN aggregates prepared with EAK16-II at pH 4 and pH 7 are stable and do not dissociate. According to the results presented in Figures 5.7 and 5.8, neither a 5- nor a 10-fold dilution can induce a break-up of the EAK-ODN aggregates formed at pH 4 and pH 7 over a period of at least 17 hrs.

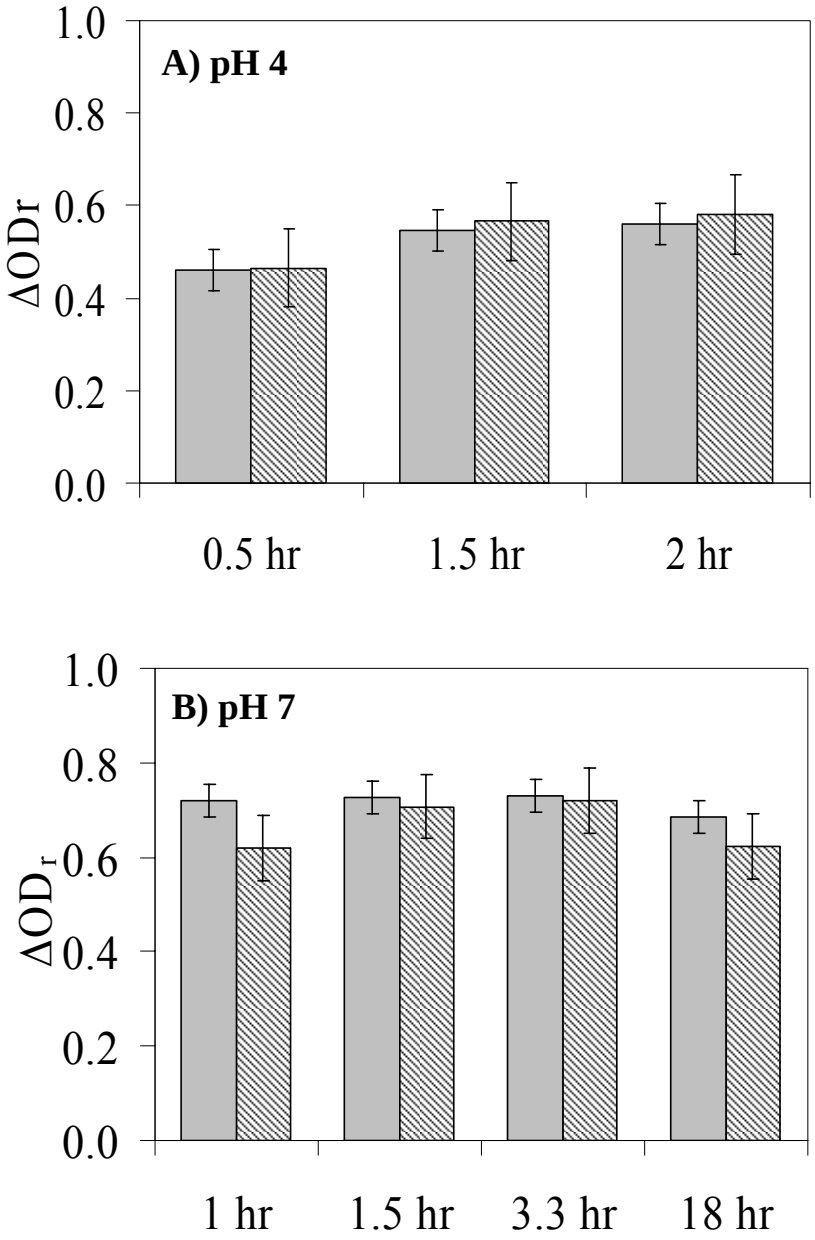

Figure 5.7. Relative UV-Vis absorbance change (ΔOD_r) over time of the dilute-5 (▭) and dilute-10 (▨) samples after diluting the EAK-ODN solutions generated by mixing 8.6 μM dG_{16} with (A) 0.0175 mg/mL EAK16-IV at pH 4 and (B) 0.08 mg/mL EAK16-IV at pH 7.

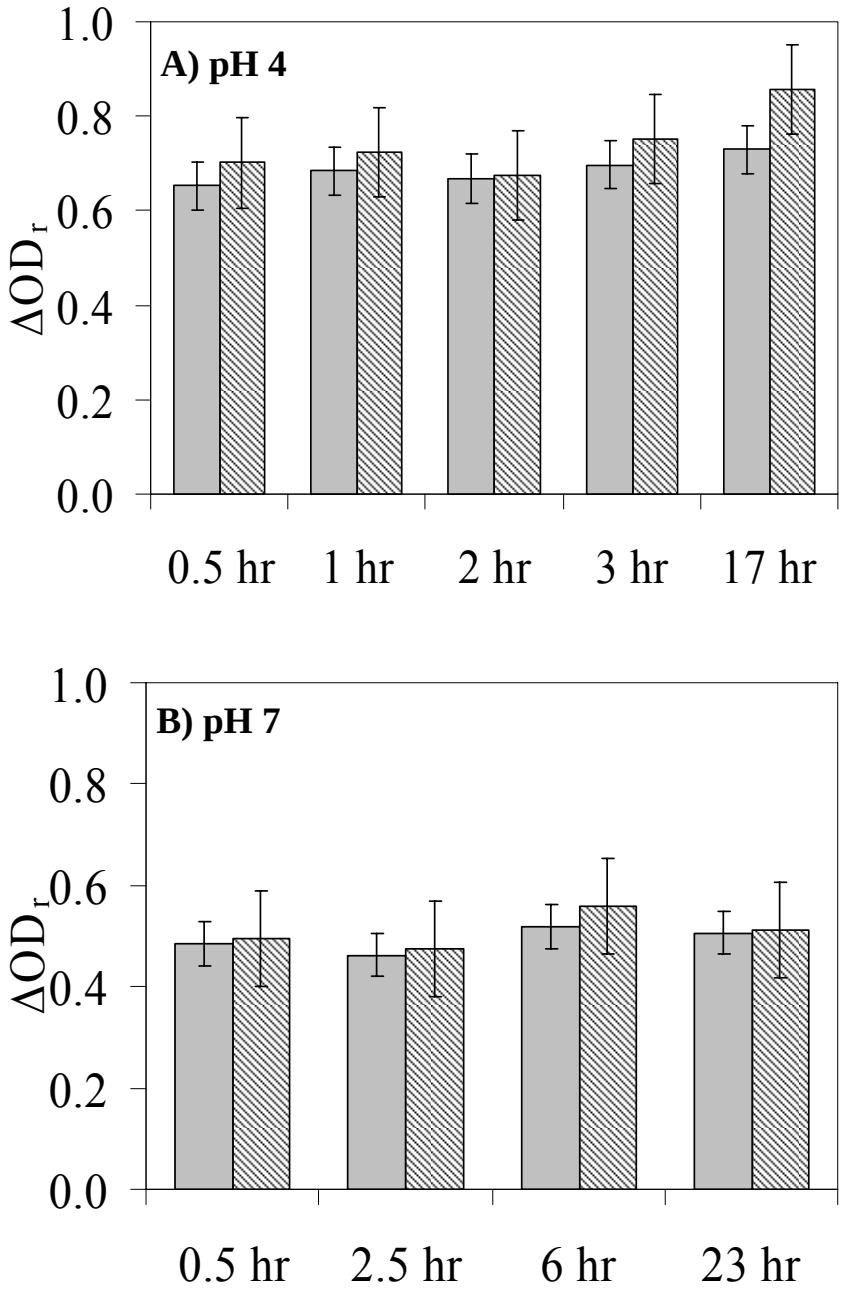

Figure 5.8. Relative UV-Vis absorbance change (ΔOD_r) over time after diluting 5- (▭) and 10-fold (▨) the solutions containing 8.6 μM dG_{16} and 0.04 mg/mL EAK16-II at pH 4 (A) and 0.1 mg/mL EAK16-II at pH 7 (B).

The stability of the EAK-ODN aggregates was also studied through a refill treatment procedure. The EAK-ODN solutions were centrifuged 30 mins after sample preparation and the

supernatant was discarded. The pellets were resuspended with the same amount of fresh buffer. The resulting samples were referred to as "refill" samples.

As shown in Figure 5.9, ΔOD_r does not change over time for the "refill" samples, regardless of the type of peptides or pH value. All ΔOD_r values range between 0.8 and 1.0. Ideally, the fraction of ODNs in the aggregates for the "refill" samples should equal unity at time zero if no dissociation of the aggregates occurred, given that only EAK-ODN aggregates were collected to prepare the "refill" samples. ΔOD_r values for the "refill" samples were found to be smaller than 1.0, ranging from 0.85 to 0.95 at time zero. This is certainly due to experimental errors introduced during the delicate centrifugation/supernatant removal steps. Nevertheless the absence of decrease for ΔOD_r in Figure 5.9 over 20 hrs together with the data shown in Figures 5.7 and 5.8 suggest that the EAK-ODN aggregates dissociate on a slow time scale upon dilution.

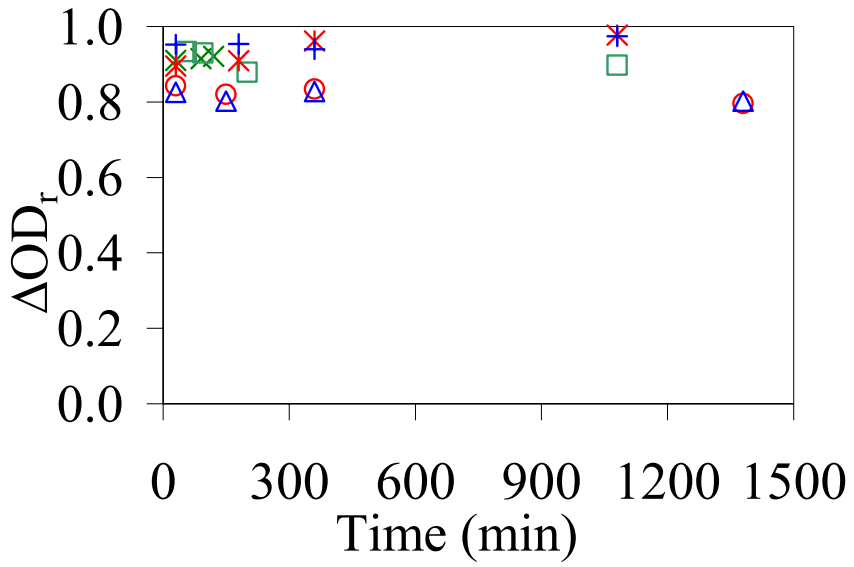

Figure 5.9. Relative UV-Vis absorbance change (ΔOD_r) over time after refilling the solutions of EAK16-IV-dG_{16} at pH 4 (×), EAK16-IV-dG_{16} at pH 7 (□), EAK16-II-dG_{16} at pH 4 (*), EAK16-II-dG_{16} at pH 7 (○), EAK16-II-dC_{16} at pH 4 (+), and EAK16-II-dC_{16} at pH 7 (Δ).

5.4 Summary

In this work, the nuclease resistance of oligonucleotides against *E.coli* exonuclease I afforded by the protection of a peptidic matrix generated by two self-assembling peptides of the EAK family at pH 4 and pH 7 was investigated using FRET. The results demonstrate a remarkable increase in nuclease resistance for the ODNs mixed with EAK16-II or EAK16-IV at pH 4. However, the protection

provided by these EAKs when the EAK-ODN aggregates are prepared at pH 7 is much lower than that at pH 4. UV-Vis absorption measurements show that the EAK-ODN aggregates prepared at pH 7 dissociate more easily than those prepared at pH 4 when the pH of the solution is raised to pH 9.5, the pH at which exonuclease I is active. These results suggest that the ability of the EAK-ODN aggregates to protect the ODNs depends on their structural integrity after being incubated with nuclease solution, and that a correlation exists between the efficiency of EAK-ODN aggregates at protection the ODNs and the binding strength of the EAK peptides to a given ODN.

The stability of the EAK-ODN aggregates after dilution was determined by UV-Vis absorption over time. The aggregates are found to be stable, undergoing no detectable dissociation over 20 hrs after the solutions are diluted 5- and 10-fold in the same buffer used for their preparation. The EAK-ODN aggregates are also shown to remain stable after the refill treatment.

The results of this work imply that the self-assembling peptides might be appropriate candidates for gene delivery, able to protect the ODNs from nuclease degradation *in vitro* and *in vivo*.

References

Agrawal, S. 1999. Importance of nucleotide sequence and chemical modifications of antisense oligonucleotides. *Biochim. Biophys. Acta* **1489:** 53-68.

Crooke, S. T. 1992. Therapeutic applications of oligonucleotides. *Biotechnology* **10:** 882-886.

Crooke, S. T. 2000. Progress in antisense technology: the end of the beginning. *Methods Enzymol.* **313:**3-45.

Dias, N., and C. A. Stein. 2002. Antisense Oligonucleotides: Basic Concepts and Mechanisms. *Mol. Cancer Therap.* **1:** 347-355.

Garcia-Chaumont, C., O. Seksek, J. Grzybowska, E. Borowski, and J. Bolard. 2000. Delivery systems for antisense oligonucleotides. *Pharm. & Therap.* **87:** 255-277.

Ghosh, M. K., J. S. Cohen, O. Dahl, and K. Ghosh. 1993. Evaluation of some properties of a phosphorodithioate oligodeoxyribonucleotide for antisense application. *Nucl. Acids Res.* **21:** 5761-5766.

Hogrefe, R. I. 1999. An antisense oligonucleotide primer. *Antisense Nucl. Acid Drug Dev.* **9:** 351-357.

Lehninger, A. L. 1993. *Principles of Biochemistry*. Worth Publishers.

Pavid, A. D. 2000. Peptide nucleic acids: versatile tools for gene therapy strategies. *Adv. Drug Del. Rev.* **44:** 81-95.

Remaut, K., B. Lucas, K. Braeckmans, N. N. Sanders, S. C. De Smedt, and J. Demeester. 2005. FRET-FCS as a tool to evaluate the stability of oligonucleotide drugs after intracellular delivery. *J. Control. Rel.* **103:** 259-271.

Uchiyama, H., K. Hirano, M. Kashiwasake-J, and K. Taira. 1996. Detection of Undegraded Oligonucleotides in Vivo by Fluorescence Resonance Energy Transfer. *J. Biol. Chem.* **271:** 380– 384.

Wang, M., M. Law, J. Duhamel, and P. Chen. 2006. Interaction of a Self-Assembling Peptide with Oligonucleotides: Complexation and Aggregation. *Biophys. J.* In Press

Zhang, S., C. Lockshin, R. Cook, and A. Rich. 1994. Unusually stable beta-sheet formation in an ionic self-complementary oligopeptide. *Biopoly.* **34:** 663-672.

Zhang, S. 2002. Emerging biological materials through molecular self-assembly. *Biotechnol. Adv.* **20:** 321-339.

Chapter 6
Conclusions and Recommendations

6.1 Conclusions

This thesis presents the first comprehensive study of the binding of self-assembling peptides to oligodeoxynucleotides (ODNs) and of the characterization of the resulting complexes/aggregates. A methodology has been successfully developed to quantitatively describe the binding of peptides to the ODNs into peptide-ODN aggregates. The effects of pH, charge distribution along peptides and oligonucleotide sequence on the peptide-ODN binding have been investigated by using different EAK self-assembling peptides, ODNs, and pHs. The size, ODN protection ability, and stability of the resulting complexes/aggregates were characterized by a series of physicochemical methods. Since formation of carrier-gene complexes is the fist step in the formulation of a gene delivery system, the detailed studies conducted in this thesis on peptide-ODN binding are expected to enable the development of strategies to control the formulation of peptide-DNA complexes and demonstrate the high potential of self-assembling peptides for gene delivery.

Self-assembling peptides bind to ODNs and form aggregates, which can be centrifuged out, as demonstrated by UV-Vis absorption and fluorescence anisotropy measurements in Chapters 3 and 4. This feature makes it possible to use UV-Vis absorption and centrifugation to obtain the fraction of ODNs incorporated in the EAK-ODN aggregates as a function of peptide concentration. The UV-Vis absorbance results were then analyzed with a binding density function to generate the binding isotherms, from which the binding parameters are extracted with the McGhee and von Hippel model. Some unique challenges were encountered in the characterization of the binding process of EAK peptides to the ODNs due to the potential for self-assembly of the peptides into nanostructures. Fluorescence anisotropy and static light scattering experiments in Chapters 3 and 4 demonstrated that the binding process of EAKs to the ODNs starts with the molecular complexation of individual EAK and ODN molecules, followed by the association of the complexes into aggregates. The remaining results obtained in this thesis are summarized as follows.

In Chapter 3, UV-Vis absorption, fluorescence anisotropy, and PAGE experiments demonstrated that at equilibrium, the EAK-ODN solutions contain free EAK, free ODNs, small EAK-ODN complexes which can not be centrifuged out, and large aggregates which are collected in the pellets after centrifugation of the solution. Equilibrium binding studies show that binding of EAK16-II to different ODNs at pH 4 is stronger than at pH 7, and that no binding occurs at pH 11. Binding

constants decrease 5-8 folds when the pH changes from 4 to 7. This result demonstrates that electrostatic interactions play an important role in the EAK-ODN binding because EAK16-II becomes less positively charged as pH increases. In addition, hydrogen bonds might promote the binding of EAK16-II to dG_{16} to a greater extent than that of EAK16-II to dC_{16}. The size of the resulting EAK-ODN aggregates measured by AFM and DLS ranges from a few hundreds of nanometers to several micrometers. The accessibility of the ODNs to the quencher is reduced by 40 % after binding to EAK16-II.

EAK16-IV, another member of the self-assembling EAK peptide family, shows some similarities to EAK16-II when it binds to the ODNs, as illustrated in Chapter 4. EAK16-IV binds to the ODNs more strongly at acidic than at basic pH. EAK16-IV also binds more strongly to dG_{16} than to the other ODN sequences studied in this thesis. The size of the EAK-ODN aggregates depends on the molar ratio of peptides to the ODNs. The accessibility of the ODNs to the quencher is reduced after binding to EAK16-IV. In particular, the charge distribution along peptides is found to have an effect on the binding. EAK16-IV, whose positively charged residues are clustered at one end of the peptide, binds to the ODNs more strongly than EAK16-II, whose positively charged residues are distributed throughout the peptide, at a same pH and for a given ODN sequence. In addition, the accessibility of the ODNs in the aggregates to the solvent is more strongly reduced upon binding to EAK16-IV than to EAK16-II.

The reduced accessibility of the ODNs described by the fluorescence quenching experiment is expected to prevent the nucleases from approaching the ODNs in the aggregates, and thus to protect the ODNs from degradation. In order to prove this, oligonucleotides complexed with EAK were incubated with *E.coli* exonuclease I to determine the level of protection afforded by the peptidic EAK matrix. The results of this study were described in Chapter 5. A remarkable increase in nuclease resistance for the ODNs mixed with EAK16-II or EAK16-IV at pH 4 is observed. However, the ODNs are protected to a much lower degree when the EAK-ODN aggregates are prepared at pH 7. The EAK-ODN aggregates prepared at pH 7 are found to dissociate more easily than those prepared at pH 4 when they are incubated with exonuclease I solution at pH 9.5. These results suggest that the ODN protection afforded by the EAK-ODN aggregates depends on their structural stability after being incubated with the nuclease solution, which correlates to the binding strength of the EAK peptides to the ODNs. The stability of the EAK-ODN aggregates after dilution was determined by UV-Vis absorption over time. The aggregates undergo no detectable dissociation over 20 hrs after the solutions are diluted 5- and 10-fold in the same buffer used for their preparation. The EAK-ODN aggregates remain stable after solutions are centrifuged, and the supernatant is discarded and replaced

by fresh buffer solutions. All in all, this thesis has demonstrated the potential of EAK self-assembling peptides at forming highly stable complexes that can protect ODNs from degradation by nucleases.

6.2 Recommendations

The binding isotherms generated in this thesis use the UV-Vis absorbance of the supernatants of the EAK-ODN solutions. This study has also shown that fluorescence anisotropy increases upon binding of the peptides to a fluorophore-labeled ODN. Since fluorescence anisotropy is a common method to study the binding of a ligand to a substrate (Arosio, *et al*., 2004), it can be used as an alternative technique to construct the binding isotherms by monitoring the changes in anisotropy as a function of peptide concentration for constant ODN concentrations. In so doing, the results obtained by UV-Vis absorption could be strengthened.

In Chapter 3 and Chapter 4, the rhodamine dimer present in the supernatants of EAK-ODN mixture solutions indicates the existence of EAK-ODN complexes, which are too small to be centrifuged out. However, none of the other techniques, such as PAGE and steady-state anisotropy were able to detect the presence of complexes. Therefore, it will be good to have additional experiments to demonstrate the formation of complexes. One option is to label the ODNs with a fluorescence donor and EAK with an acceptor, and then to monitor the FRET change after mixing relatively low concentration of EAK and ODN. Another option would be use time-resolved anisotropy, which reflects the species with different sizes. The percentage of each specie could be quantified.

The current binding study has shown that the self-assembling peptides have some of the desired features expected for oligonucleotide carriers, such as conferring ODN protection and undergoing slow dissociation from the ODNs after many folds dilution. However, the morphology of the peptide-ODN complexes together with surface features, such as charges or hydrophobicity, may affect where the ODN is being delivered *in vivo* and ultimately influence the ability of the delivery system to reach the target site (Simeoni, *et al*., 2003). Thus, it becomes important to investigate these physicochemical properties as well. The morphologies of the EAK-ODN aggregates prepared at different ratios of peptide-to-ODN can be investigated by atomic force microscopy. The surface charges of the EAK-ODN complexes/aggregates can be investigated based on zeta potentials measured by electrophoretic light scattering. The surface hydrophobicity can be examined by surface tension measurements (Adamson and Gast, 1997).

The EAK-ODN aggregates have been shown to protect the ODNs from exonuclease I degradation in the current study. However, there are numerous other nucleases in any biological

system. For the EAK-ODN complexes to be a useable gene delivery system, it is necessary to investigate whether the EAK matrix can protect the ODNs from degradation against different nucleases. This can be done by studying with FRET the nuclease resistance of the ODNs provided by the EAK-ODN aggregates in cell culture medium containing serum.

The ODNs used in the current study, containing hexadecamer cytosine or guanine only, are more homogenous than the antisense oligonucletides typically used. In order to use the EAK self-assembling peptide to carry oligonucleotides, it is important to extend the current studies to real antisense oligonucleotides, which can be chosen based on a particular disease target.

Once the peptide-ODN aggregates with ODN protection have been constructed, one must examine whether these constructs can enhance the cellular uptake of the ODN cargoes, which together with rapid ODN degradation are two major challenges in the gene delivery. The cellular distribution and release of the oligonucleotides can be studied by fluorescence microscopy.

Appendices

A. Resolution Limit of Fluorescence Anisotropy Measurement

To evaluate the resolution limit of fluorescence anisotropy, the anisotropy of mixtures of 1 μM of FAM-labeled dC_{16} and EAK with concentrations ranging from 0 to 6 μM at pH 4 was measured 30 mins after sample preparation without centrifugation. Samples were excited at 452 nm and the fluorescence intensity was monitored at 514 nm (the peak of the FAM-dC_{16} emission spectra). The percentage of dC_{16} bound to EAK was calculated at each EAK concentration from the binding parameters obtained from the MvH model, Equation 3-5.

The fluorescence anisotropy of FAM-dC_{16} is shown in Figure A (empty circle) as a function of EAK concentration at pH 4. The error bars in Figure A represent the standard deviation obtained with 50 data points.

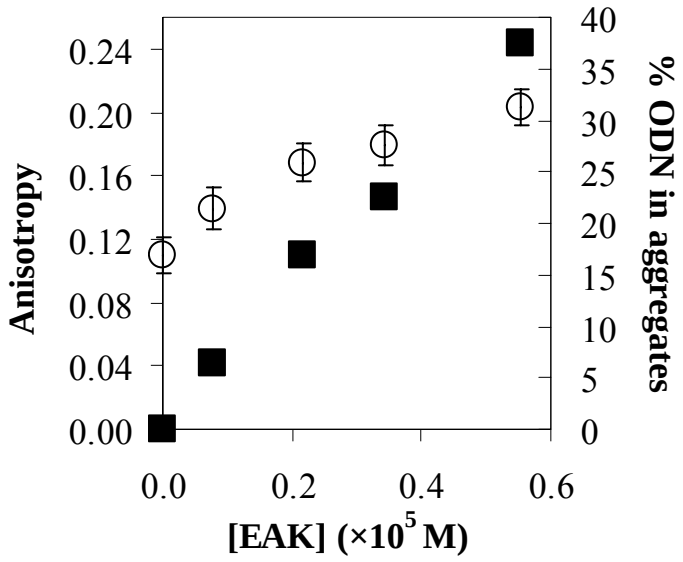

Figure A. Anisotropy (○) and the calculated percentage (■) of the FAM-dC_{16} in aggregates upon the addition of EAK.

Although the MvH model is not suitable to describe the two-step kinetics, it was found to fit the experimental data shown in Figure 3.2 very well. Thus, it was used to calculate the fraction of ODNs in the aggregates given in Figure A (solid squares). The anisotropy increases from 0.11 to 0.14 as the fraction of the ODN in aggregates increases from 0 to 9 mol%. This result demonstrates that the presence of 10 mol% of the ODNs in aggregates will be detected by fluorescence anisotropy.

B. AFM images of dG_{16} and EAK at pH 4. (A) 0.1 mg/mL EAK after 45 minutes; (B) 1.6 μM dG_{16} after 45 minutes; the experimental conditions were described in the Experimental Section of Chapter 3. No EAK-ODN aggregates were observed, especially in the form of fibers.